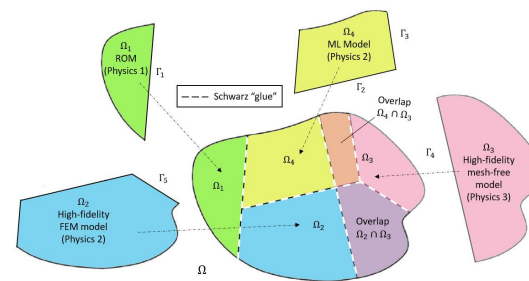
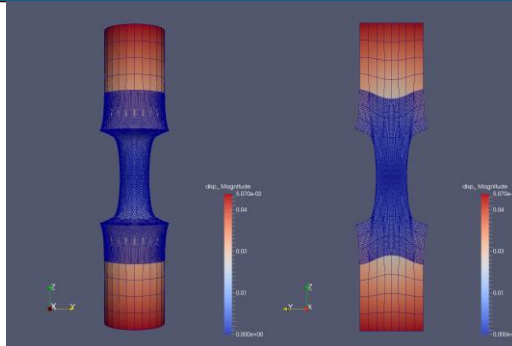
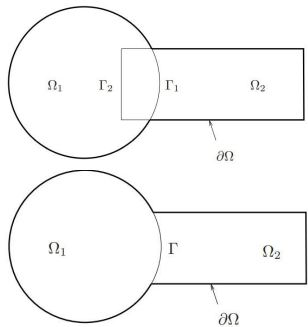


Alternating Schwarz-based coupling of conventional and data-driven models



Irina Tezaur¹, Joshua Barnett^{1,2}, Alejandro Mota¹,
Chris Wentland¹, Will Snyder^{1,3}

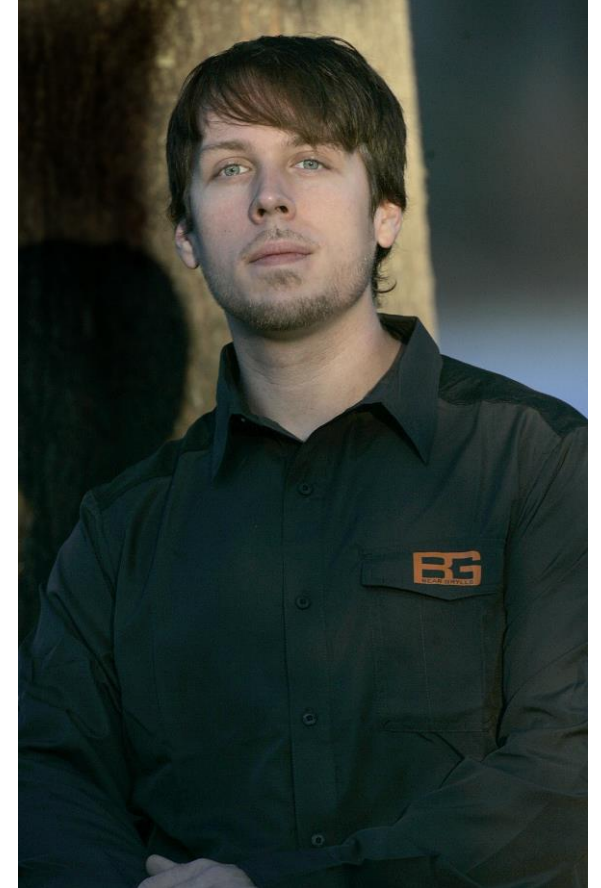
¹Sandia National Laboratories, ²Stanford University, ³Virginia Tech University

COUPLED 2023
Chania, Greece, June 5-7, 2023

SAND2023-04302C

In memory of minisymposium co-organizer K. Chad Sockwell

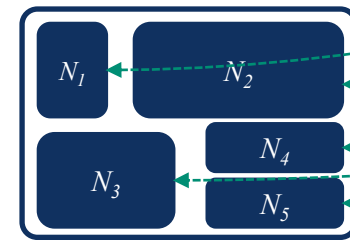
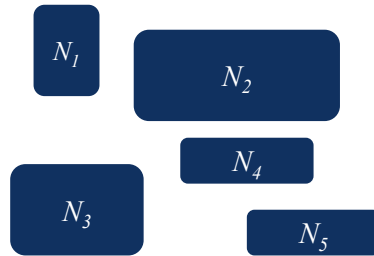
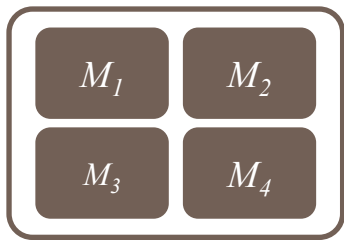
April 30, 1991 – May 18, 2022



Motivation: multi-scale & multi-physics coupling



There exist established **rigorous mathematical theories** for **coupling** multi-scale and multi-physics components based on **traditional discretization methods** (“Full Order Models” or FOMs).



Complex System Model

- PDEs, ODEs
- Nonlocal integral
- Classical DFT
- Atomistic, ...

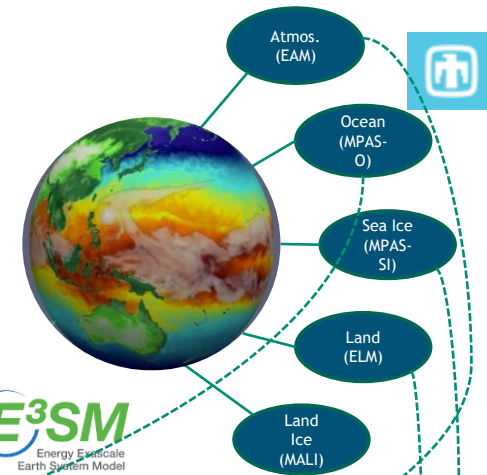
Traditional Methods

- Mesh-based (FE, FV, FD)
- Meshless (SPH, MLS)
- Implicit, explicit
- Eulerian, Lagrangian...

Coupled Numerical Model

- Monolithic (Lagrange multipliers)
- Partitioned (loose) coupling
- Iterative (Schwarz, optimization)

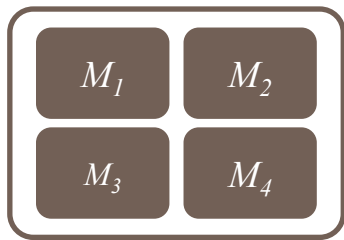
E³SM
Energy-Euscale
Earth System Model



Motivation: multi-scale & multi-physics coupling

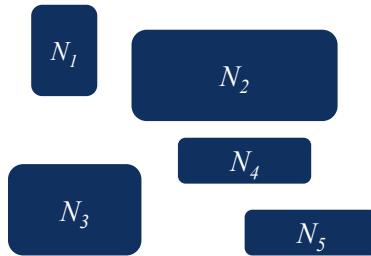


There exist established **rigorous mathematical theories** for **coupling** multi-scale and multi-physics components based on **traditional discretization methods** (“Full Order Models” or FOMs).



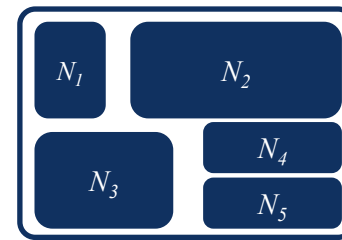
Complex System Model

- PDEs, ODEs
- Nonlocal integral
- Classical DFT
- Atomistic, ...



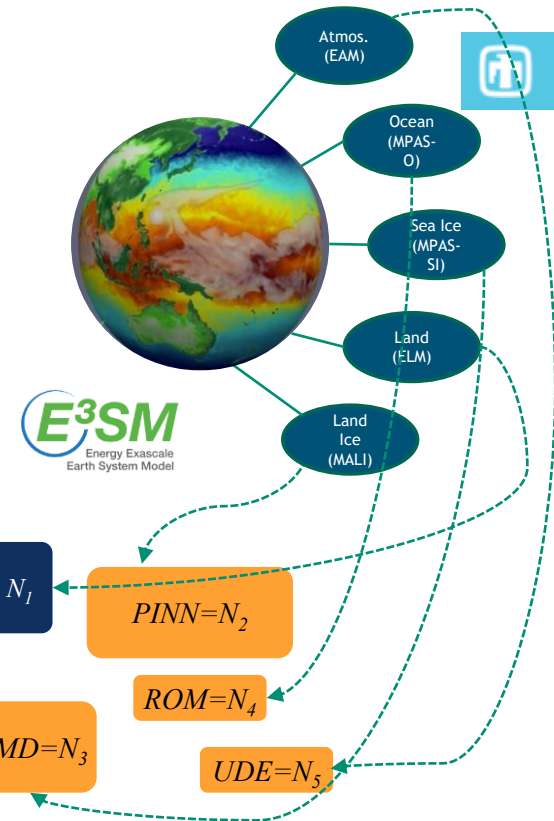
Traditional Methods

- Mesh-based (FE, FV, FD)
- Meshless (SPH, MLS)
- Implicit, explicit
- Eulerian, Lagrangian, ...



Coupled Numerical Model

- Monolithic (Lagrange multipliers)
- Partitioned (loose) coupling
- Iterative (Schwarz, optimization)



Traditional + Data-Driven Methods

- PINNs
- Neural ODEs
- Projection-based ROMs, ...

While there is currently a big push to integrate **data-driven methods** into modeling & simulation toolchains, existing algorithmic and software infrastructures are **ill-equipped** to handle **rigorous** plug-and-play integration of **non-traditional, data-driven models**!



fHNM (flexible Heterogeneous Numerical Methods) Project:

aims to **discover** the mathematical principles guiding the **assembly** of **standard** and **data-driven numerical models** in stable, accurate and physically consistent ways

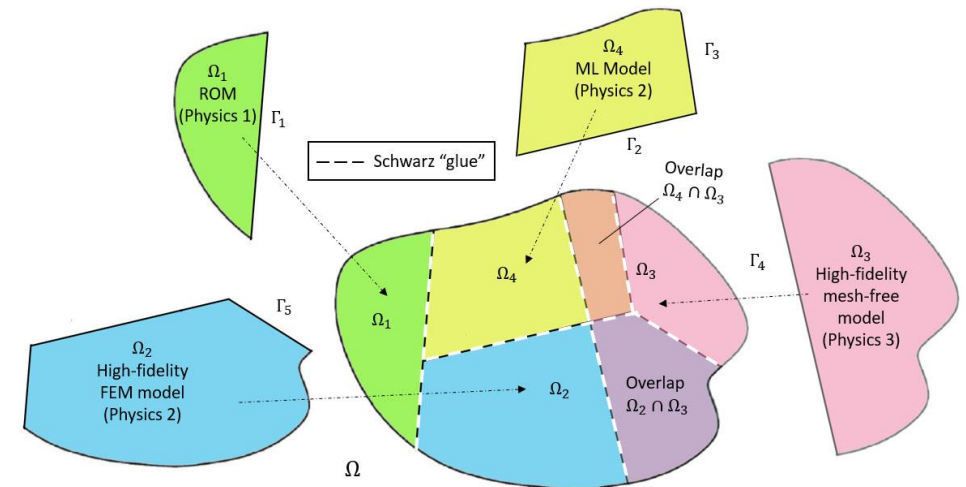
Data-driven models: to be “mixed-and-matched” with each other and first-principles models

- *Class A*: projection-based reduced order models (ROMs)
- *Class B*: machine-learned models, i.e., Physics-Informed Neural Networks (PINNs)
- *Class C*: flow map approximation models, i.e., dynamic model decomposition (DMD) models



Coupling methods:

- *Method 1*: Alternating Schwarz-based coupling
- *Method 2*: Optimization-based coupling
- *Method 3*: Coupling via generalized mortar methods (GMMs)



fHNM (flexible Heterogeneous Numerical Methods) Project:

aims to **discover** the mathematical principles guiding the **assembly** of **standard** and **data-driven numerical models** in stable, accurate and physically consistent ways

Data-driven models: to be “mixed-and-matched” with each other and first-principles models

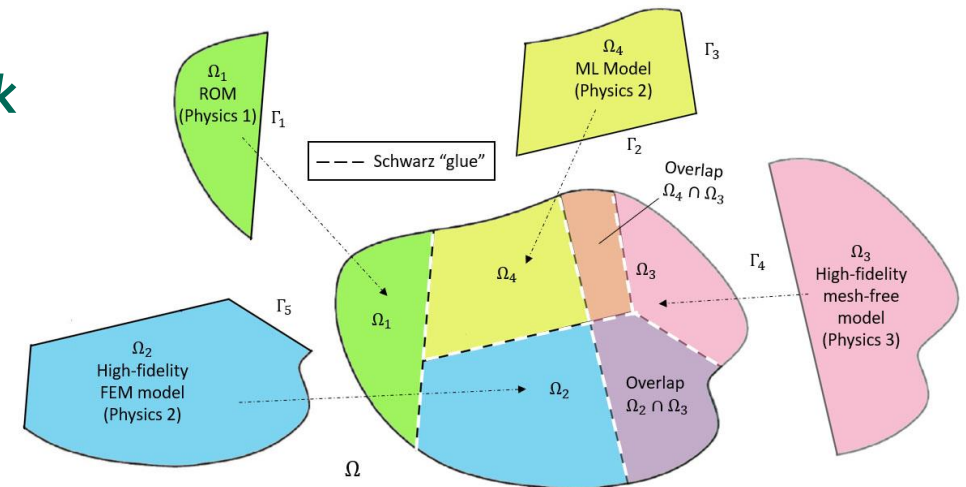
- **Class A:** projection-based reduced order models (ROMs)
- *Class B:* machine-learned models, i.e., Physics-Informed Neural Networks (PINNs)
- *Class C:* flow map approximation models, i.e., dynamic model decomposition (DMD) models



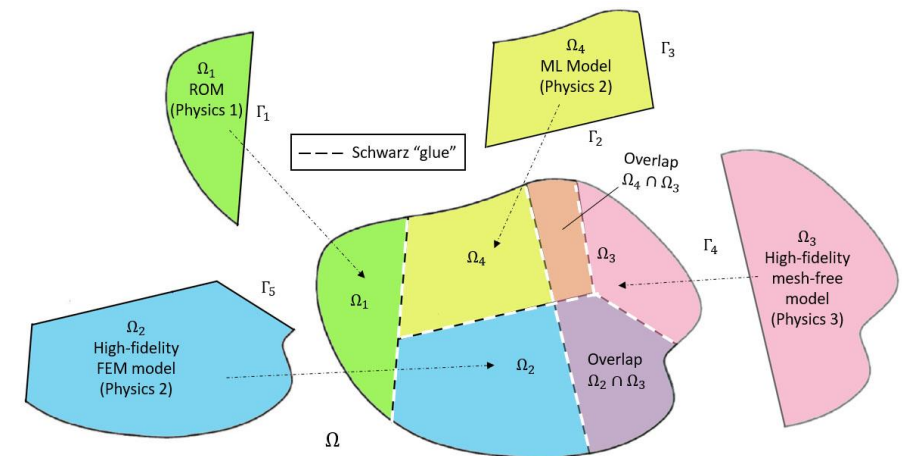
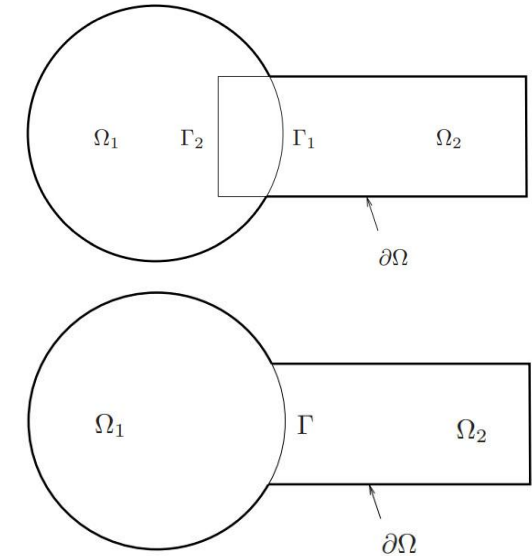
Coupling methods:

- **Method 1:** Alternating Schwarz-based coupling
- *Method 2:* Optimization-based coupling
- *Method 3:* Coupling via generalized mortar methods (GMMs)

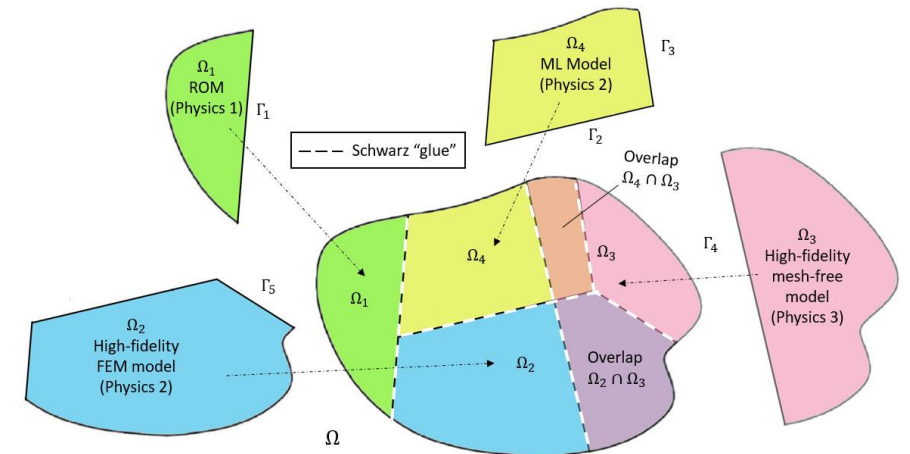
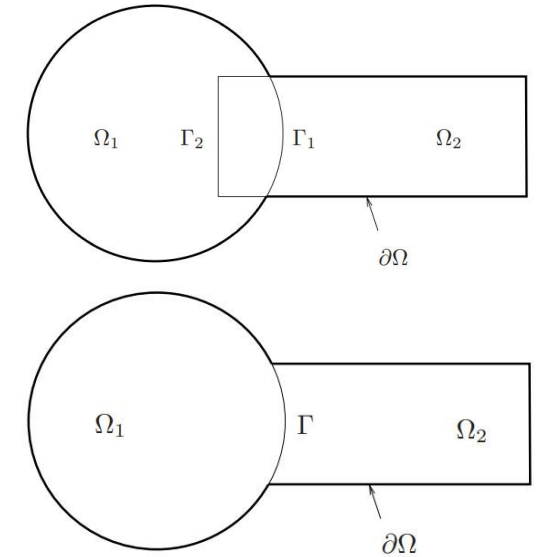
This talk



- The Schwarz Alternating Method for Domain Decomposition-Based Coupling
- Extension to FOM*-ROM[#] and ROM-ROM Coupling
- Numerical Examples
 - 1D Dynamic Wave Propagation in Hyperelastic Bar
 - 2D Burgers Equation
- Summary & Future Work



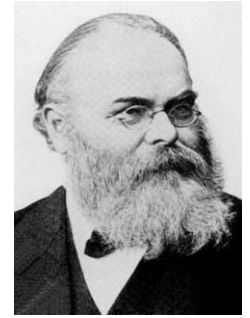
- **The Schwarz Alternating Method for Domain Decomposition-Based Coupling**
- Extension to FOM*-ROM[#] and ROM-ROM Coupling
- Numerical Examples
 - 1D Dynamic Wave Propagation in Hyperelastic Bar
 - 2D Burgers Equation
- Summary & Future Work



9 Schwarz Alternating Method for Domain Decomposition

- Proposed in 1870 by H. Schwarz for solving Laplace PDE on irregular domains.

Crux of Method: if the solution is known in regularly shaped domains, use those as pieces to iteratively build a solution for the more complex domain.



H. Schwarz (1843-1921)

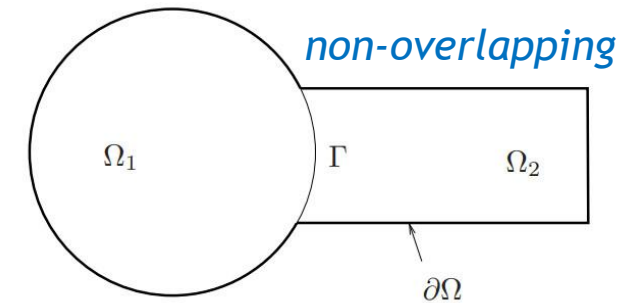
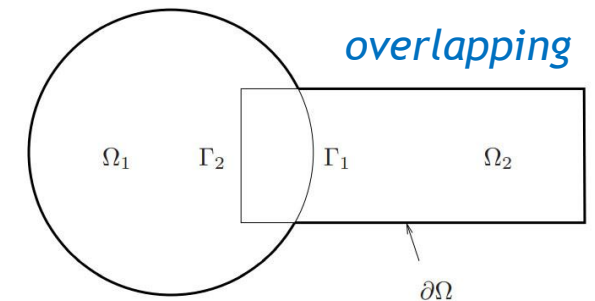
Basic Schwarz Algorithm

Initialize:

- Solve PDE by any method on Ω_1 w/ initial guess for transmission BCs on Γ_1 .

Iterate until convergence:

- Solve PDE by any method on Ω_2 w/ transmission BCs on Γ_2 based on values just obtained for Ω_1 .
- Solve PDE by any method on Ω_1 w/ transmission BCs on Γ_1 based on values just obtained for Ω_2 .



Overlapping Schwarz: convergent with all-Dirichlet transmission BCs¹ if $\Omega_1 \cap \Omega_2 \neq \emptyset$.

Non-overlapping Schwarz: convergent with Robin-Robin² or alternating Neumann-Dirichlet³ transmission BCs.

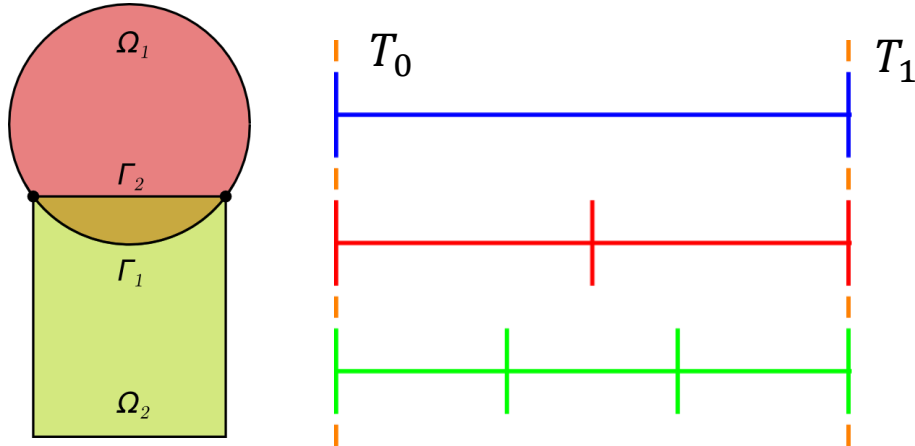
¹Schwarz, 1870; Lions, 1988. ²Lions, 1990. ³Zanolli *et al.*, 1987.



AS A *PRECONDITIONER*
FOR THE LINEARIZED
SYSTEM



AS A *SOLVER* FOR THE
COUPLED
FULLY NONLINEAR
PROBLEM



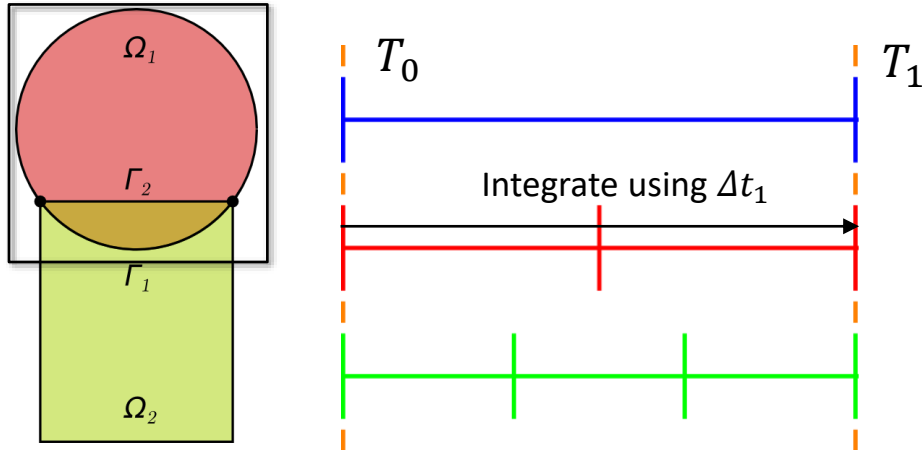
Controller time stepper

Time integrator for Ω_1

Time integrator for Ω_2

Step 0: Initialize $i = 0$ (controller time index).

$$\text{Model PDE: } \begin{cases} \dot{\mathbf{u}} + N(\mathbf{u}) = \mathbf{f}, & \text{in } \Omega \\ \mathbf{u}(\mathbf{x}, t) = \mathbf{g}(t), & \text{on } \partial\Omega \\ \mathbf{u}(\mathbf{x}, 0) = \mathbf{u}_0, & \text{in } \Omega \end{cases}$$



Controller time stepper

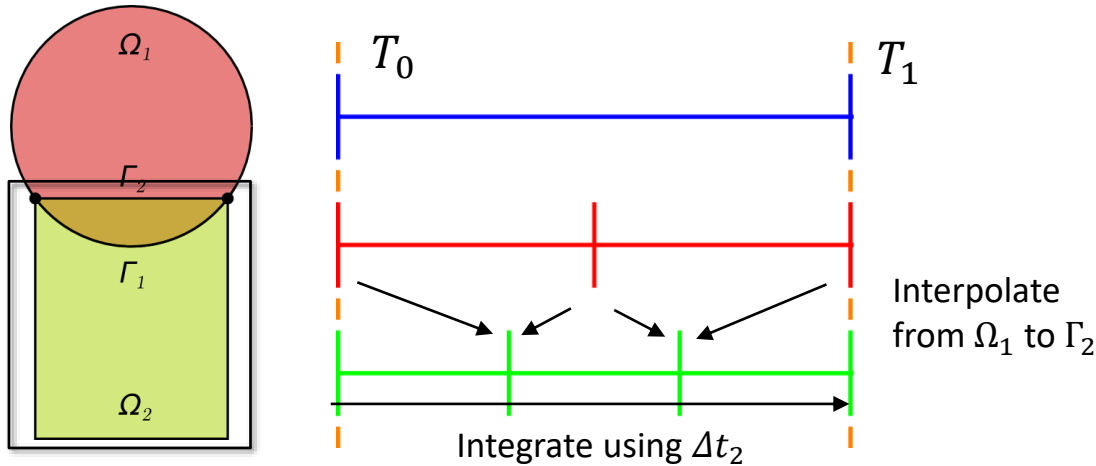
Time integrator for Ω_1

Time integrator for Ω_2

Step 0: Initialize $i = 0$ (controller time index).

Step 1: Advance Ω_1 solution from time T_i to time T_{i+1} using time-stepper in Ω_1 with time-step Δt_1 , using solution in Ω_2 interpolated to Γ_1 at times $T_i + n\Delta t_1$.

$$\text{Model PDE: } \begin{cases} \dot{\mathbf{u}} + N(\mathbf{u}) = \mathbf{f}, & \text{in } \Omega \\ \mathbf{u}(\mathbf{x}, t) = \mathbf{g}(t), & \text{on } \partial\Omega \\ \mathbf{u}(\mathbf{x}, 0) = \mathbf{u}_0, & \text{in } \Omega \end{cases}$$



Controller time stepper

Time integrator for Ω_1

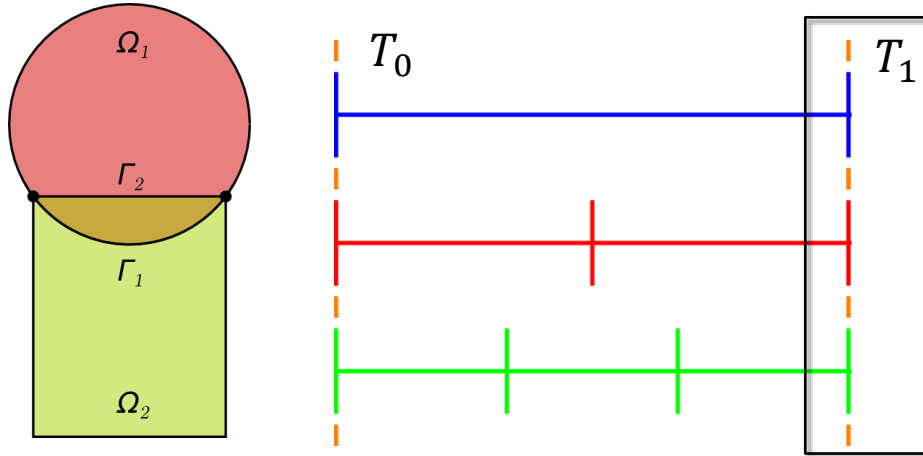
Time integrator for Ω_2

Step 0: Initialize $i = 0$ (controller time index).

Step 1: Advance Ω_1 solution from time T_i to time T_{i+1} using time-stepper in Ω_1 with time-step Δt_1 , using solution in Ω_2 interpolated to Γ_1 at times $T_i + n\Delta t_1$.

Step 2: Advance Ω_2 solution from time T_i to time T_{i+1} using time-stepper in Ω_2 with time-step Δt_2 , using solution in Ω_1 interpolated to Γ_2 at times $T_i + n\Delta t_2$.

$$\text{Model PDE: } \begin{cases} \dot{\mathbf{u}} + N(\mathbf{u}) = \mathbf{f}, & \text{in } \Omega \\ \mathbf{u}(\mathbf{x}, t) = \mathbf{g}(t), & \text{on } \partial\Omega \\ \mathbf{u}(\mathbf{x}, 0) = \mathbf{u}_0, & \text{in } \Omega \end{cases}$$



Controller time stepper

Time integrator for Ω_1

Time integrator for Ω_2

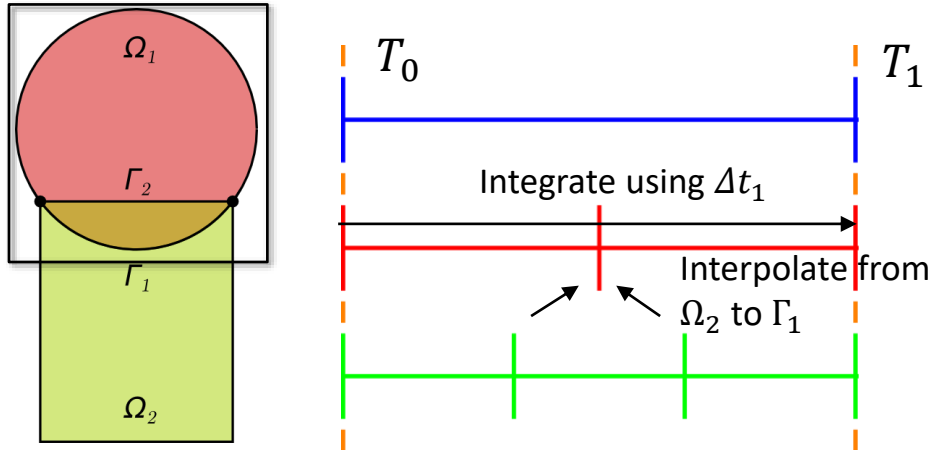
Step 0: Initialize $i = 0$ (controller time index).

Step 1: Advance Ω_1 solution from time T_i to time T_{i+1} using time-stepper in Ω_1 with time-step Δt_1 , using solution in Ω_2 interpolated to Γ_1 at times $T_i + n\Delta t_1$.

Step 2: Advance Ω_2 solution from time T_i to time T_{i+1} using time-stepper in Ω_2 with time-step Δt_2 , using solution in Ω_1 interpolated to Γ_2 at times $T_i + n\Delta t_2$.

Step 3: Check for convergence at time T_{i+1} .

$$\text{Model PDE: } \begin{cases} \dot{\mathbf{u}} + N(\mathbf{u}) = \mathbf{f}, & \text{in } \Omega \\ \mathbf{u}(\mathbf{x}, t) = \mathbf{g}(t), & \text{on } \partial\Omega \\ \mathbf{u}(\mathbf{x}, 0) = \mathbf{u}_0, & \text{in } \Omega \end{cases}$$



Controller time stepper

Time integrator for Ω_1

Time integrator for Ω_2

Step 0: Initialize $i = 0$ (controller time index).

Step 1: Advance Ω_1 solution from time T_i to time T_{i+1} using time-stepper in Ω_1 with time-step Δt_1 , using solution in Ω_2 interpolated to Γ_1 at times $T_i + n\Delta t_1$.

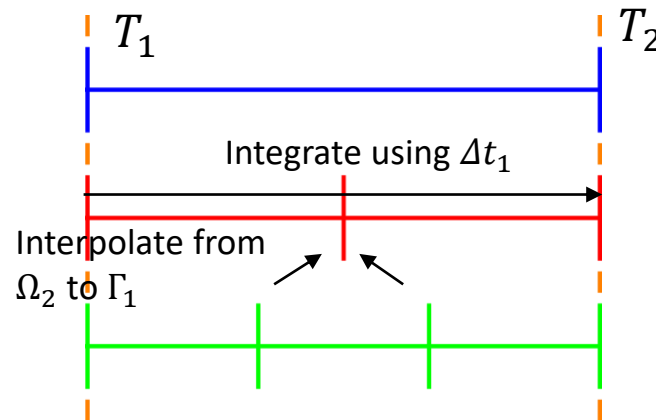
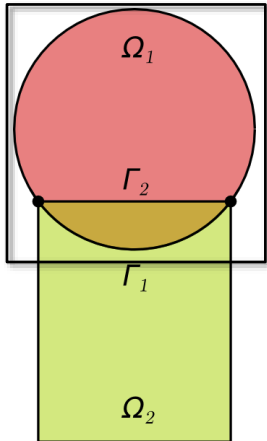
Step 2: Advance Ω_2 solution from time T_i to time T_{i+1} using time-stepper in Ω_2 with time-step Δt_2 , using solution in Ω_1 interpolated to Γ_2 at times $T_i + n\Delta t_2$.

Step 3: Check for convergence at time T_{i+1} .

➤ If unconverged, return to Step 1.

Model PDE:

$$\begin{cases} \dot{\mathbf{u}} + N(\mathbf{u}) = \mathbf{f}, & \text{in } \Omega \\ \mathbf{u}(\mathbf{x}, t) = \mathbf{g}(t), & \text{on } \partial\Omega \\ \mathbf{u}(\mathbf{x}, 0) = \mathbf{u}_0, & \text{in } \Omega \end{cases}$$



Controller time stepper

Time integrator for Ω_1

Time integrator for Ω_2

Can use ***different integrators*** with ***different time steps*** within each domain!

Step 0: Initialize $i = 0$ (controller time index).

Step 1: Advance Ω_1 solution from time T_i to time T_{i+1} using time-stepper in Ω_1 with time-step Δt_1 , using solution in Ω_2 interpolated to Γ_1 at times $T_i + n\Delta t_1$.

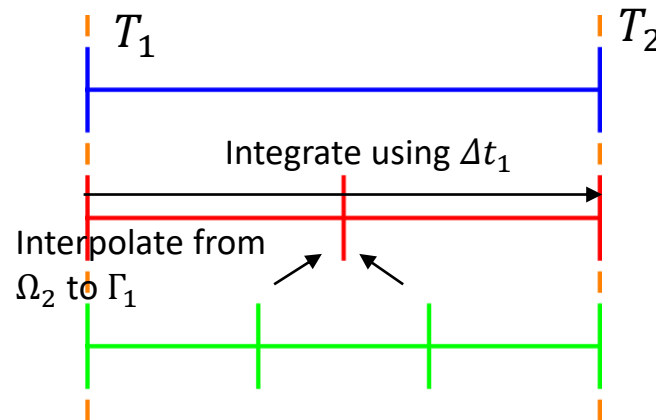
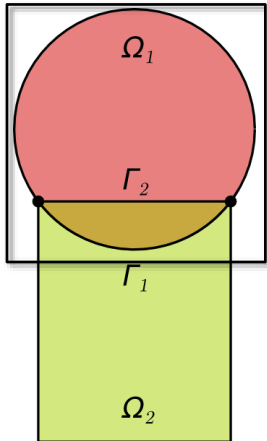
Step 2: Advance Ω_2 solution from time T_i to time T_{i+1} using time-stepper in Ω_2 with time-step Δt_2 , using solution in Ω_1 interpolated to Γ_2 at times $T_i + n\Delta t_2$.

Step 3: Check for convergence at time T_{i+1} .

- If unconverged, return to Step 1.
- If converged, set $i = i + 1$ and return to Step 1.

Model PDE:

$$\begin{cases} \dot{\mathbf{u}} + N(\mathbf{u}) = \mathbf{f}, & \text{in } \Omega \\ \mathbf{u}(x, t) = \mathbf{g}(t), & \text{on } \partial\Omega \\ \mathbf{u}(x, 0) = \mathbf{u}_0, & \text{in } \Omega \end{cases}$$



Controller time stepper

Time integrator for Ω_1

Time integrator for Ω_2

Time-stepping procedure is **equivalent** to doing Schwarz on **space-time domain** [Mota *et al.* 2022].

Step 0: Initialize $i = 0$ (controller time index).

Step 1: Advance Ω_1 solution from time T_i to time T_{i+1} using time-stepper in Ω_1 with time-step Δt_1 , using solution in Ω_2 interpolated to Γ_1 at times $T_i + n\Delta t_1$.

Step 2: Advance Ω_2 solution from time T_i to time T_{i+1} using time-stepper in Ω_2 with time-step Δt_2 , using solution in Ω_1 interpolated to Γ_2 at times $T_i + n\Delta t_2$.

Step 3: Check for convergence at time T_{i+1} .

- If unconverged, return to Step 1.
- If converged, set $i = i + 1$ and return to Step 1.

Model PDE:

$$\begin{cases} \dot{\mathbf{u}} + N(\mathbf{u}) = \mathbf{f}, & \text{in } \Omega \\ \mathbf{u}(x, t) = \mathbf{g}(t), & \text{on } \partial\Omega \\ \mathbf{u}(x, 0) = \mathbf{u}_0, & \text{in } \Omega \end{cases}$$

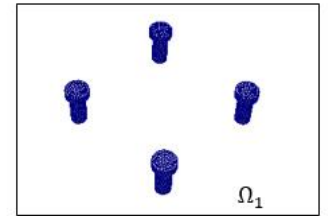
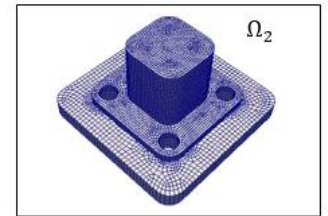
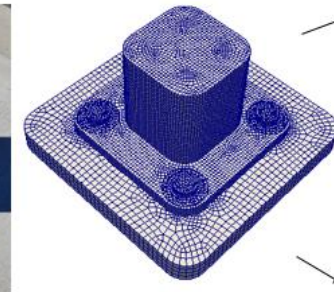


Model Solid Mechanics PDEs:

$$\text{Quasistatic: } \operatorname{Div} \mathbf{P} + \rho_0 \mathbf{B} = \mathbf{0} \quad \text{in } \Omega$$

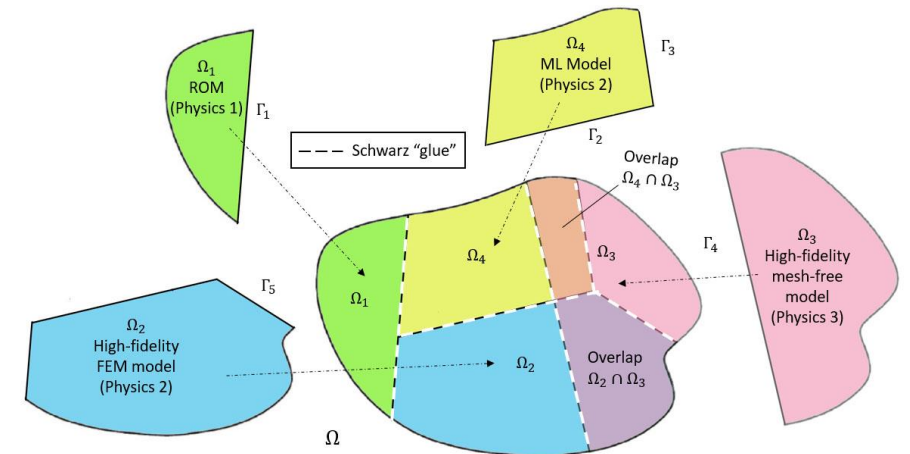
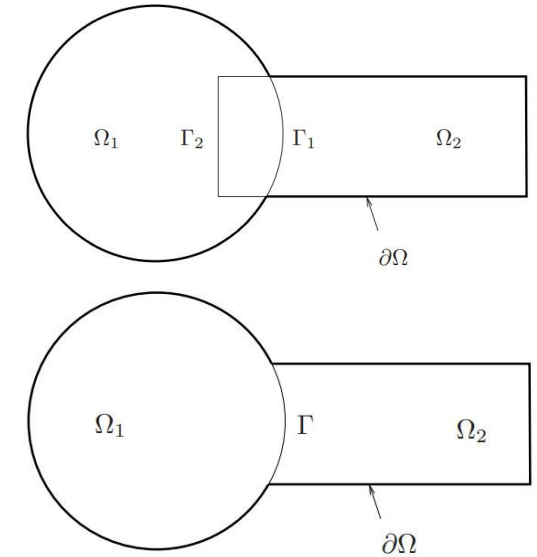
$$\text{Dynamic: } \operatorname{Div} \mathbf{P} + \rho_0 \mathbf{B} = \rho_0 \ddot{\boldsymbol{\varphi}} \quad \text{in } \Omega \times I$$

- Coupling is *concurrent* (two-way).
- *Ease of implementation* into existing massively-parallel HPC codes.
- *Scalable, fast, robust* (we target *real* engineering problems, e.g., analyses involving failure of bolted components!).
- Coupling does not introduce *nonphysical artifacts*.
- *Theoretical* convergence properties/guarantees¹.
- “*Plug-and-play*” framework:
 - Ability to couple regions with *different non-conformal meshes*, *different element types* and *different levels of refinement* to simplify task of *meshing complex geometries*.
 - Ability to use *different solvers/time-integrators* in different regions.



¹ Mota et al. 2017; Mota et al. 2022. ² <https://github.com/sandialabs/LCM>.

- The Schwarz Alternating Method for Domain Decomposition-Based Coupling
- **Extension to FOM*-ROM[#] and ROM-ROM Coupling**
- Numerical Examples
 - 1D Dynamic Wave Propagation in Hyperelastic Bar
 - 2D Burgers Equation
- Summary & Future Work

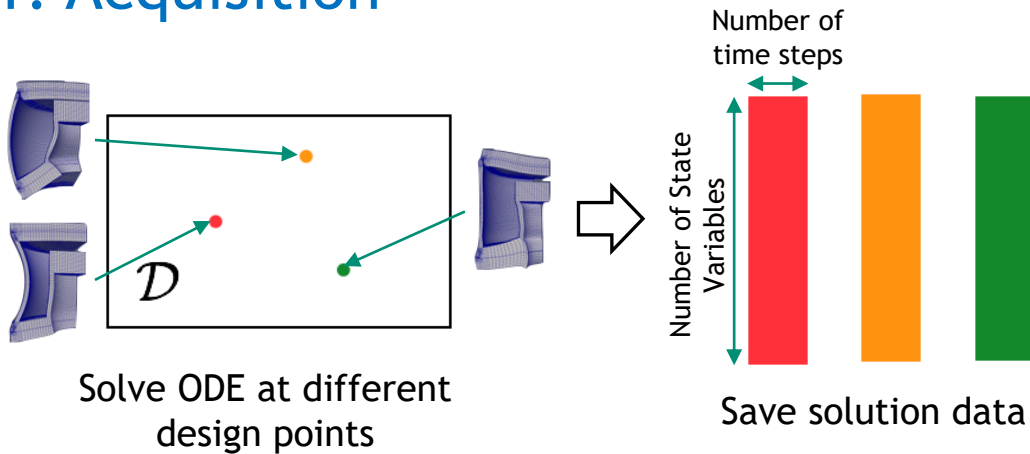


Projection-Based Model Order Reduction via the POD/Galerkin Method



$$\text{Full Order Model (FOM): } \mathbf{M} \frac{d^2 \mathbf{u}}{dt^2} + \mathbf{f}_{\text{int}}(\mathbf{u}) = \mathbf{f}_{\text{ext}}$$

1. Acquisition



2. Learning

Proper Orthogonal Decomposition (POD):

$$\mathbf{X} = \begin{bmatrix} \text{red} & \text{orange} & \text{green} \end{bmatrix} = \begin{bmatrix} \text{brown} & \text{blue} \end{bmatrix} \begin{bmatrix} \text{blue} \end{bmatrix} \begin{bmatrix} \text{blue} \end{bmatrix}^T$$

Σ

ROM = projection-based Reduced Order Model

3. Projection-Based Reduction

Reduce the number of unknowns

$$\mathbf{u}(t) \approx \tilde{\mathbf{u}}(t) = \Phi \hat{\mathbf{u}}(t)$$

Perform Galerkin projection

$$\Phi^T \mathbf{M} \Phi \frac{d^2 \hat{\mathbf{u}}}{dt^2} + \Phi^T \mathbf{f}_{\text{int}}(\Phi \hat{\mathbf{u}}) = \Phi^T \mathbf{f}_{\text{ext}}$$

Hyper-reduce nonlinear terms

$$\mathbf{f}_{\text{int}}(\Phi \hat{\mathbf{u}}) \approx \mathbf{A} \mathbf{f}_{\text{int}}(\Phi \hat{\mathbf{u}})$$



$$\begin{bmatrix} \text{purple} & \text{purple} & \text{purple} & \text{purple} \end{bmatrix} \left(\begin{bmatrix} \text{brown} & \text{grey} & \text{black} \end{bmatrix} \right)$$

HROM = Hyper-reduced ROM

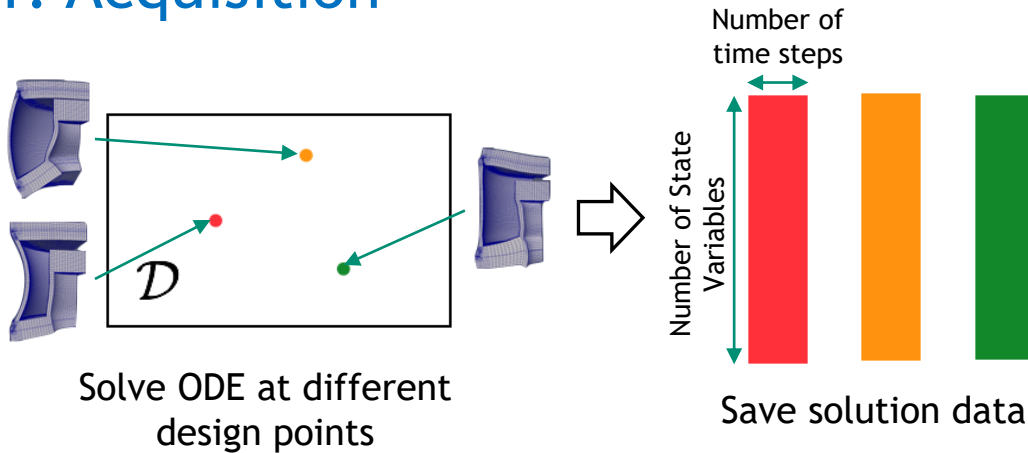
Projection-Based Model Order Reduction via the POD/LSPG* Method



Full Order Model (FOM): $\frac{du}{dt} = f(u; t, \mu)$

* Least-Squares Petrov-Galerkin

1. Acquisition



2. Learning

Proper Orthogonal Decomposition (POD):

$$\mathbf{X} = \mathbf{\Phi} \mathbf{U} \mathbf{\Sigma} \mathbf{V}^T$$

ROM = projection-based Reduced Order Model

3. Projection-Based Reduction

Choose ODE temporal discretization

$$\frac{du}{dt} = f(u; t, \mu) \Downarrow r^n(u^n; \mu) = 0, \quad n = 1, \dots, T$$

Reduce the number of unknowns

$$u(t) \approx \tilde{u}(t) = \Phi \hat{u}(t)$$

Minimize residual

$$\min_{\hat{v}} \left\| \mathbf{A} \hat{v} - \mathbf{r}^n(\Phi \hat{v}; \mu) \right\|_2$$



HROM = Hyper-reduced ROM



Enforcement of Dirichlet boundary conditions (DBC) in ROM at indices i_{Dir}

- Method I in [Gunzburger *et al.* 2007] is employed

$$\mathbf{u}(t) \approx \bar{\mathbf{u}} + \Phi \hat{\mathbf{u}}(t), \quad \mathbf{v}(t) \approx \bar{\mathbf{v}} + \Phi \hat{\mathbf{v}}(t), \quad \mathbf{a}(t) \approx \bar{\mathbf{a}} + \Phi \hat{\mathbf{a}}(t)$$

- POD modes made to satisfy homogeneous DBCs: $\Phi(i_{\text{Dir}}, :) = \mathbf{0}$
- BCs imposed by modifying $\bar{\mathbf{u}}, \bar{\mathbf{v}}, \bar{\mathbf{a}}$: $\bar{\mathbf{u}}(i_{\text{Dir}}) \leftarrow \chi_u, \bar{\mathbf{v}}(i_{\text{Dir}}) \leftarrow \chi_v, \bar{\mathbf{a}}(i_{\text{Dir}}) \leftarrow \chi_a$

Hyper-reduction considerations

- Boundary points must be included in sample mesh for DBC enforcement
- We employ the Energy-Conserving Sampling & Weighting Method (ECSW) [Farhat *et al.* 2015] → preserves Hamiltonian structure for solid mechanics problems

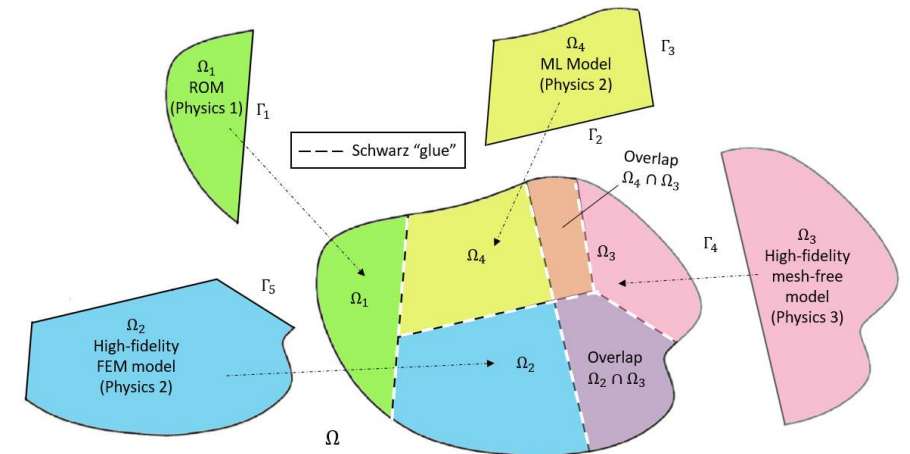
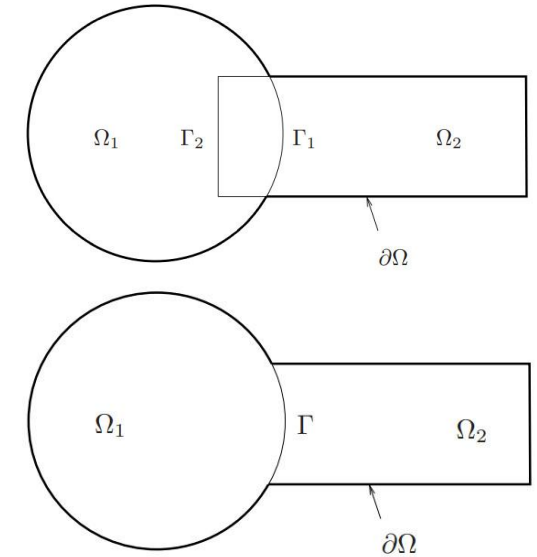
Choice of domain decomposition

- Error-based indicators that help decide in what region of the domain a ROM can be viable should drive domain decomposition [Bergmann *et al.* 2018] (future work)

Snapshot collection and reduced basis construction

- POD results presented herein use snapshots obtained via FOM-FOM coupling on $\Omega = \bigcup_i \Omega_i$
- Future work: generate snapshots/bases separately in each Ω_i [Hoang *et al.* 2021, Smetana *et al.* 2022]

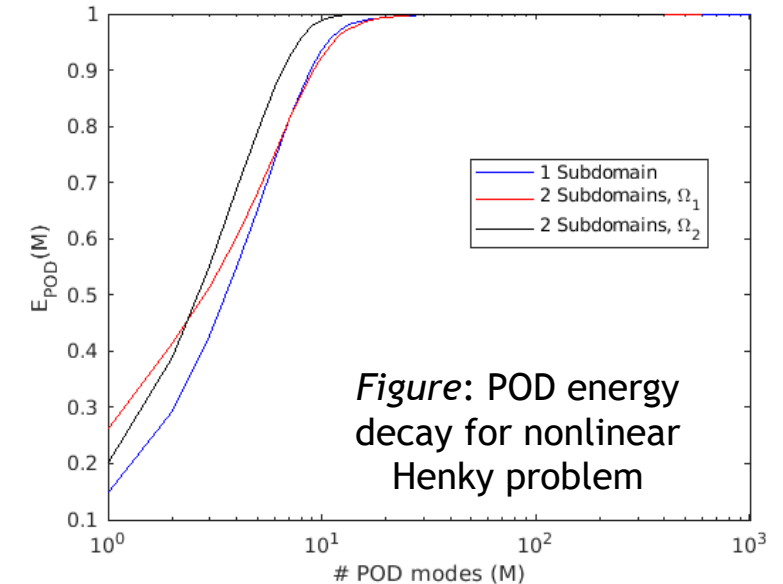
- The Schwarz Alternating Method for Domain Decomposition-Based Coupling
- Extension to FOM*-ROM[#] and ROM-ROM Coupling
- Numerical Examples
 - 1D Dynamic Wave Propagation in Hyperelastic Bar
 - 2D Burgers Equation
- Summary & Future Work



Numerical Example: 1D Dynamic Wave Propagation Problem



- **1D beam** geometry $\Omega = (0,1)$, clamped at both ends, with prescribed initial condition discretized using FEM + Newmark- β
- Simple problem but very **stringent test** for discretization/coupling methods, and **difficult problem for ROMs**.
- Two **constitutive models** considered:
 - Linear elastic (problem has exact analytical solution)
 - Nonlinear hyperelastic Henky **This talk**
- ROMs results are **reproductive** and **predictive**, and are based on the **POD/Galerkin** method, with POD calculated from FOM-FOM coupled model.
 - 50 POD modes capture $\sim 100\%$ snapshot energy for linear variant of this problem.
 - 536 POD modes capture $\sim 100\%$ snapshot energy for Henky variant of this problem.
- Hyper-reduced ROMs (HROMs) perform **hyper-reduction** using ECSW [Farhat *et al.*, 2015]
 - Ensures that **Lagrangian structure** of problem is preserved in HROM.
- **Couplings tested**: overlapping, non-overlapping, FOM-FOM, FOM-ROM, ROM-ROM, FOM-HROM, HROM-HROM, implicit-explicit, implicit-implicit, explicit-explicit. **This talk**



Numerical Example: 1D Dynamic Wave Propagation Problem



- **Two variants** of problem, with different initial conditions (ICs):
 - Symmetric Gaussian IC (top right)
 - Rounded Square IC (bottom right)
- **Non-overlapping domain decomposition (DD)** of $\Omega = \Omega_1 \cup \Omega_2$, where $\Omega_1 = [0, 0.6]$ and $\Omega_2 = [0.6, 1.0]$
 - DD is based on heuristics: during time-interval considered ($0 \leq t \leq 1 \times 10^3$), sharper gradient forms in Ω_1 , suggesting FOM or larger ROM is needed there.
- **Reproductive problem:**
 - Displacement snapshots collected using FOM-FOM non-overlapping coupling with **Symmetric Gaussian IC**
 - FOM-ROM, FOM-HROM, ROM-ROM and HROM-HROM run with **Symmetric Gaussian IC**
- **Predictive problem:**
 - Displacement snapshots collected using FOM-FOM non-overlapping coupling with **Symmetric Gaussian IC**
 - FOM-ROM, FOM-HROM, ROM-ROM and HROM-HROM run with **Rounded Square IC**

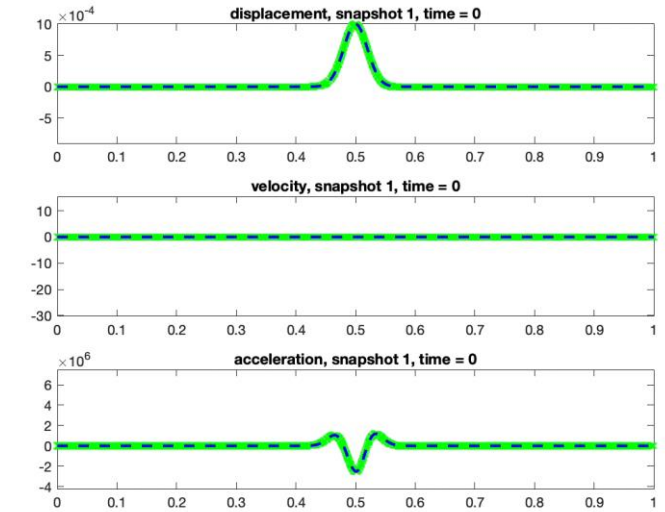
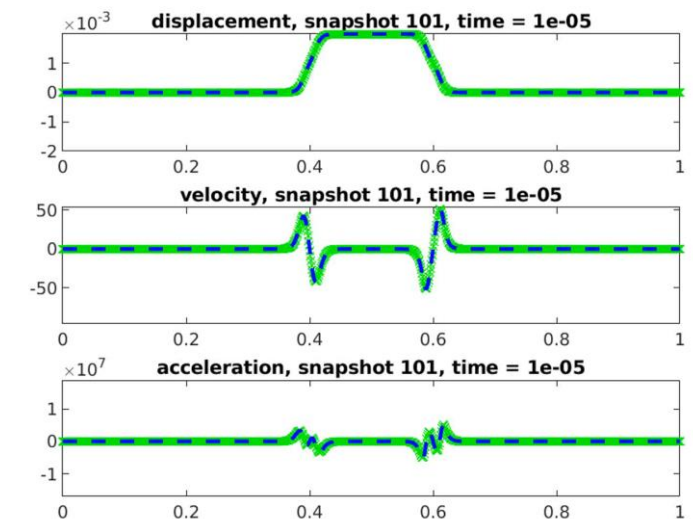
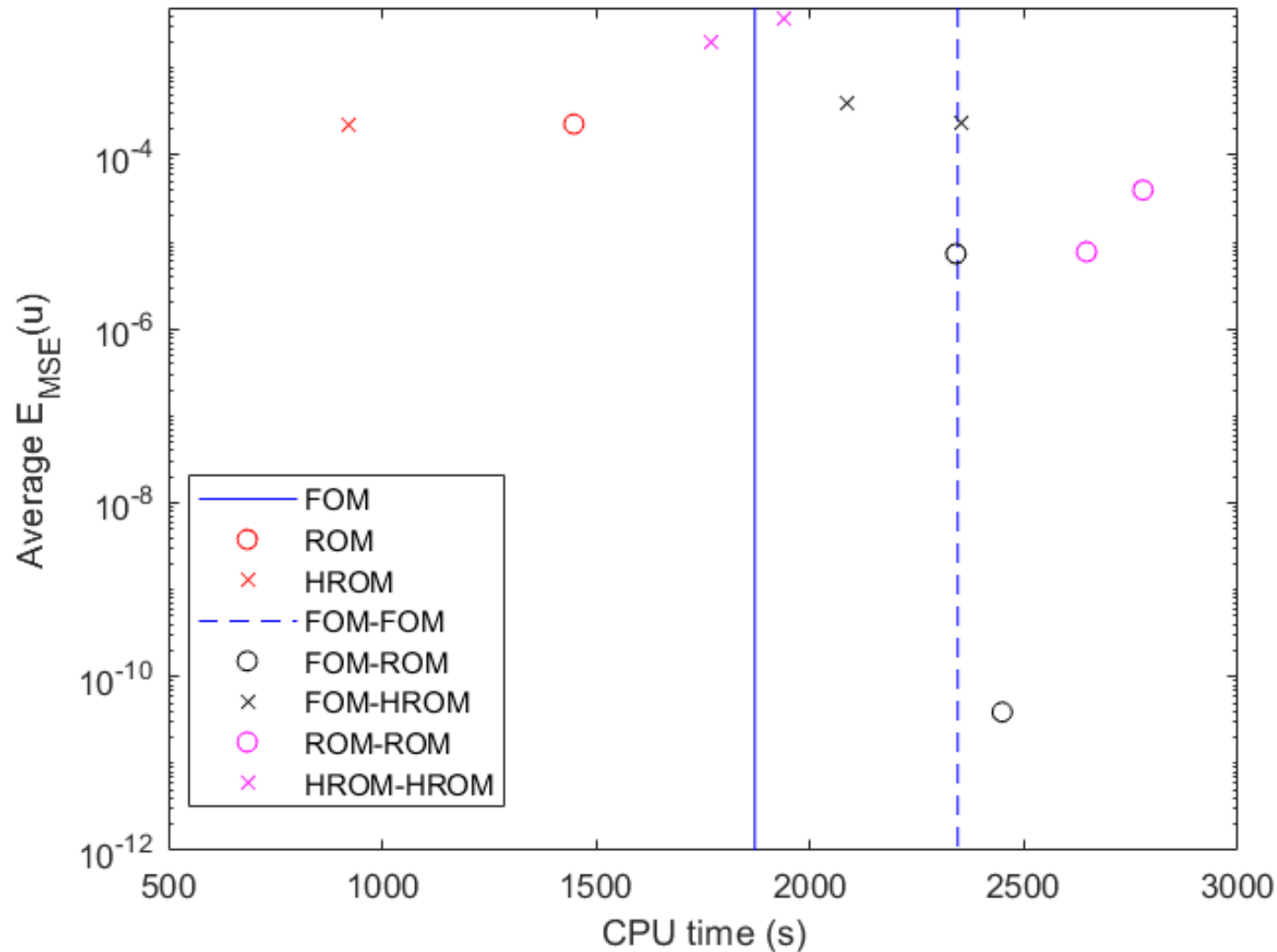


Figure above: Symmetric Gaussian IC problem solution
Figure below: Rounded Square IC problem solution



Numerical Example: Reproductive Problem Results



- **Single-domain ROM and HROM are most efficient**
- Couplings involving ROMs and HROMs enable one to achieve **smaller errors**
- Benefits of **hyper-reduction** are **limited on 1D problem**
- **FOM-HROM and HROM-HROM couplings outperform the FOM-FOM coupling** in terms of CPU time by 12.5-32.6%

Numerical Example: Reproductive Problem Results

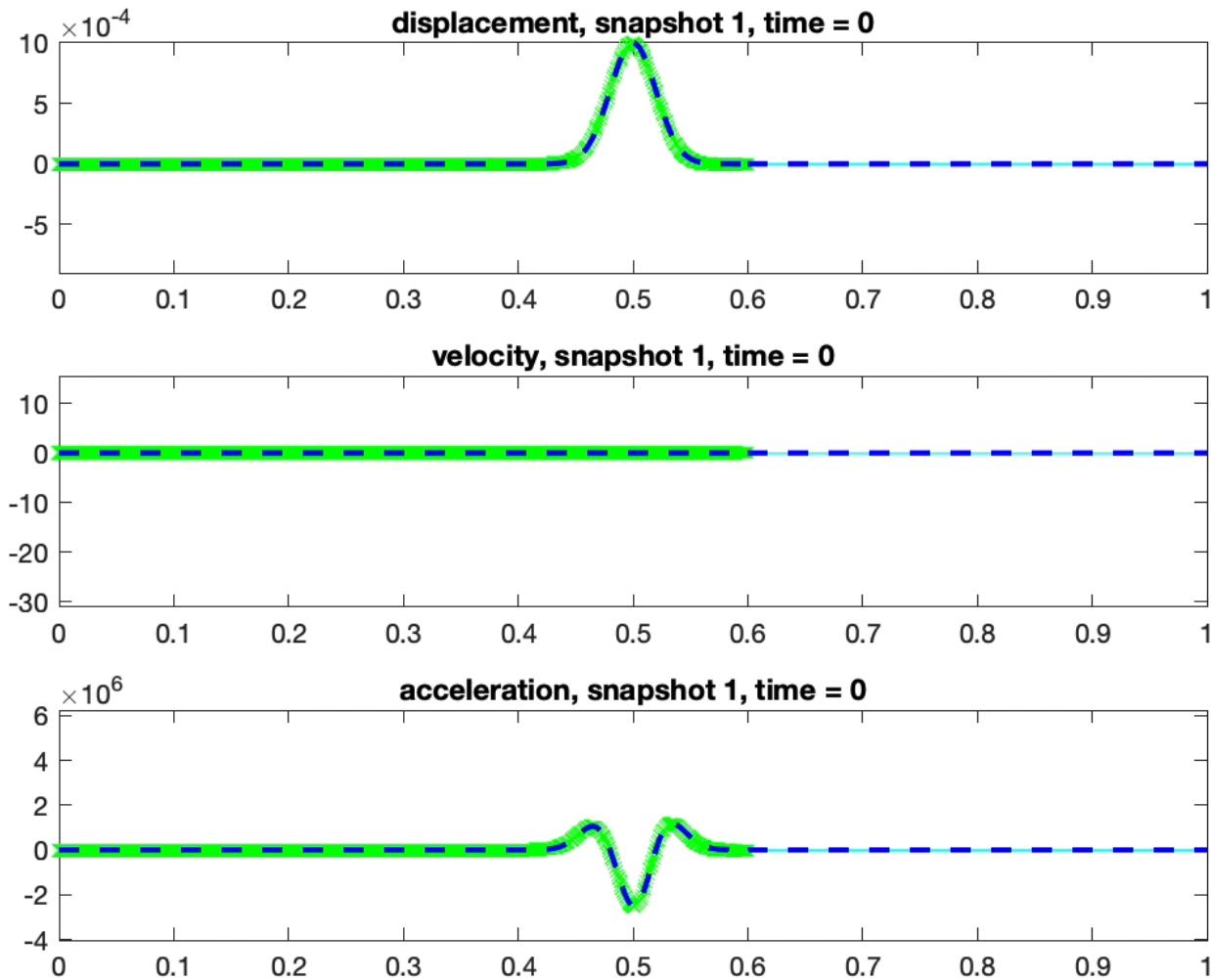
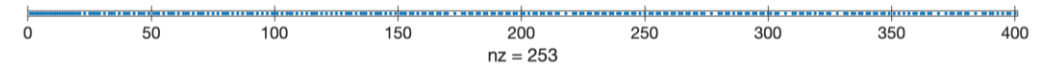


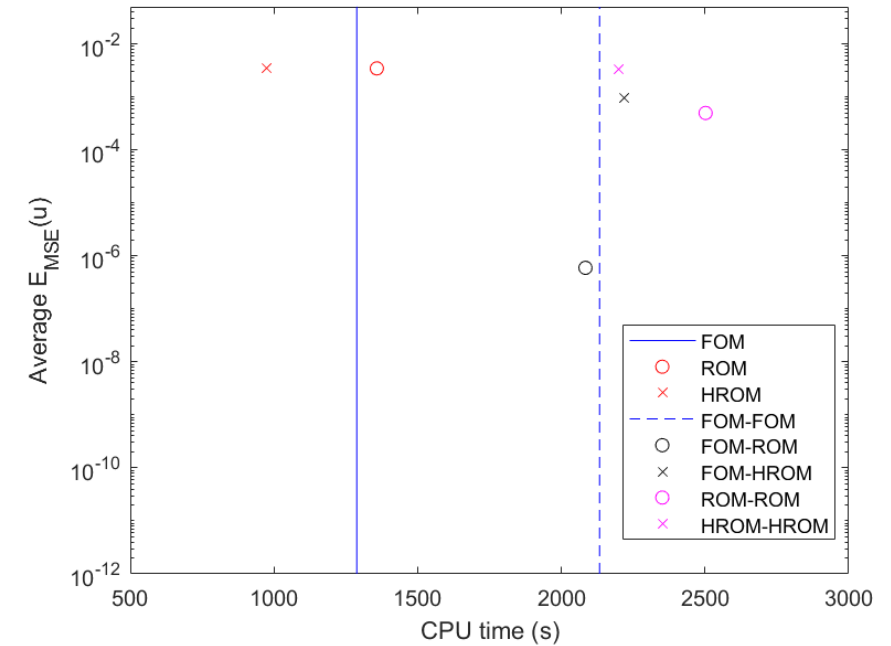
Figure left: FOM (green) - HROM (cyan) coupling compared with single-domain FOM solution (blue). HROM has 200 modes.

Figure below: ECSW algorithm samples 253/400 elements



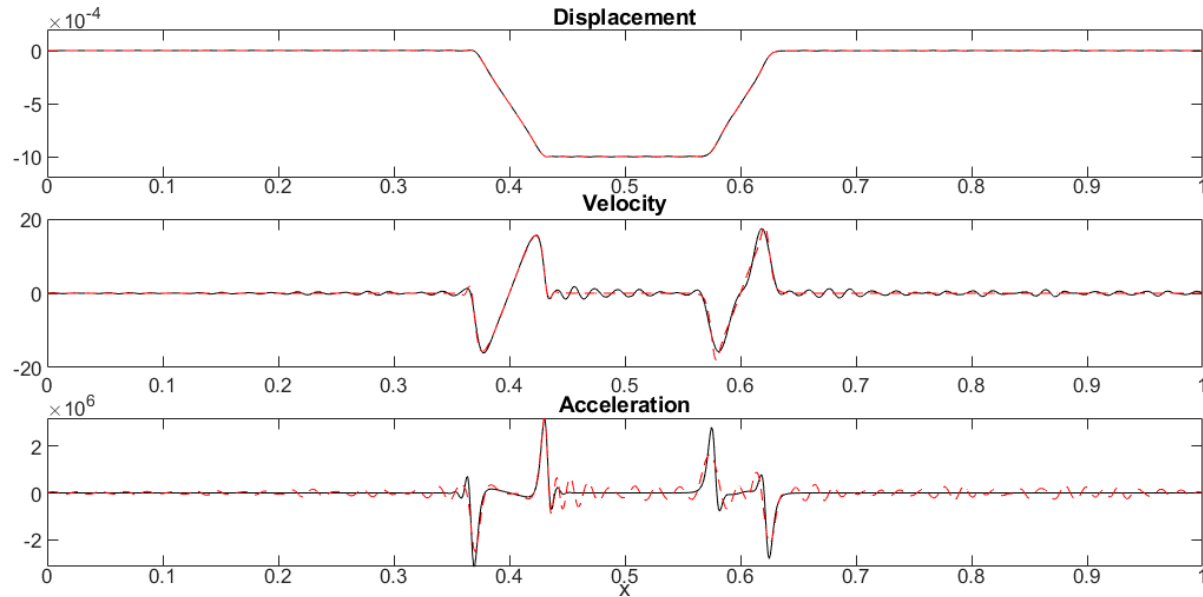
Numerical Example: Predictive Problem Results

Model	CPU time (s)	$N_{e,1}/N_{e,2}$	$\mathcal{E}_{\text{MSE}}(\tilde{\mathbf{u}}_1)/\mathcal{E}_{\text{MSE}}(\tilde{\mathbf{u}}_2)$	$\mathcal{E}_{\text{MSE}}(\tilde{\mathbf{v}}_1)/\mathcal{E}_{\text{MSE}}(\tilde{\mathbf{v}}_2)$	$\mathcal{E}_{\text{MSE}}(\tilde{\mathbf{a}}_1)/\mathcal{E}_{\text{MSE}}(\tilde{\mathbf{a}}_2)$	N_S
FOM	1.288×10^3	—/—	—/—	—/—	—/—	—
ROM	1.358×10^3	—/—	$3.451 \times 10^{-3}/-$	$6.750 \times 10^{-2}/-$	$3.021 \times 10^{-1}/-$	—
HROM	9.759×10^2	614/—	$3.463 \times 10^{-3}/-$	$6.750 \times 10^{-2}/-$	$3.021 \times 10^{-1}/-$	—
FOM-FOM	2.133×10^3	—/—	—/—	—/—	—/—	23,280
FOM-ROM	2.084×10^3	—/—	$1.907 \times 10^{-8}/1.170 \times 10^{-6}$	$1.461 \times 10^{-6}/9.882 \times 10^{-5}$	$3.973 \times 10^{-5}/1.757 \times 10^{-3}$	23,288
FOM-HROM	2.219×10^3	—/253	$1.967 \times 10^{-4}/1.720 \times 10^{-3}$	$4.986 \times 10^{-3}/4.185 \times 10^{-2}$	$2.768 \times 10^{-2}/2.388 \times 10^{-1}$	29,700
ROM-ROM	2.502×10^3	—/—	$5.592 \times 10^{-4}/4.346 \times 10^{-4}$	$1.575 \times 10^{-2}/1.001 \times 10^{-2}$	$9.197 \times 10^{-2}/5.304 \times 10^{-2}$	26,220
HROM-HROM	2.200×10^3	405/253	$4.802 \times 10^{-3}/1.960 \times 10^{-3}$	$8.500 \times 10^{-2}/4.630 \times 10^{-2}$	$3.744 \times 10^{-1}/2.580 \times 10^{-1}$	30,067

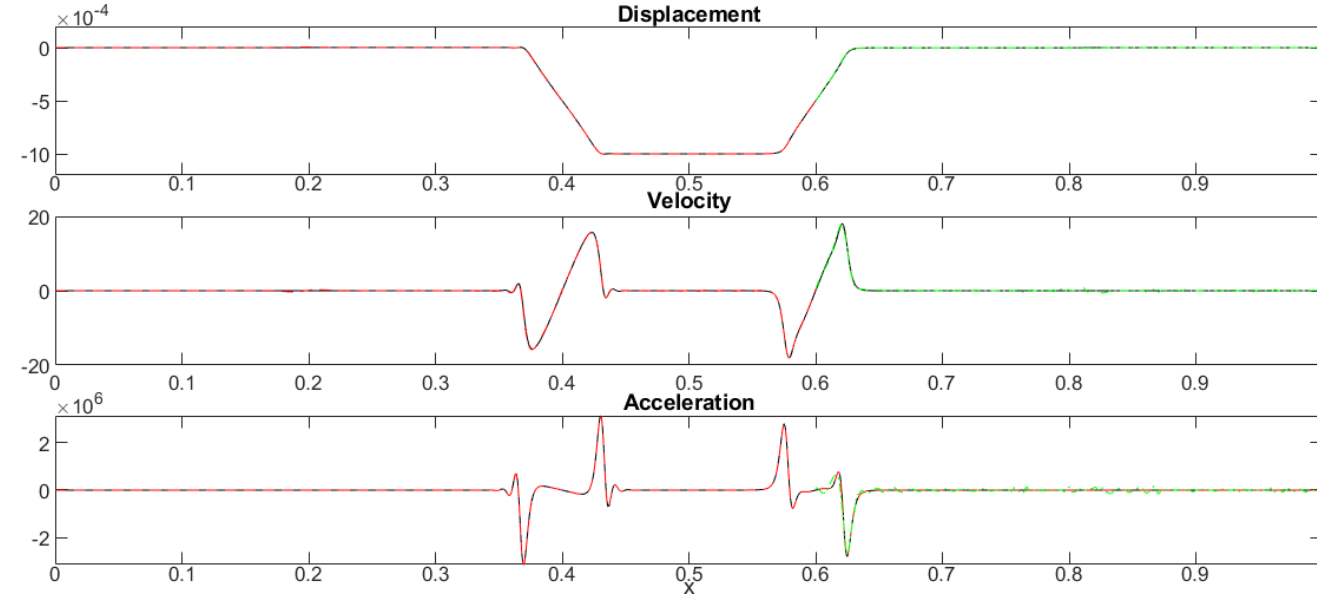


- Results indicate that **predictive accuracy/robustness** can be improved by coupling ROM or HROM to FOM
 - FOM-ROM coupling is **remarkably accurate**, achieving displacement error $O(1 \times 10^{-8})$
 - FOM-HROM and ROM-ROM couplings are **more accurate** than single-domain ROMs
 - HROM-HROM **on par** with single-domain HROM in terms of accuracy
- Wall-clock times** of coupled models can be improved
 - FOM-HROM, ROM-ROM and HROM-HROM models are **slower** than FOM-FOM model as **more Schwarz iterations** required to achieve convergence
 - **Hyper-reduction** samples $\sim 60\%$ of total mesh points for this 1D traveling wave problem
 - ❖ Greater gains from hyper-reduction anticipated for 2D/3D problems

Numerical Example: Predictive Problem Results



Predictive single-domain ROM ($M_1 = 300$)
solution at final time



Predictive FOM-HROM ($M_2 = 200$)
solution at final time

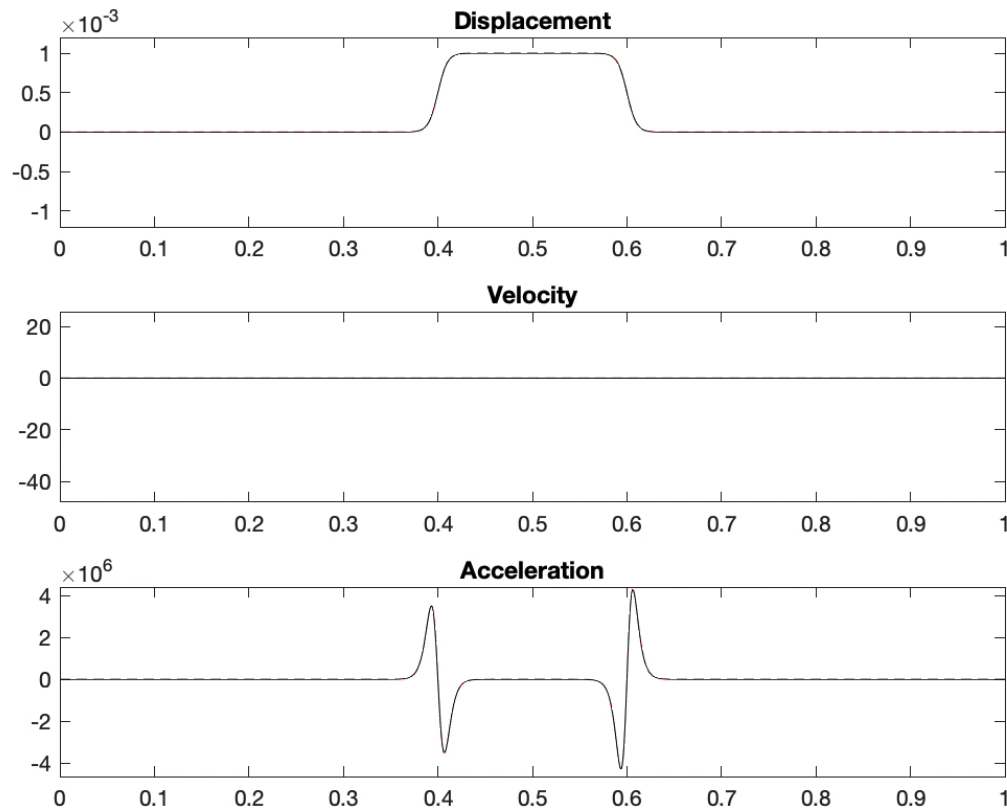
— Single-domain FOM solution

— Solution in Ω_1

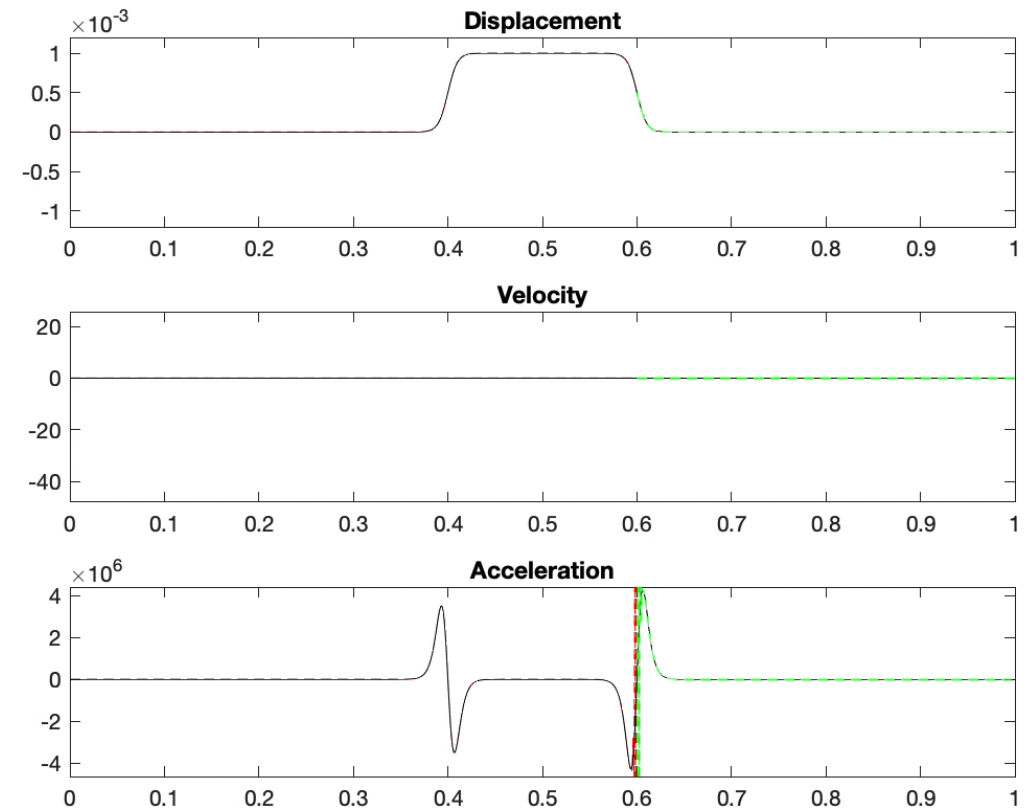
— Solution in Ω_2

- Predictive **single-domain ROM** solution exhibits **spurious oscillations** in velocity and acceleration
- Predictive **FOM-HROM** solution is **smooth** and **oscillation-free**
 - Highlights coupling method's ability to improve ROM predictive accuracy

Numerical Example: Predictive Problem Results



Predictive single-domain ROM ($M_1 = 300$)



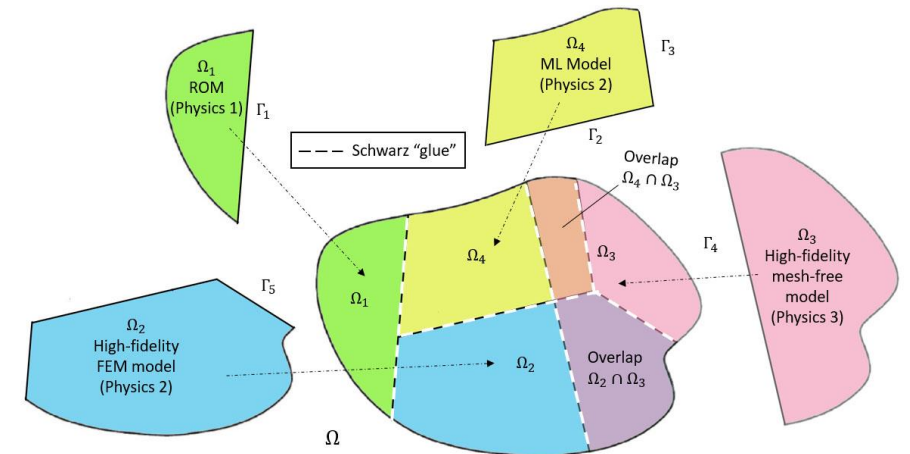
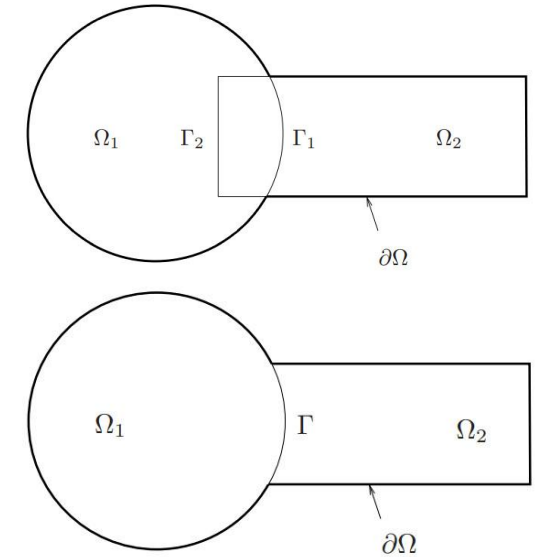
Predictive FOM-HROM ($M_2 = 200$)

— Single-domain FOM solution

— Solution in Ω_1

— Solution in Ω_2

- The Schwarz Alternating Method for Domain Decomposition-Based Coupling
- Extension to FOM*-ROM[#] and ROM-ROM Coupling
- Numerical Examples
 - 1D Dynamic Wave Propagation in Hyperelastic Bar
 - 2D Burgers Equation
- Summary & Future Work



Numerical Example: 2D Inviscid Burgers Problem



$$\frac{\partial u}{\partial t} + \frac{1}{2} \left(\frac{\partial u^2}{\partial x} + \frac{\partial uv}{\partial y} \right) = 0.02 \exp(\mu_2 x)$$

$$\frac{\partial v}{\partial t} + \frac{1}{2} \left(\frac{\partial vu}{\partial x} + \frac{\partial v^2}{\partial y} \right) = 0$$

$$u(x=0, y, t; \mu) = \mu_1$$

$$u(x, y, t=0) = v(x, y, t=0) = 1$$

$$x, y \in [0, 100], t \in [0, T_f]$$

FOM discretization:

- Spatial discretization given by a **Godunov-type scheme** with $N = 250$ elements in each dimension
- Implicit temporal discretization: **trapezoidal method** with fixed $\Delta t = 0.05$; Choose $T_f = 25.0$

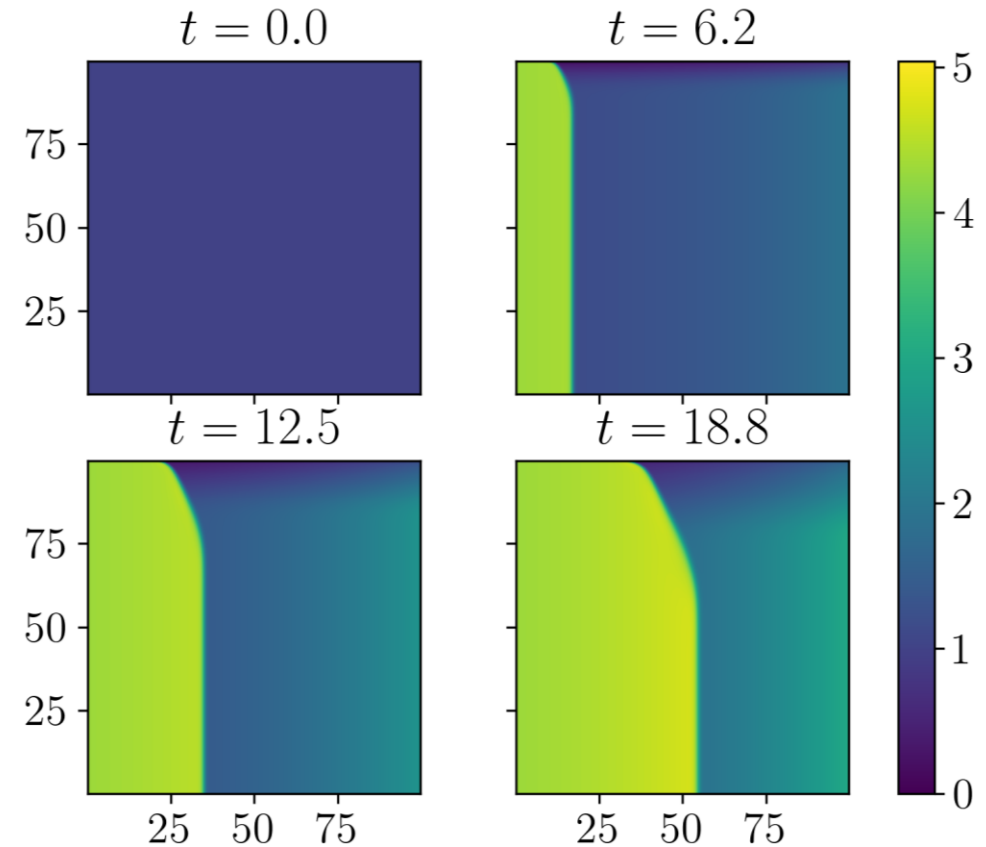
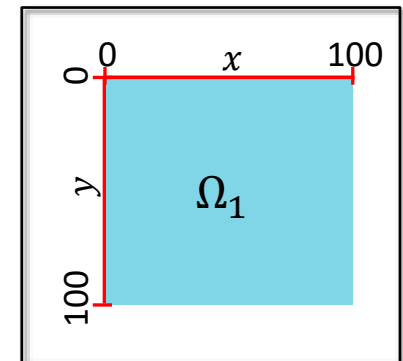


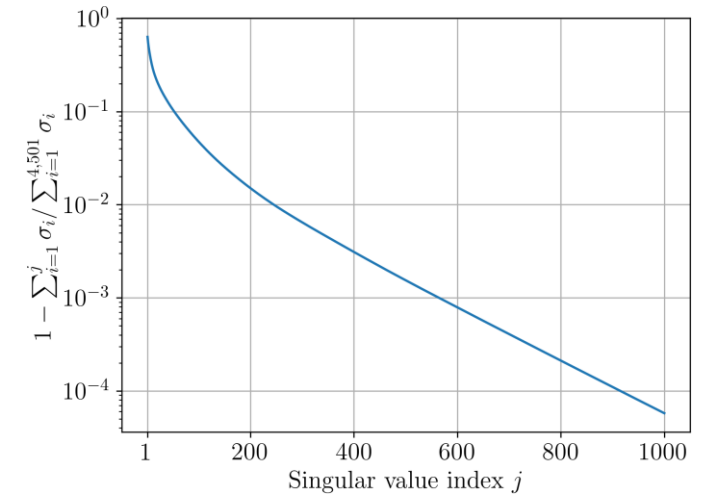
Figure above: solution of u component at various times



Numerical Example: 2D Inviscid Burgers Problem



- **2D** makes for a more appropriate testing of potential speedups from coupling subdomains to ROMs
- The **inviscid Burgers' equation** is a popular analog for fluid problems where shocks are possible, and is particularly difficult for conventional projection-based ROMs
- Two **parameters** considered:
 - Dirichlet BC parameterization μ_1
 - Source term parameterization μ_2
- ROMs results are **predictive and** are based on the **Least-Squares Petrov-Galerkin (LSPG)** method, with POD calculated from FOM coupling models.
 - Greater than 200 POD modes required to capture 99% snapshot energy for when sampling 9 $\mu = [\mu_1, \mu_2]$ values
- Hyper-reduced ROMs (HROMs) perform **hyper-reduction** using ECSW [Farhat *et al.*, 2015]
- **Couplings tested:** overlapping, FOM-FOM, FOM-ROM, ROM-ROM, FOM-HROM, HROM-HROM, implicit-explicit, implicit-implicit, explicit-explicit.



This talk

Single Domain ROM

- **Spatial/temporal resolution:** $\Delta x_i = 0.4$, $\Delta y_i = 0.4$, $\Delta t_i = 0.05$
- **Uniform sampling** of $\mathcal{D} = [4.25, 5.50] \times [0.015, 0.03]$ by a 3×3 grid \Rightarrow 9 training parameter points characterized by $\Delta \mu_1 = 0.625$ and $\Delta \mu_2 = 0.0075$
- Queried but **unsampled parameter point** $\mu = [4.75, 0.02]$ with reduced dimension of $M = 95$
- **Reduced mesh** resulting from solving non-negative least squares problem formulate by ECSW gives $n_e = 5,689$ elements (9.1% of $N_e = 62,500$ elements).

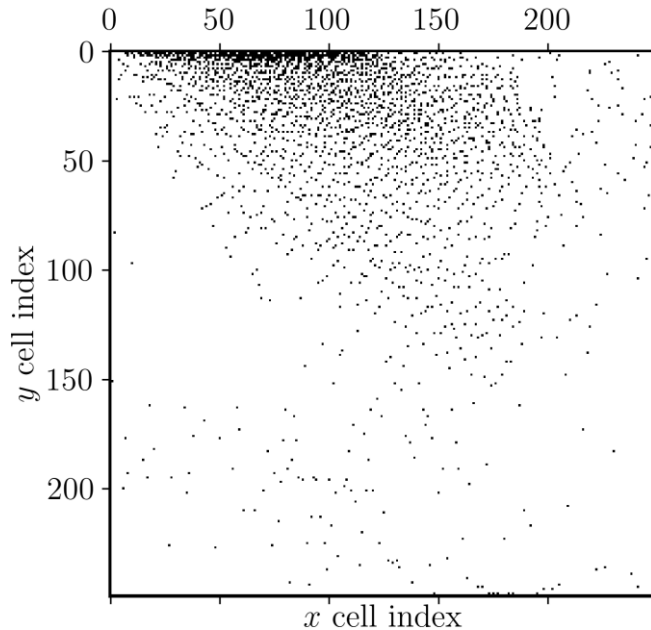


Figure above: Reduced mesh of single domain HROM

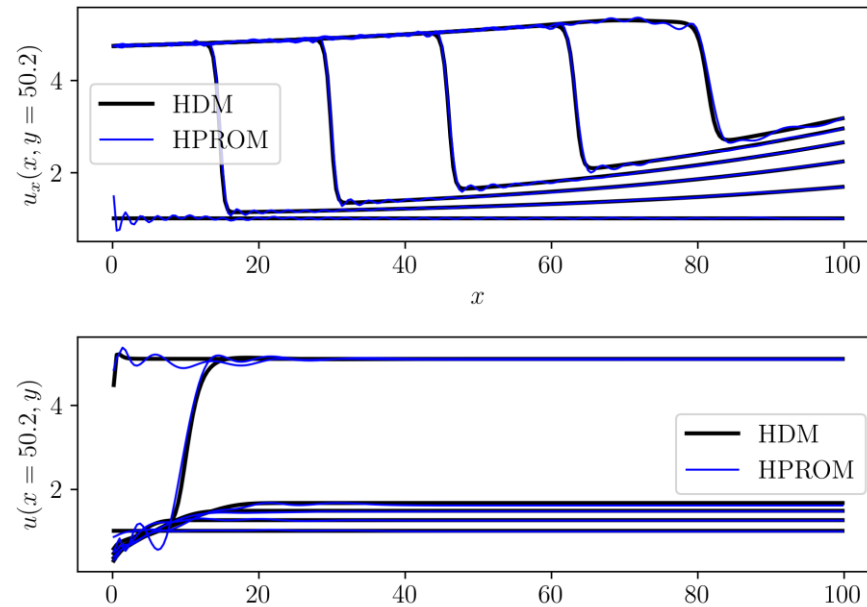
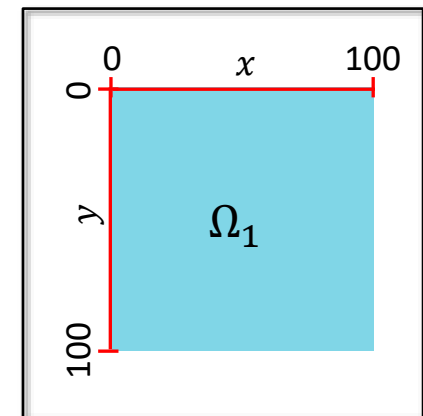


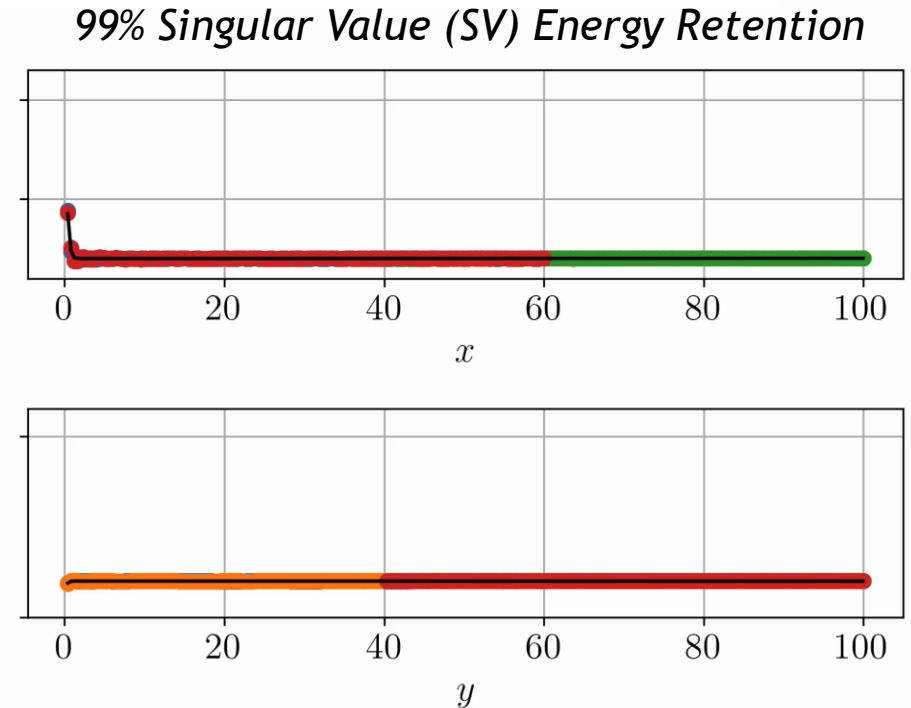
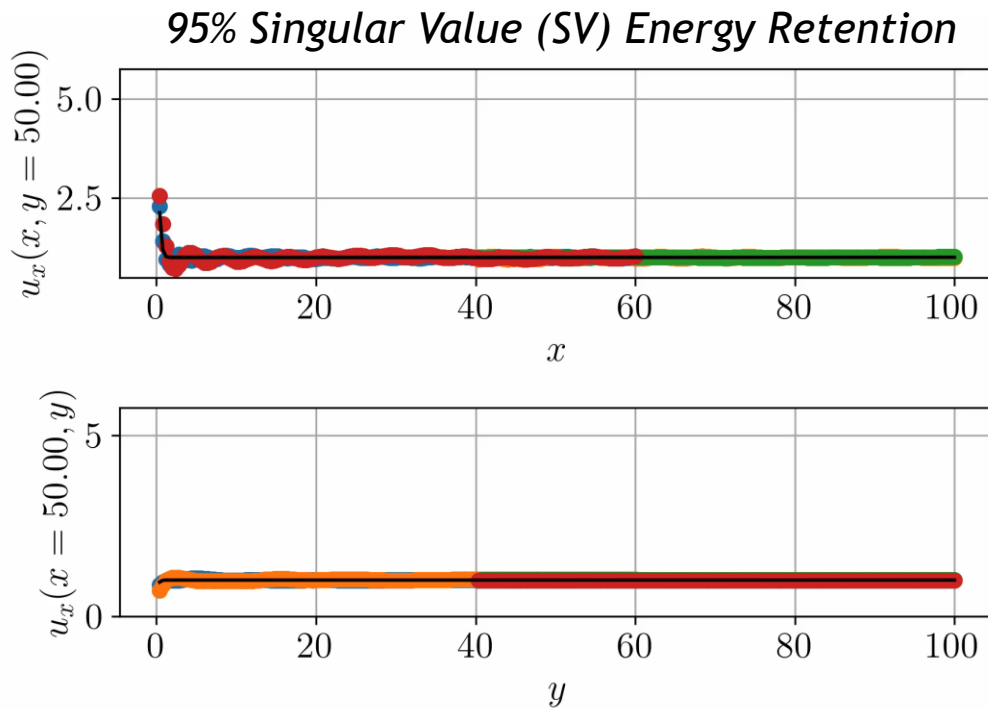
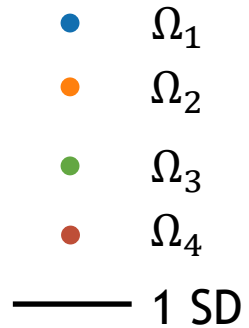
Figure above: HROM and FOM results at various time steps

% SV Energy	M	MSE* (%)	CPU time* (s)
95	69	1.1	138
99	177	0.17	447

* Numbers in table are w/o hyper-reduction

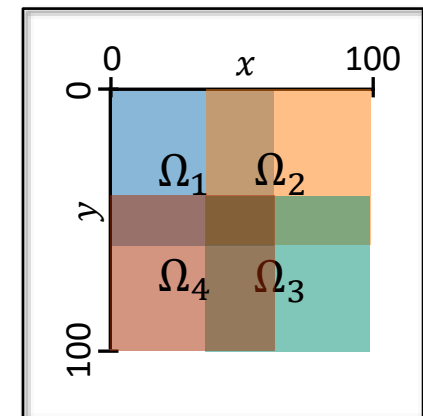


ROM-ROM-ROM-ROM Coupling

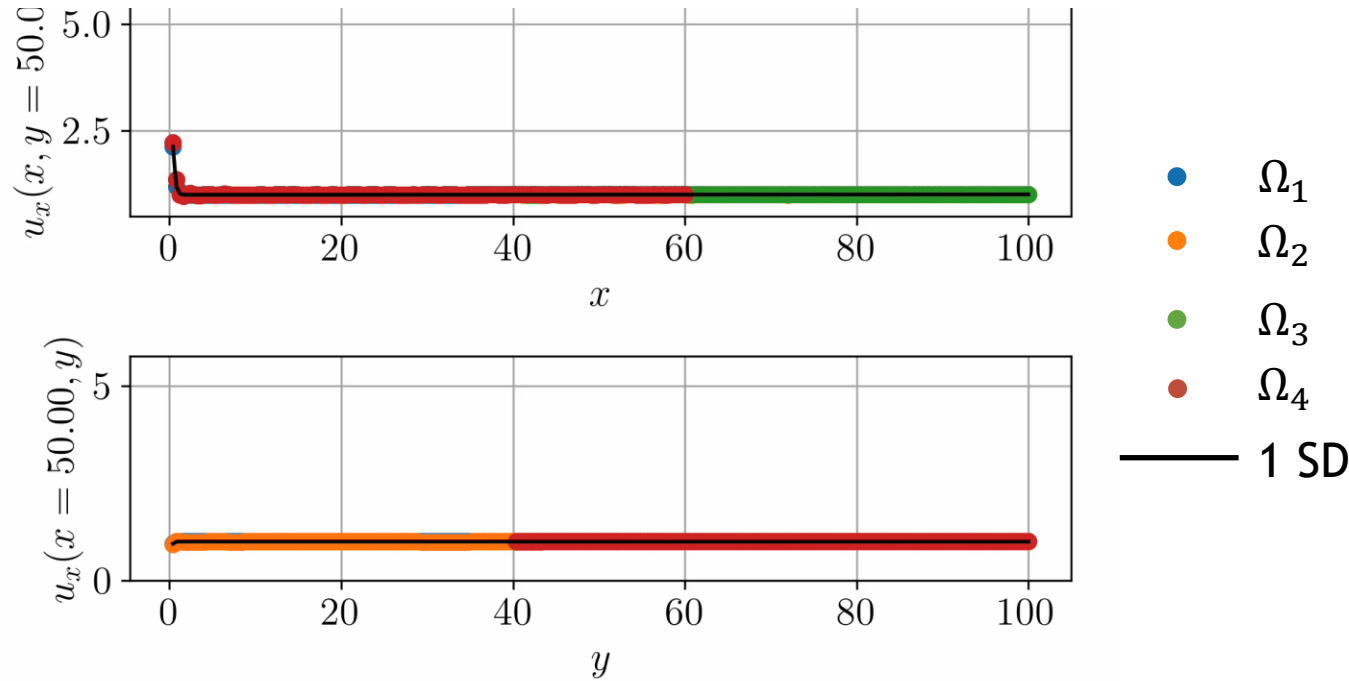


- Method converges in **only 3 Schwarz iterations** per controller time-step
- Errors $O(1\%)$ or less**
- $1.47\times$ speedup** over all-FOM coupling for 95% SV energy retention case

Subdomains	95% SV Energy			99% SV Energy		
	M	MSE (%)	CPU time (s)	M	MSE (%)	CPU time (s)
Ω_1	57	1.1	85	146	0.18	295
Ω_2	44	1.2	56	120	0.18	216
Ω_3	24	1.4	43	60	0.16	89
Ω_4	32	1.9	61	66	0.25	100
Total			245			700



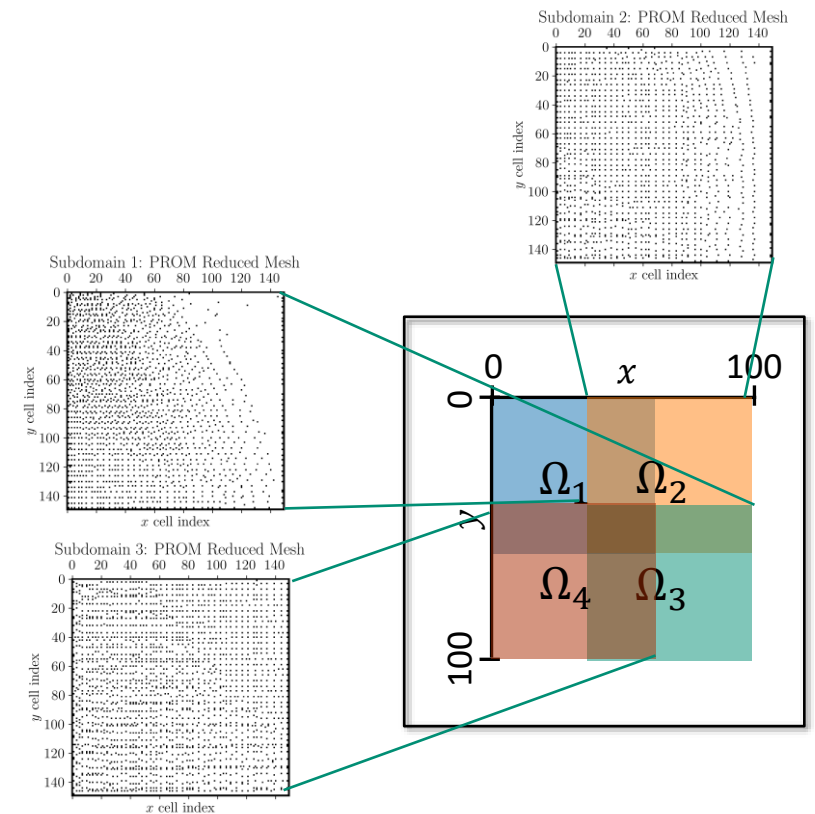
FOM-HROM-HROM-HROM Coupling



- FOM in Ω_1 as this is “hardest” subdomain for ROM
- HROMs in $\Omega_2, \Omega_3, \Omega_4$ capture 99% snapshot energy
- Method converges in 3 Schwarz iterations per controller time-step
- Errors $O(0.1\%)$ with 0 error in Ω_1
- $2.26\times$ speedup achieved over all-FOM coupling

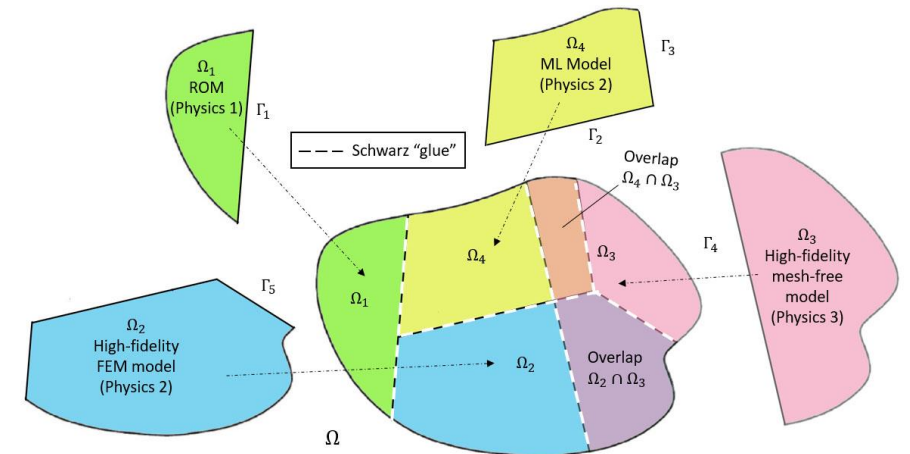
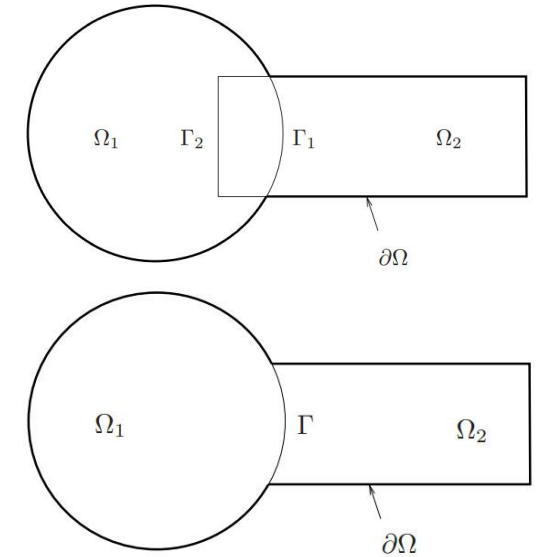
Further speedups possible via code optimizations and additive Schwarz.

Subdomains	99% SV Energy		
	M	MSE (%)	CPU time (s)
Ω_1	—	0.0	95
Ω_2	120	0.26	26
Ω_3	60	0.43	17
Ω_4	66	0.34	21
Total			159





- The Schwarz Alternating Method for Domain Decomposition-Based Coupling
- Extension to FOM*-ROM[#] and ROM-ROM Coupling
- Numerical Examples
 - 1D Dynamic Wave Propagation in Hyperelastic Bar
 - 2D Burgers Equation
- Summary & Future Work

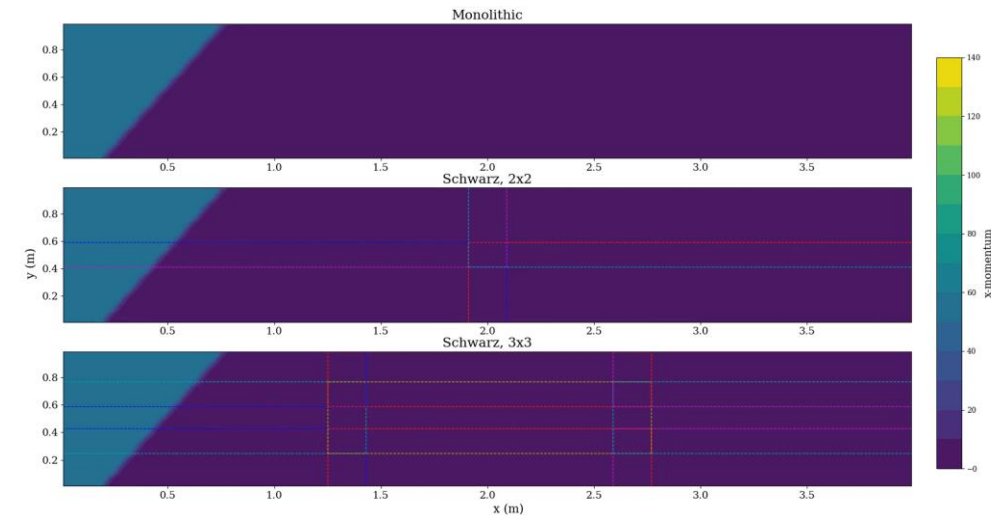


Summary:

- In a 1D solid mechanics and 2D hyperbolic PDE setting, Schwarz has been demonstrated for coupling of FOMs & (H)ROMs
- Computational gains can be achieved by coupling (H)ROMs

Ongoing & future work:

- Extension to other applications and HPC codes
- Improving method efficiency (e.g., additive Schwarz)
- Coupling nonlinear approximation manifold methods
- Dynamic adaptation of domain partitioning & “on-the-fly” ROM-FOM switching
- Learning of “optimal” transmission conditions to ensure structure preservation
- Extension of Schwarz to coupling of Physics Informed Neural Networks (PINNs)



Movie above: FOM-FOM coupling via Schwarz for 2D Euler problem using pressio-demoapps*

* <https://https://pressio.github.io>

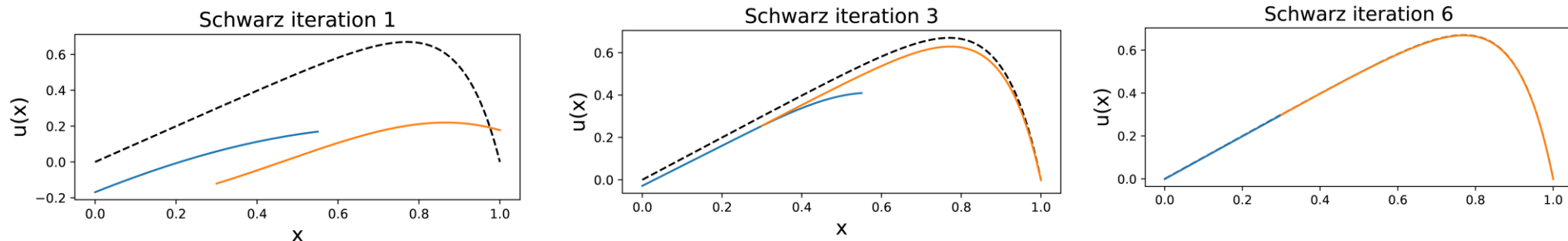
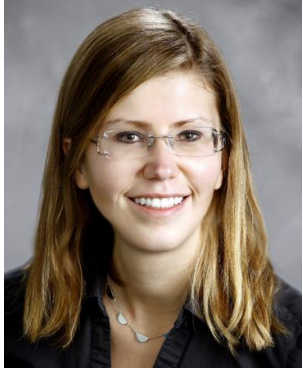


Figure above: overlapping alternating Schwarz PINN-PINN coupling for advection-diffusion problem.

Team & Acknowledgments



Irina Tezaur



Joshua Barnett
Year-Round Intern



Alejandro Mota



Chris Wentland
Postdoc



Will Snyder
Summer Intern

Thank you! Questions?



- [1] A. Salinger, *et al.* "Albany: Using Agile Components to Develop a Flexible, Generic Multiphysics Analysis Code", *Int. J. Multiscale Comput. Engng.* 14(4) (2016) 415-438.
- [2] H. Schwarz. "Über einen Grenzübergang durch alternierendes Verfahren". In: Vierteljahrsschrift der Naturforschenden Gesellschaft in Zurich 15 (1870), pp. 272-286.
- [3] S.L. Sobolev. "Schwarz's Algorithm in Elasticity Theory". In: Selected Works of S.L Sobolev. Volume I: equations of mathematical physics, computational mathematics and cubature formulats. Ed. By G.V. Demidenko and V.L. Vaskevich. New York: Springer, 2006.
- [4] S. Mikhlin. "On the Schwarz algorithm". In: Proceedings of the USSR Academy of Sciences 77 (1951), pp. 569-571.
- [5] P.L. Lions. "On the Schwarz alternating method I." In: 1988, First International Symposium on Domain Decomposition methods for Partial Differential Equations, SIAM, Philadelphia.
- [6] SIERRA Solid Mechanics Team. Sierra/SM 4.48 User's Guide. Tech. rep. SAND2018-2961. SNL Report, Oct. 2018.
- [7] M. Gunzburger, J. Peterson, J. Shadid. "Reduced-order modeling of time-dependent PDEs with multiple parameters in the boundary data". *CMAME* 196 (2007) 1030-1047.
- [8] C. Hoang, Y. Choi, K. Carlberg. "Domain-decomposition least-squares Petrov-Galerkin (DD-LSPG) nonlinear model reduction". *CMAME* 384 (2021) 113997.
- [9] K. Smetana, T. Taddei. "Localized model reduction for nonlinear elliptic partial differential equations: localized training, partition of unity, and adaptive enrichment", *ArXiv pre-print*, 2022.
- [10] C. Farhat, T. Chapman, P. Avery. "Structure-preserving, stability & accuracy properties of the energy-conserving sampling and weighting method for the hyper reduction of nonlinear FE dynamic models", *IJNME* 102 (2015) 1077-1110.
- [11] M. Bergmann, A. Ferrero, A. Iollo, E. Lombardi, A. Scardigli, H. Telib. "A zonal Galerkin-free POD model for incompressible flows." *JCP* 352 (2018) 301-325.



- [12] C. Sockwell, P. Bochev, K. Peterson, P. Kuberry. Interface Flux Recovery Framework for Constructing Partitioned Heterogeneous Time-Integration Methods. *Methods Numer. Meth. PDEs*, 2023 (in press). **Talk by P. Kuberry (IS03-II)**
- [13] A. de Castro, P. Bochev, P. Kuberry, I. Tezaur. A synchronous partitioned scheme for coupled reduced order models based on separate reduced order bases for interior and interface nodes”, *submitted to special issue of CMAME in honor of Tom Hughes’ 80th birthday*.
- [14] C. Sockwell, K. Peterson, P. Kuberry, P. Bochev, Interface Flux Recovery Framework for Constructing Partitioned Heterogeneous Time-Integration Methods, to appear. **Talk by J. Connors (IS03-I)**
- [15] A. Mota, I. Tezaur, G. Phlipot. "The Schwarz Alternating Method for Dynamic Solid Mechanics”, *Comput. Meth. Appl. Mech. Engng.* 121 (21) (2022) 5036-5071.
- [16] J. Hoy, I. Tezaur, A. Mota. "The Schwarz alternating method for multiscale contact mechanics". in *Computer Science Research Institute Summer Proceedings 2021*, J.D. Smith and E. Galvan, eds., Technical Report SAND2021-0653R, Sandia National Labs, 360-378, 2021.
- [17] J. Barnett, I. Tezaur, A. Mota. "The Schwarz alternating method for the seamless coupling of nonlinear reduced order models and full order models", in *Computer Science Research Institute Summer Proceedings 2022*, S.K. Seritan and J.D. Smith, eds., Technical Report SAND2022-10280R, Sandia National Laboratories, 2022, pp. 31-55. **This talk**

Journal article on ROM-FOM/ROM-ROM coupling using Schwarz is in preparation.

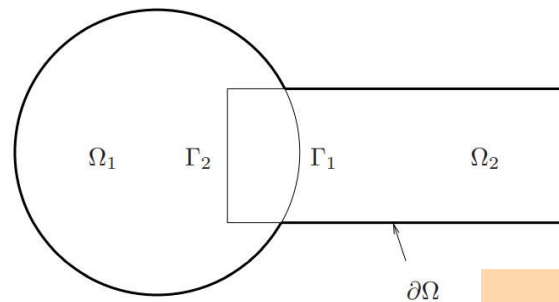
Email: ikalash@sandia.gov
URL: www.sandia.gov/~ikalash

Start of Backup Slides

Overlapping Domain Decomposition

$$\begin{cases} N(\mathbf{u}_1^{(n+1)}) = f, & \text{in } \Omega_1 \\ \mathbf{u}_1^{(n+1)} = \mathbf{g}, & \text{on } \partial\Omega_1 \setminus \Gamma_1 \\ \mathbf{u}_1^{(n+1)} = \mathbf{u}_2^{(n)} & \text{on } \Gamma_1 \end{cases}$$

$$\begin{cases} N(\mathbf{u}_2^{(n+1)}) = f, & \text{in } \Omega_2 \\ \mathbf{u}_2^{(n+1)} = \mathbf{g}, & \text{on } \partial\Omega_2 \setminus \Gamma_2 \\ \mathbf{u}_2^{(n+1)} = \mathbf{u}_1^{(n+1)} & \text{on } \Gamma_2 \end{cases}$$



$$\text{Model PDE: } \begin{cases} N(\mathbf{u}) = \mathbf{f}, & \text{in } \Omega \\ \mathbf{u} = \mathbf{g}, & \text{on } \partial\Omega \end{cases}$$

- Dirichlet-Dirichlet transmission BCs [Schwarz 1870; Lions 1988; Mota *et al.* 2017; Mota *et al.* 2022]

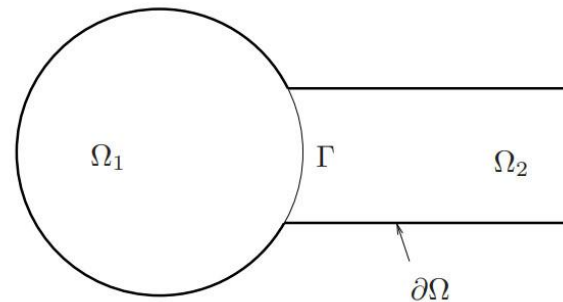
This talk: sequential subdomain solves (*multiplicative Schwarz*). Parallel subdomain solves (*additive Schwarz*) also possible.

Non-overlapping Domain Decomposition

$$\begin{cases} N(\mathbf{u}_1^{(n+1)}) = f, & \text{in } \Omega_1 \\ \mathbf{u}_1^{(n+1)} = \mathbf{g}, & \text{on } \partial\Omega_1 \setminus \Gamma \\ \mathbf{u}_1^{(n+1)} = \lambda_{n+1}, & \text{on } \Gamma \end{cases}$$

$$\begin{cases} N(\mathbf{u}_2^{(n+1)}) = f, & \text{in } \Omega_2 \\ \mathbf{u}_2^{(n+1)} = \mathbf{g}, & \text{on } \partial\Omega_2 \setminus \Gamma \\ \nabla \mathbf{u}_2^{(n+1)} \cdot \mathbf{n} = \nabla \mathbf{u}_1^{(n+1)} \cdot \mathbf{n}, & \text{on } \Gamma \end{cases}$$

$$\lambda_{n+1} = \theta \varphi_2^{(n)} + (1 - \theta) \lambda_n, \text{ on } \Gamma, \text{ for } n \geq 1$$



- Relevant for multi-material and multi-physics coupling
- Alternating Dirichlet-Neumann transmission BCs [Zanolli *et al.* 1987]
- Robin-Robin transmission BCs also lead to convergence [Lions 1990]
- $\theta \in [0,1]$: relaxation parameter (can help convergence)

Numerical Example: 1D Dynamic Wave Propagation Problem



- **Basis sizes** M_1 and M_2 vary from 60 to 300
 - Larger ROM used in Ω_1 , since solution has **steeper gradient** here
- For couplings involving FOM and ROM/HROM, **FOM** is placed in Ω_1 , since solution has steeper gradient here
- **Non-negative least-squares optimization problem** for ECSW weights solved using MATLAB's lsqnonneg function with early termination criterion (solution step-size tolerance = 10^{-4})
 - Ensures all HROMs have **consistent termination criterion** w.r.t. MATLAB implementation
 - However, **relative error tolerance** of selected reduced elements will differ
 - ❖ Switching to termination criterion based on relative error is work in progress and expected to improve HROM results
 - Convergence tolerance determines **size of sample mesh** $N_{e,i}$
 - **Boundary points** must be in sample mesh for application of Schwarz BC

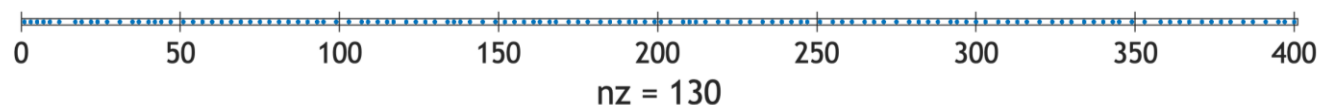


Figure left: sample sample mesh for 1D wave propagation problem

J. Barnett, I. Tezaur, A. Mota. "The Schwarz alternating method for the seamless coupling of nonlinear reduced order models and full order models", in [Computer Science Research Institute Summer Proceedings 2022](#), S.K. Seritan and J.D. Smith, eds., Technical Report SAND2022-10280R, Sandia National Laboratories, 2022, pp. 31-55. (<https://arxiv.org/abs/2210.12551>)

Numerical Example: Reproductive Problem Results



Model	M_1/M_2	$N_{e,1}/N_{e,2}$	CPU time (s)	$\frac{\mathcal{E}_{\text{MSE}}(\tilde{\mathbf{u}}_1)}{\mathcal{E}_{\text{MSE}}(\tilde{\mathbf{u}}_2)}$	$\frac{\mathcal{E}_{\text{MSE}}(\tilde{\mathbf{v}}_1)}{\mathcal{E}_{\text{MSE}}(\tilde{\mathbf{v}}_2)}$	$\frac{\mathcal{E}_{\text{MSE}}(\tilde{\mathbf{a}}_1)}{\mathcal{E}_{\text{MSE}}(\tilde{\mathbf{a}}_2)}$	N_S
FOM	—/—	—/—	1.871×10^3	—/—	—/—	—/—	—
ROM	60/—	—/—	1.398×10^3	1.659×10^{-2} /—	1.037×10^{-1}	4.681×10^{-1} /—	—
HROM	60/—	155/—	5.878×10^2	1.730×10^{-2} /—	1.063×10^{-1} /—	4.741×10^{-1} /—	—
ROM	200/—	—/—	1.448×10^3	2.287×10^{-4} /—	4.038×10^{-3} /—	4.542×10^{-2} /—	—
HROM	200/—	428/—	9.229×10^2	8.396×10^{-4} /—	8.947×10^{-3} /—	7.462×10^{-2} /—	—
FOM-FOM	—/—	—/—	2.345×10^3	—	—	—	24,630
FOM-ROM	—/80	—/—	2.341×10^3	2.171×10^{-6} / 1.253×10^{-5}	3.884×10^{-5} / 2.401×10^{-4}	2.982×10^{-4} / 2.805×10^{-3}	25,227
FOM-HROM	—/80	—/130	2.085×10^3	2.022×10^{-4} / 5.734×10^{-4}	$1.723e \times 10^{-3}$ / 5.776×10^{-3}	7.421×10^{-3} / 3.791×10^{-2}	29,678
FOM-ROM	—/200	—/—	2.449×10^3	4.754×10^{-12} / 7.357×10^{-11}	1.835×10^{-10} / 4.027×10^{-9}	5.550×10^{-9} / 1.401×10^{-7}	24,630
FOM-HROM	—/200	—/252	2.352×10^3	1.421×10^{-5} / 4.563×10^{-4}	1.724×10^{-4} / 2.243×10^{-3}	9.567×10^{-4} / 1.364×10^{-2}	27,156
ROM-ROM	200/80	—/—	2.778×10^3	4.861×10^{-5} / 3.093×10^{-5}	1.219×10^{-3} / 4.177×10^{-4}	1.586×10^{-2} / 3.936×10^{-3}	27,810
HROM-HROM	200/80	315/130	1.769×10^3	3.410×10^{-3} / 6.662×10^{-4}	4.110×10^{-2} / 6.432×10^{-3}	2.485×10^{-1} / 4.307×10^{-2}	29,860
ROM-ROM	300/80	—/—	2.646×10^3	2.580×10^{-6} / 1.292×10^{-5}	6.226×10^{-5} / 2.483×10^{-4}	9.470×10^{-4} / 2.906×10^{-3}	25,059
HROM-HROM	300/80	405/130	1.938×10^3	6.960×10^{-3} / 7.230×10^{-4}	6.328×10^{-2} / 7.403×10^{-3}	3.137×10^{-1} / 4.960×10^{-2}	29,896

Green shading highlights most competitive coupled models

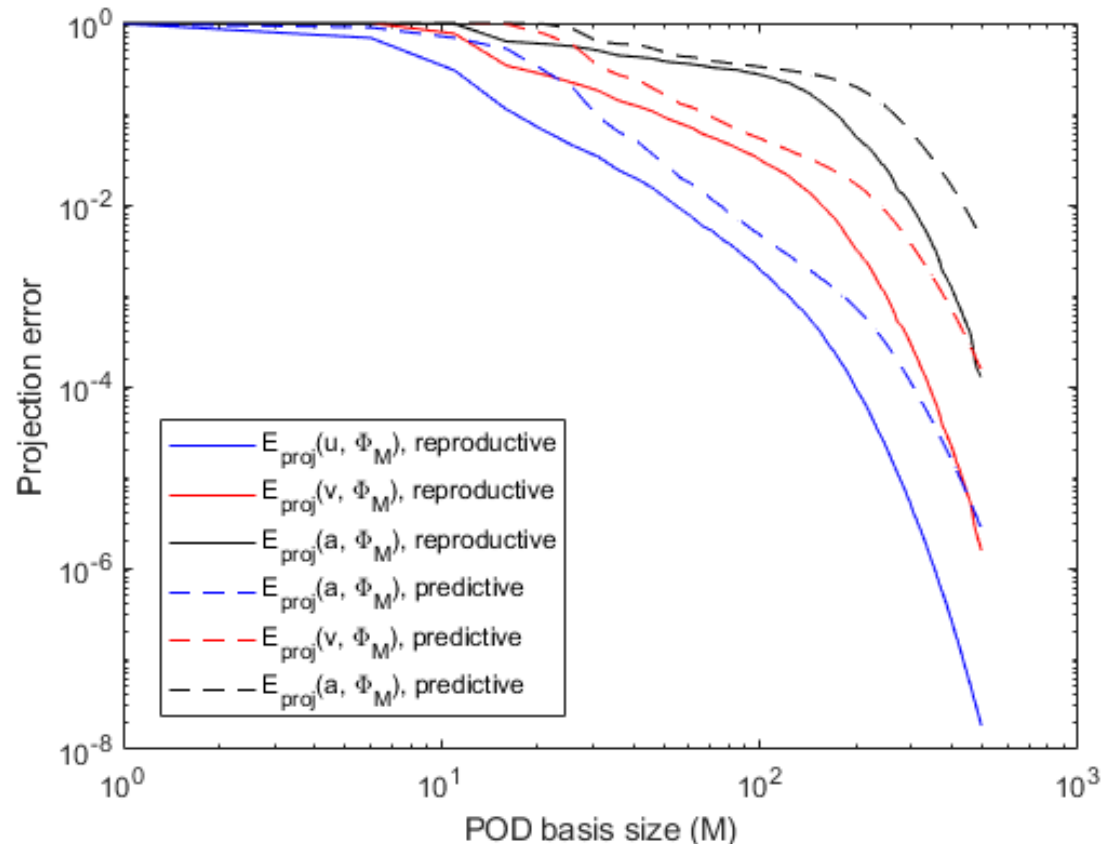
- All coupled models evaluated converged on average in **<3 Schwarz iterations** per time-step
- Larger FOM-ROM coupling has **same total # Schwarz iters** (N_S) as FOM-FOM coupling
- Other couplings require more Schwarz iters than FOM-FOM coupling to converge
 - **More Schwarz iters** required when coupling **less accurate models**
 - Larger 300/80 mode ROM-ROM takes less wall-clock time than smaller 200/80 mode ROM-ROM
- **FOM-HROM** and **HROM-HROM** couplings **outperform** the **FOM-FOM** coupling in terms of CPU time by 12.5-32.6%
- All couplings involving ROMs/HROMs are **at least as accurate** as single-domain ROMs/HROMs

Numerical Example: Predictive Problem Results



- Start by calculating **projection error** for reproductive and predictive version of the Rounded Square IC problem:

$$\mathcal{E}_{\text{proj}}(\mathbf{u}, \Phi_M) := \frac{\|\mathbf{u} - \Phi_M(\Phi_M^T \Phi_M)^{-1} \Phi_M^T \mathbf{u}\|_2}{\|\mathbf{u}\|_2}$$



- Projection error suggests **predictive ROM** can achieve **accuracy** and **convergence** with **basis refinement**
- O(100) modes** are needed to achieve sufficiently accurate ROM
 - Larger ROMs containing O(100) modes considered in our coupling experiments: $M_1 = 300$, $M_2 = 200$

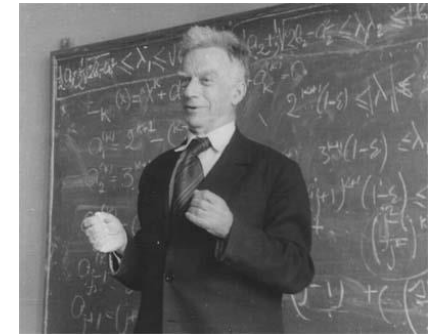
Theoretical Foundation

Using the Schwarz alternating as a **discretization method** for PDEs is natural idea with a sound **theoretical foundation**.

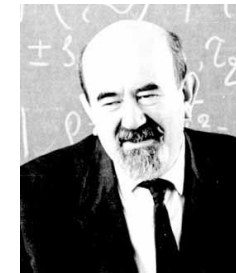
- **S.L. Sobolev (1936)**: posed Schwarz method for **linear elasticity** in variational form and **proved method's convergence** by proposing a convergent sequence of energy functionals.
- **S.G. Mikhlin (1951)**: **proved convergence** of Schwarz method for general linear elliptic PDEs.
- **P.-L. Lions (1988)**: studied convergence of Schwarz for **nonlinear monotone elliptic problems** using max principle.
- **A. Mota, I. Tezaur, C. Alleman (2017)**: proved **convergence** of the alternating Schwarz method for **finite deformation quasi-static nonlinear PDEs** (with energy functional $\Phi[\varphi]$) with a **geometric convergence rate**.

$$\Phi[\varphi] = \int_B A(F, Z) dV - \int_B \mathbf{B} \cdot \boldsymbol{\varphi} dV$$

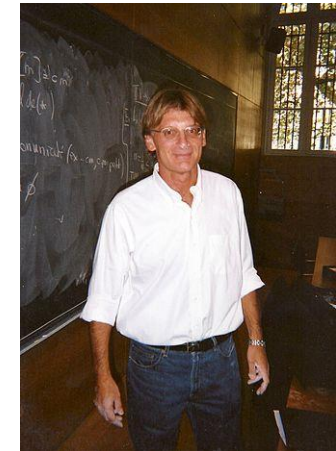
$$\nabla \cdot \mathbf{P} + \mathbf{B} = \mathbf{0}$$



S.L. Sobolev (1908 – 1989)



S.G. Mikhlin
(1908 – 1990)



P.-L. Lions (1956-)



A. Mota, I. Tezaur, C. Alleman

Convergence Proof*



2 Formulation of the Schwarz Alternating Method

We start by defining the standard finite deformation variational formulation to establish notation before presenting the formulation of the coupling method.

2.1 Variational Formulation on a Single Domain

Consider a body as the open set $\Omega \subset \mathbb{R}^2$ undergoing a motion described by the mapping $x = \varphi(\mathbf{X}) : \Omega \rightarrow \mathbb{R}^2$, $\mathbf{X} \in \Omega$. Assume that the boundary of the body is $\partial\Omega = \partial\Omega_D \cup \partial\Omega_N$ with unit normal \mathbf{n} , where $\partial\Omega_D$ is a displacement boundary, $\partial\Omega_N$ is a traction boundary, and $\partial\Omega_D \cap \partial\Omega_N = \emptyset$. The prescribed boundary displacements or Dirichlet boundary conditions are $\chi : \partial\Omega_D \rightarrow \mathbb{R}^2$. The prescribed boundary tractions or Neumann boundary conditions are $\mathbf{T} : \partial\Omega_N \rightarrow \mathbb{R}^2$. Let $\mathbf{P} = \text{Grad } \varphi$ be the deformation gradient. Let also $\text{RB} : \Omega \rightarrow \mathbb{R}^2$ be the body force, with RB the mass density in the reference configuration. Furthermore, introduce the energy functional

$$\Phi[\varphi] = \int_{\Omega} A(\mathbf{F}, \mathbf{X}) d\mathbf{X} - \int_{\Omega} \text{RB} \cdot \varphi d\mathbf{X} - \int_{\partial\Omega_N} \mathbf{T} \cdot \varphi dS, \quad (1)$$

in which $A(\mathbf{F}, \mathbf{X})$ is the Helmholtz free energy density and \mathbf{X} is a collection of internal variables. The weak form of the problem is obtained by minimizing the energy functional $\Phi[\varphi]$ over the Sobolev space $H^1(\Omega)$ that is comprised of all functions that are square-integrable and have square-integrable first derivatives. Define

$$S := \{\varphi \in H^1(\Omega) : \varphi = \chi \text{ on } \partial\Omega_D\} \quad (2)$$

and

$$V := \{\xi \in H^1_0(\Omega) : \xi = 0 \text{ on } \partial\Omega_D\} \quad (3)$$

where $\xi \in V$ is a test function. The potential energy is minimized if and only if $\Phi[\varphi] \leq \Phi[\varphi + \xi]$ for all $\xi \in V$ and $\varphi \in S$. It is straightforward to show that the minimum of $\Phi[\varphi]$ is the mapping $\varphi : S$ that satisfies

$$D\Phi[\varphi](\xi) = \int_{\Omega} \mathbf{P} \cdot \text{Grad} \xi d\mathbf{X} - \int_{\Omega} \text{RB} \cdot \xi d\mathbf{X} - \int_{\partial\Omega_N} \mathbf{T} \cdot \xi dS = 0, \quad (4)$$

where $\mathbf{P} = \partial A / \partial \mathbf{F}$ denotes the first Piola-Kirchhoff stress. The Euler-Lagrange equation corresponding to the variational statement (1) is

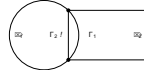


Figure 1: Two subdomains Ω_1 and Ω_2 and the corresponding boundary Γ , and Γ_1 and Γ_2 used by the Schwarz alternating method.

that is $i = 1$ and $j = 2$ if n is odd, and $i = 2$ and $j = 1$ if n is even. Introduce the following definitions for each subdomain:

- Closure $\bar{\Omega}_i := \Omega_i \cup \partial\Omega_i$
- Dirichlet boundary: $\partial\Omega_i := \partial\Omega_i \cap \partial\Omega_D$
- Neumann boundary: $\partial\Omega_i := \partial\Omega_i \cap \partial\Omega_N$
- Schwarz boundary: $\Gamma_i := \partial\Omega_i \cap \Gamma$

Note that with these definitions we guarantee that $\partial\Omega_1 \cap \partial\Omega_2 = \emptyset$, $\partial\Omega_1 \cap \Gamma_1 = \emptyset$, and $\partial\Omega_2 \cap \Gamma_2 = \emptyset$. Now define the spaces

$$S_i := \{\varphi : 2 \text{ W}(\Omega_i) : \varphi = \chi \text{ on } \partial\Omega_{i,D}, \varphi = P_{\Omega_j}(\varphi) \text{ on } \Gamma_i\}, \quad (7)$$

and

$$V_i := \{\varphi : 2 \text{ W}(\Omega_i) : \varphi = 0 \text{ on } \partial\Omega_{i,D}\}. \quad (8)$$

where the symbol $P_{\Omega_j}(\varphi)$ denotes the projection from the subdomain Ω_j onto the Schwarz boundary Γ_i . This projection operator plays a central role in the Schwarz alternating method. Its form and implementation are discussed in subsequent sections. For the moment it is sufficient to assume that the operator is able to project a field φ from one subdomain to the Schwarz boundary of the other subdomain.

The Schwarz alternating method solves a sequence of problems on Ω_1 and Ω_2 . The solution $\varphi^{(n)}$ for the

$$\begin{aligned} 1. & \varphi_1^{(n)} = X_1^{(n)} \text{ on } \Omega_1, \varphi_1^{(n)} = \chi_1(X_1^{(n)}) \text{ on } \partial\Omega_{1,D}, &> \text{variation for } \Omega_1 \\ 2. & \varphi_2^{(n)} = X_2^{(n)} \text{ on } \Omega_2, \varphi_2^{(n)} = \chi_2(X_2^{(n)}) \text{ on } \partial\Omega_{2,D}, &> \text{variation for } \Omega_2 \\ 3. & \text{repeat} &> \text{Non-stochastic loop} \\ 4. & \begin{cases} \varphi_1^{(n+1)} = \left(K_{11}^{(n)} + K_{12}^{(n)} H_{21} \right) \begin{pmatrix} K_{11}^{(n)} H_{11} \\ K_{12}^{(n)} H_{21} \end{pmatrix} \begin{pmatrix} -R_1^{(n)} \\ -R_2^{(n)} \end{pmatrix} \\ \varphi_2^{(n+1)} = \left(K_{21}^{(n)} + K_{22}^{(n)} H_{12} \right) \begin{pmatrix} K_{21}^{(n)} H_{11} \\ K_{22}^{(n)} H_{21} \end{pmatrix} \begin{pmatrix} -R_1^{(n)} \\ -R_2^{(n)} \end{pmatrix} \end{cases} &> \text{linear system} \\ 5. & \varphi_1^{(n+1)} = \varphi_1^{(n)} + \Delta\varphi_1^{(n)} \\ 6. & \varphi_2^{(n+1)} = \varphi_2^{(n)} + \Delta\varphi_2^{(n)} \\ 7. & \text{until } \left\| \left(\left\| \varphi_1^{(n+1)} - \varphi_1^{(n)} \right\| \right)^2 + \left(\left\| \varphi_2^{(n+1)} - \varphi_2^{(n)} \right\| \right)^2 \right\|^{1/2} \leq \epsilon_{\text{tolerance}} &> \text{stop criterion} \end{aligned}$$

Algorithm 1: Stochastic Schwarz Method

(1), (3), (4). Although we do not provide here formal convergence proofs for the remaining variants of the Schwarz method, we offer some numerical results illustrating their convergence in Section 4.

Consider the energy functional $\Phi[\varphi]$ defined in (1). We will denote by (\cdot, \cdot) the usual L^2 inner product over Ω , that is,

$$(\varphi_1, \varphi_2) := \int_{\Omega} \varphi_1 \cdot \varphi_2 d\mathbf{X}. \quad (5)$$

for $\varphi_1, \varphi_2 \in W_0^{1,2}(\Omega)$, with corresponding norm $\|\cdot\|$. The proof of the convergence of the Schwarz alternating method requires that the functional $\Phi[\varphi]$ satisfy the following properties over the space S defined in (2):

1. $\Phi[\varphi]$ is coercive.
2. $\Phi[\varphi]$ is Fréchet differentiable, with $\Phi'[\varphi]$ denoting its Fréchet derivative.
3. $\Phi[\varphi]$ is strictly convex.
4. $\Phi[\varphi]$ is lower semi-continuous.
5. $\Phi'[\varphi]$ is uniformly continuous on K_∞ , where

$$K_\infty := \{\varphi \in S : \Phi[\varphi] \leq B, B \in \mathbb{R}, B < \infty\}. \quad (6)$$

It can be shown that the energy functional $\Phi[\varphi]$ defined in (1) is strictly convex in S (property 2) provided that the Helmholtz free energy density $A(\mathbf{F}, \mathbf{X})$ is a convex function of \mathbf{F} (property 1) and

Theorem 1. Assume that the energy functional $\Phi[\varphi]$ satisfies properties 1–5 above. Consider the Schwarz alternating method of Section 2 defined by (9)–(13) and its equivalent form (39). Then

- (a) $\Phi[\tilde{\varphi}^{(0)}] \geq \Phi[\tilde{\varphi}^{(1)}] \geq \dots \geq \Phi[\tilde{\varphi}^{(n-1)}] \geq \Phi[\tilde{\varphi}^{(n)}] \geq \dots \geq \Phi[\varphi]$, where φ is the minimizer of $\Phi[\varphi]$ over S .
- (b) The sequence $\{\tilde{\varphi}^{(n)}\}$ defined in (39) converges to the minimizer φ of $\Phi[\varphi]$ in S .
- (c) The Schwarz minimum values $\Phi[\tilde{\varphi}^{(n)}]$ converge monotonically to the minimum value $\Phi[\varphi]$ in S starting from any initial guess $\tilde{\varphi}^{(0)}$.

Remark 1 By the coercivity of $\Phi[\varphi]$, it follows from the Lax-Milgram theorem that a unique minimizer to the functional over S exists, i.e., the minimization of $\Phi[\varphi]$ is well-posed.

Remark 2 By the Stampacchia theorem, the minimization of $\Phi[\varphi]$ in S is equivalent to finding $\varphi \in S$ such that

$$(\Phi'[\varphi], \xi - \varphi) \geq 0 \quad (11)$$

for all $\xi \in S$.

Remark 3 Recall that the strict convexity property of $\Phi[\varphi]$ can be written as

$$\Phi[\varphi_2] - \Phi[\varphi_1] - (\Phi'[\varphi_1], \varphi_2 - \varphi_1) \geq 0. \quad (12)$$

$\forall \varphi_1, \varphi_2 \in S$. From (10), remark that if $\Phi[\varphi]$ is strictly convex over $S \forall B \in \mathbb{R}$ such that $B < \infty$, we can find an $\alpha_B > 0$ such that $\forall \varphi_1, \varphi_2 \in K_B$ we have

$$\Phi[\varphi_2] - \Phi[\varphi_1] - (\Phi'[\varphi_1], \varphi_2 - \varphi_1) \geq \alpha_B \|\varphi_2 - \varphi_1\|^2. \quad (13)$$

Remark 4 By property 5, the uniform continuity of $\Phi'[\varphi]$, the uniform modulus of continuity $\omega \rightarrow 0$, with $\omega : K_\infty \rightarrow K_\infty$, such that

$$\|\Phi'[\varphi_1] - \Phi'[\varphi_2]\| \leq \omega(\|\varphi_1 - \varphi_2\|). \quad (14)$$

$\forall \varphi_1, \varphi_2 \in K_B$. By definition, $\omega(t) \rightarrow 0$ as $t \rightarrow 0$.

Remark 5 It was shown in (13) that in the case $\Omega_1 \cap \Omega_2 \neq \emptyset$, $\forall \varphi \in S$, there exist $\xi_1 \in S_1$ and $\xi_2 \in S_2$ such that

$$\varphi = \xi_1 + \xi_2. \quad (15)$$

and

$$\max\{\|\xi_1\|, \|\xi_2\|\} \leq C_0 \|\varphi\|, \quad (16)$$

for some $C_0 > 0$ independent of φ .

Remark 6 Note that (39) can be written as

$$(\Phi'[\varphi^{(n)}], \varphi^{(n+1)} - \varphi^{(n)}) = 0, \text{ for } \varphi^{(n)} \in \tilde{S}_n, \varphi^{(n+1)} \in \tilde{S}_n, \quad (17)$$

for $n \in \{1, 2, 3, \dots\}$ and $n \in \{1, 2, 3, \dots\}$ (recall from (6) the relation between i and n). This is due to the uniqueness of the solution to each minimization problem over S_i , and the definition of $\varphi^{(n)}$ as the minimizer of $\Phi[\varphi]$ over \tilde{S}_n .

Remark 7 Let $\varphi^{(n)} \in \tilde{S}_n$ and let $\xi \in S$. By **Remark 5**, there exist $\xi_1 \in S_1$ and $\xi_2 \in S_2$ such that

$$(\Phi'[\varphi^{(n)}], \xi) - (\Phi'[\varphi^{(n)}], \xi_1 + \xi_2). \quad (18)$$

Again using (57) and also (58) in (18) leads to

$$(\Phi'[\varphi^{(n)}], \xi) - (\Phi'[\varphi^{(n)}], \xi_1) - (\Phi'[\varphi^{(n)}], \xi_2) \leq \|(\Phi'[\varphi^{(n)}] - \Phi'[\varphi^{(n+1)}])\| \cdot \|\xi\|, \quad (19)$$

and substituting (56) into (19) we finally obtain that

$$(\Phi'[\varphi^{(n)}], \xi) \leq C_0 (\Phi'[\varphi^{(n)}] - \Phi'[\varphi^{(n+1)}]) \cdot \|\xi\|, \quad (20)$$

$\forall \xi \in S$.

Remark 8 For part (a) of Theorem 1, recall the definition of geometric convexity:

$$K_{n+1} \subseteq C K_n, \quad (21)$$

$\forall n \in \{0, 1, 2, \dots\}$ for some $C > 0$, where

$$K_n := \{\varphi^{(n+1)} - \varphi^{(n)}\}. \quad (22)$$

Remark 9 Recall from the definition of continuity that if $\Phi'[\varphi]$ is Lipschitz continuous at $\varphi^{(n)}$ near φ , then there exists a constant $K > 0$ such that

$$\left\| \frac{\Phi'[\varphi^{(n)}] - \Phi'[\varphi]}{\|\varphi^{(n)} - \varphi\|} \right\| \leq K. \quad (23)$$

Considering that $\Phi'[\varphi] = 0$ since φ is the minimizer of $\Phi[\varphi]$, (23) is equivalent to

$$\|\Phi'[\varphi^{(n)}]\| \leq K \|\varphi^{(n)} - \varphi\|. \quad (24)$$

Proof of Theorem 1

Proof of (a). Let $\varphi^{(1)} = \arg \min_{\varphi \in \tilde{S}_1} \Phi[\varphi]$. By (10), $\varphi^{(1)} \in \tilde{S}_1$. Let φ^* be the minimizer of $\Phi[\varphi]$ over S and suppose $\Phi[\varphi^*] > \Phi[\varphi^{(1)}]$. But this is a contradiction, since we can take $\varphi^* = \varphi^{(1)}$. Hence, it cannot be that $\Phi[\varphi^{(1)}] < \Phi[\varphi^*]$ where $\varphi^* = \arg \min_{\varphi \in \tilde{S}_1} \Phi[\varphi]$. It follows by induction that

$$\Phi[\varphi^{(n)}] \leq \Phi[\varphi^{(n+1)}] \quad (25)$$

for $n \in \{1, 2, 3, \dots\}$. Now let φ be the minimizer of $\Phi[\varphi]$ over S . Since the problem is well-posed φ is unique. Hence $\Phi[\varphi] \leq \Phi[\varphi^{(n)}]$ for all $n \in \{1, 2, 3, \dots\}$. \square

Proof of (b). By (10), for large enough n , there exists some $C_1 > 0$ independent of n such that

$$\|\varphi^{(n)} - \varphi\| \leq C_1 \|\varphi^{(n+1)} - \varphi^{(n)}\|. \quad (26)$$

Let us choose C_1 such that $C_1 > \alpha_B/K$, where K is the Lipschitz continuity constant in (16). Combining (16) with (26) leads to

$$\frac{1}{\alpha_B} (\Phi'[\varphi^{(n)}] - \Phi'[\varphi^{(n+1)}]) \geq \|\varphi^{(n+1)} - \varphi^{(n)}\| \geq \frac{1}{C_1} \|\varphi^{(n)} - \varphi\|. \quad (27)$$

By (10), $\|\varphi^{(n)} - \varphi^{(n+1)}\| \rightarrow 0$ as $n \rightarrow \infty$. From this we obtain the result, namely that $\varphi^{(n)} \rightarrow \varphi$ in S .

Proof of (c). This follows immediately from (a) and (b). \square

Proof of (d). By (10), for large enough n , there exists some $C_1 > 0$ independent of n such that

$$\|\varphi^{(n)} - \varphi\| \leq C_1 \|\varphi^{(n+1)} - \varphi^{(n)}\|. \quad (28)$$

Let us choose C_1 such that $C_1 > \alpha_B/K$, where K is the Lipschitz continuity constant in (16). Combining (16) with (28) leads to

$$\frac{1}{\alpha_B} (\Phi'[\varphi^{(n)}] - \Phi'[\varphi^{(n+1)}]) \geq \|\varphi^{(n+1)} - \varphi^{(n)}\| \geq \frac{1}{C_1} \|\varphi^{(n)} - \varphi\|. \quad (29)$$

Remark that (30)

$$\tilde{S}_n = \varphi^{(n-1)} + \tilde{V}_n \text{ for } \varphi^{(n-1)} \in \tilde{S}_{n-1} \Rightarrow \varphi^{(n-1)} \in \tilde{S}_n. \quad (30)$$

Theorem 1. Assume that the energy functional $\Phi[\varphi]$ satisfies properties 1–5 above. Consider the Schwarz alternating method of Section 2 defined by (9)–(13) and its equivalent form (39). Then

(a) $\Phi[\tilde{\varphi}^{(0)}] \geq \Phi[\tilde{\varphi}^{(1)}] \geq \dots \geq \Phi[\tilde{\varphi}^{(n-1)}] \geq \Phi[\tilde{\varphi}^{(n)}] \geq \dots \geq \Phi[\varphi]$, where φ is the minimizer of $\Phi[\varphi]$ over S .

(b) The sequence $\{\tilde{\varphi}^{(n)}\}$ defined in (39) converges to the minimizer φ of $\Phi[\varphi]$ in S .

(c) The Schwarz minimum values $\Phi[\tilde{\varphi}^{(n)}]$ converge monotonically to the minimum value $\Phi[\varphi]$ in S starting from any initial guess $\tilde{\varphi}^{(0)}$.

(d) If $\Phi'[\varphi]$ is Lipschitz continuous in a neighborhood of φ , then the sequence $\{\varphi^{(n)}\}$ converges geometrically to the minimizer φ . \square

Proof. See Appendix A. \square

Finally, while most of works cited above present their analysis for the specific case of two subdomains, extension to multiple subdomains is a general straightforward. The case of multiple subdomains is considered specifically in Lions [13], Badoia [14], and Li-Shun and Evans [14].

4 Numerical Examples

In this section, we present numerical examples of the behavior of the Schwarz alternating method for two different implementations. First, we briefly describe the two implementations, one in MATLAB and the other in the open-source software FEniCS [15]. Next, we discuss the error estimates used throughout the numerical examples. Then, we continue with four examples that demonstrate different features of the Schwarz alternating method and our implementation. The first example, a two-dimensional singular bar, is used to demonstrate the behavior of the four Schwarz variants of Section 2.4. The second example, a cuboid body of square base, aims to study the effect of the size of the overlap region on the convergence of the method. The objective of the third example, a notched cantilever, is to analyze the numerical error in the results and demonstrate the ability of the method to coarse different element topologies. The last example, a laser

$$(\Phi'[\varphi^{(n)}], \varphi - \varphi^{(n)}) \leq (\Phi'[\varphi^{(n)}], \varphi - \varphi^{(n+1)}) + \alpha(\|\varphi - \varphi^{(n)}\| \leq \Phi[\varphi] - \Phi[\varphi^{(n+1)}]) \quad (31)$$

since $\alpha_B > 0$. Now, by the Cauchy-Schwarz inequality followed by the application of the Lipschitz continuity of $\Phi'[\varphi]$ (16) we can write

$$(\Phi'[\varphi^{(n)}], \varphi - \varphi^{(n)}) \leq \|(\Phi'[\varphi^{(n)}])\| \cdot \|\varphi - \varphi^{(n)}\| \leq K \|\varphi - \varphi^{(n)}\|^2. \quad (32)$$

Hence, from (31),

$$\Phi[\varphi^{(n+1)}] - \Phi[\varphi] \leq K \|\varphi^{(n)} - \varphi\|^2. \quad (33)$$

Moreover, by (33) since $\Phi'[\varphi] = 0$,

$$\Phi[\varphi^{(n+1)}] - \Phi[\varphi] \geq \alpha_B \|\varphi^{(n)} - \varphi\|^2. \quad (34)$$

Using (33) and (32) we obtain

$$(\Phi'[\varphi^{(n)}] - \Phi'[\varphi]) - (\Phi'[\varphi^{(n+1)}] - \Phi'[\varphi]) \leq K \|\varphi^{(n)} - \varphi\|^2 - \alpha_B \|\varphi^{(n+1)} - \varphi\|^2. \quad (35)$$

Combining (33) and (35) leads to

$$\frac{1}{C_1} \|\varphi^{(n)} - \varphi\|^2 \leq (\Phi'[\varphi^{(n)}] - \Phi'[\varphi]) - (\Phi'[\varphi^{(n+1)}] - \Phi'[\varphi]) \leq K \|\varphi^{(n)} - \varphi\|^2 - \alpha_B \|\varphi^{(n+1)} - \varphi\|^2, \quad (36)$$

or

$$\|\varphi^{(n+1)} - \varphi\| \leq B \|\varphi^{(n)} - \varphi\| \quad (37)$$

with

$$B := \left(\frac{K}{\alpha_B} - \frac{1}{C_1} \right). \quad (38)$$

and $B \in \mathbb{R}$ as we chose $C_1 > \alpha_B/K$. Furthermore, since the sequence $\{\varphi^{(n)}\}$ converges monotonically to the minimizer φ of $\Phi[\varphi]$ by (b) and (c), it follows that $B \in (0, 1)$. Define $C := 1 - B \in (0, 1)$, then (37) can be recast as

$$\|\varphi^{(n+1)} - \varphi\| \leq C \|\varphi^{(n)} - \varphi\| \quad (39)$$

whenever the claim is proven. \square

B Analytic Solution for Linear-Elastic Singular Bar

As reference, herein we provide the solution of the singular bar of Section 4.3 for linear elasticity. The equilibrium equation is

$$P = \sigma(X)/E(X) = \text{const}, \quad \sigma(X) = E(X) \cdot \epsilon(X) = \sigma(X), \quad A(X) = A_0 \left(\frac{X}{L} \right)^{\frac{1}{\alpha}}, \quad (40)$$



- Like for quasistatics, dynamic alternating Schwarz method converges provided each single-domain problem is **well-posed** and **overlap region** is **non-empty**, under some **conditions** on Δt .
- **Well-posedness** for the dynamic problem requires that action functional $S[\boldsymbol{\varphi}] := \int_I \int_{\Omega} L(\boldsymbol{\varphi}, \dot{\boldsymbol{\varphi}}) dV dt$ be **strictly convex** or **strictly concave**, where $L(\boldsymbol{\varphi}, \dot{\boldsymbol{\varphi}}) := T(\dot{\boldsymbol{\varphi}}) + V(\boldsymbol{\varphi})$ is the Lagrangian.
 - This is studied by looking at its second variation $\delta^2 S[\boldsymbol{\varphi}_h]$
- We can show assuming a **Newmark** time-integration scheme that for the **fully-discrete** problem:

$$\delta^2 S[\boldsymbol{\varphi}_h] = \mathbf{x}^T \left[\frac{\gamma^2}{(\beta \Delta t)^2} \mathbf{M} - \mathbf{K} \right] \mathbf{x}$$

- $\delta^2 S[\boldsymbol{\varphi}_h]$ can always be made positive by choosing a **sufficiently small** Δt
- Numerical experiments reveal that Δt requirements for **stability/accuracy** typically lead to automatic satisfaction of this bound.

Schwarz for Multiscale FOM-FOM Coupling in Solid Mechanics¹

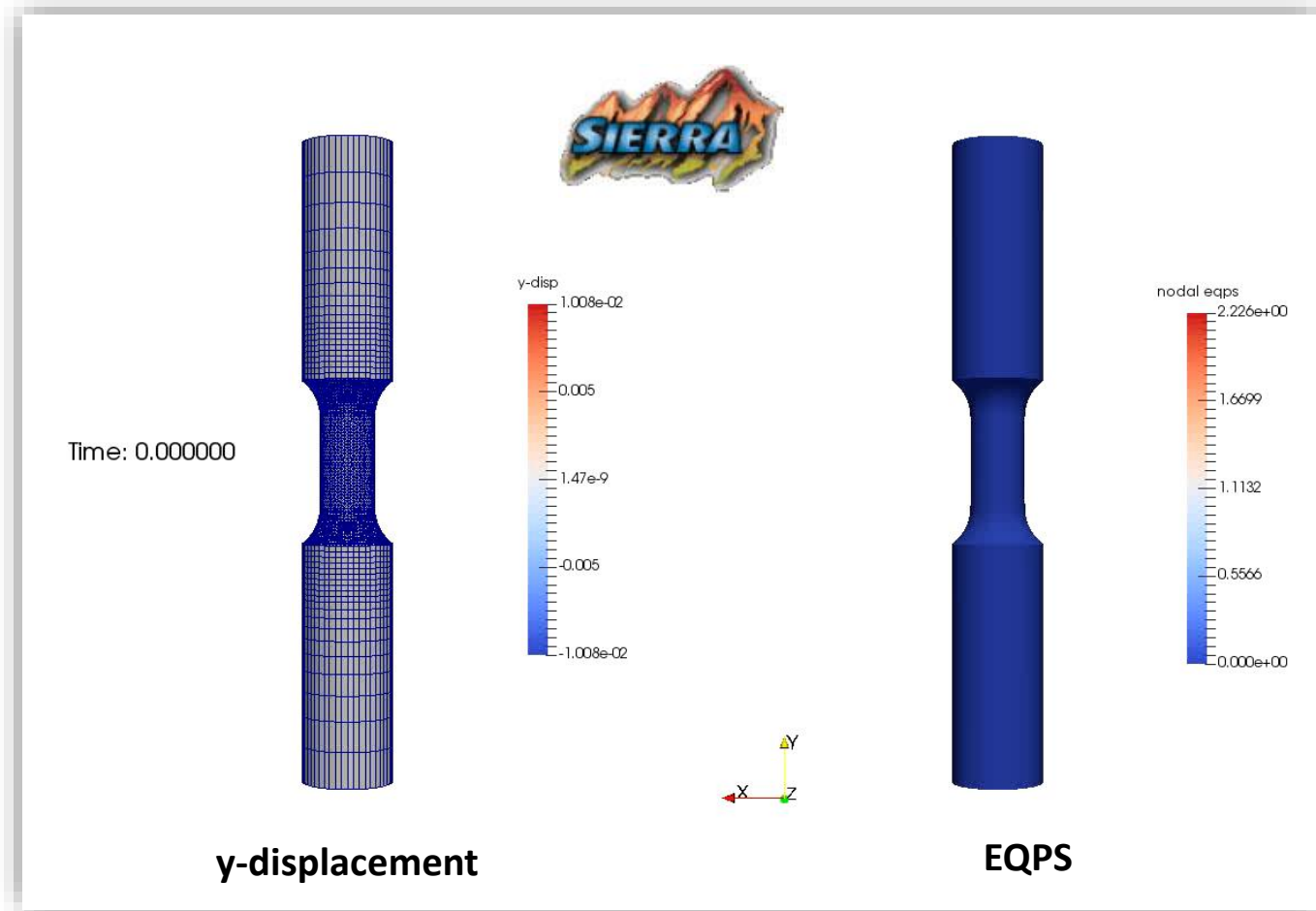
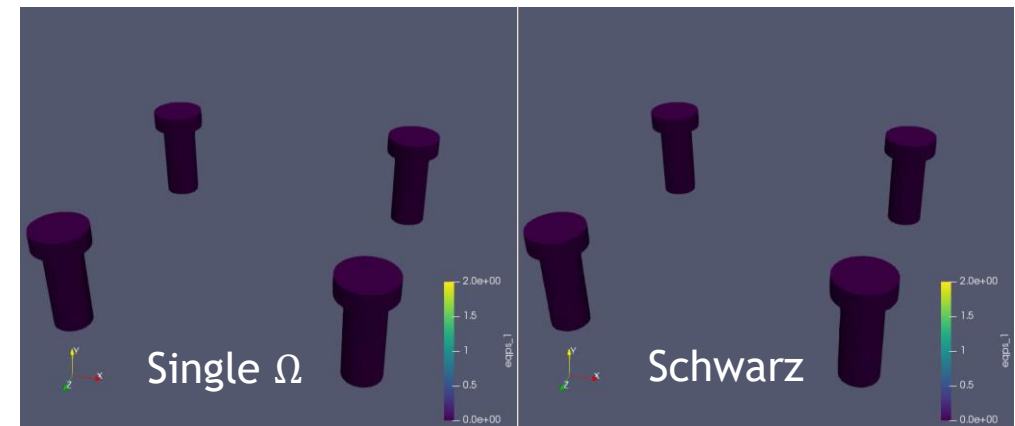
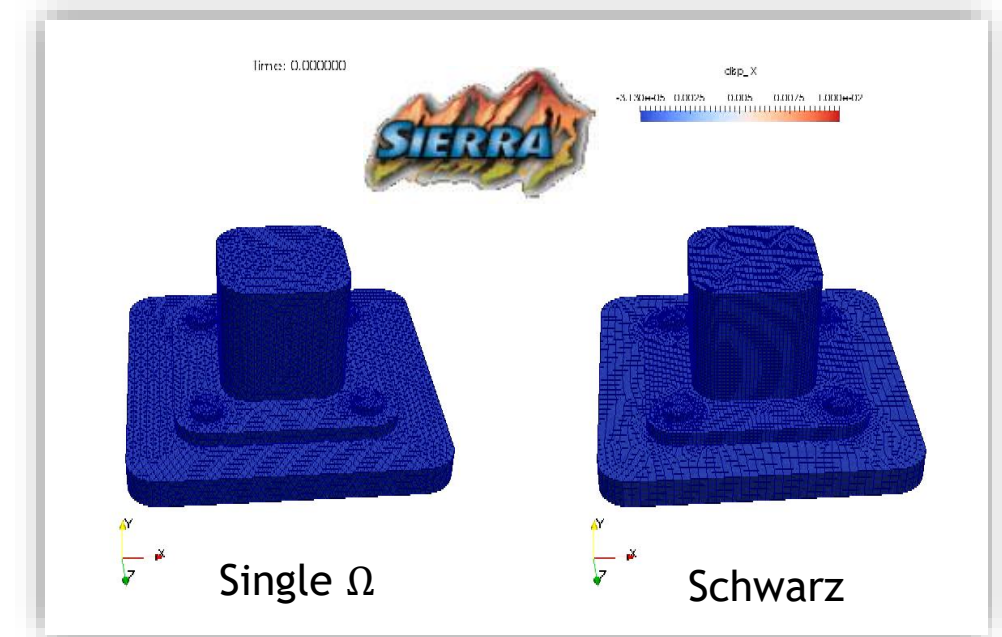


Figure above: tension specimen simulation coupling composite TET10 elements with HEX elements in Sierra/SM.

Figures right: bolted joint simulation coupling composite TET10 elements with HEX elements in Sierra/SM.



¹ Mota *et al.* 2017; Mota *et al.* 2022.

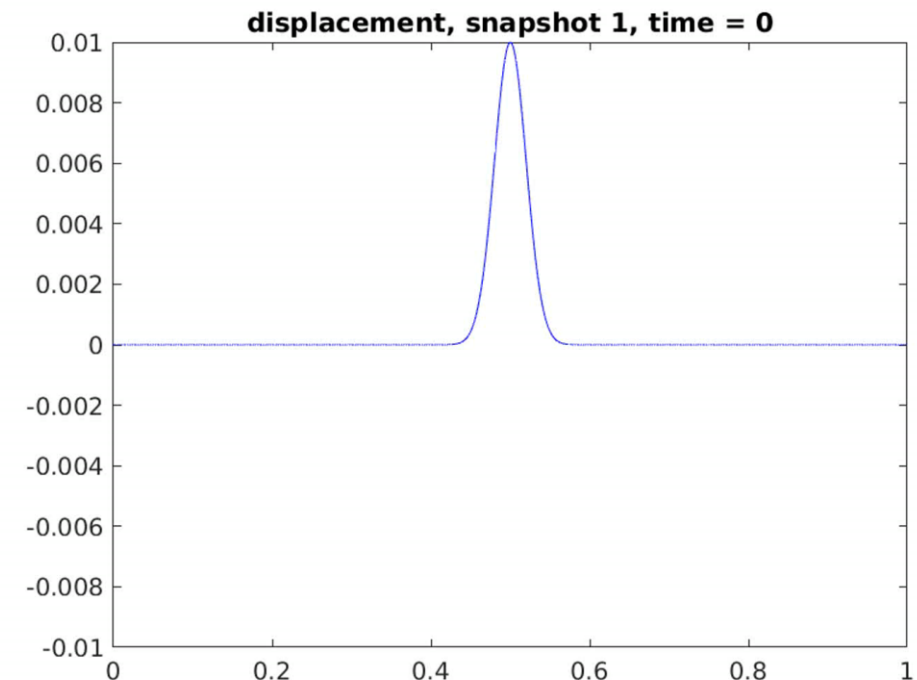
Numerical Example: Linear Elastic Wave Propagation Problem



- Linear elastic **clamped beam** with Gaussian initial condition.
- Simple problem with analytical exact solution but very **stringent test** for discretization/coupling methods.
- **Couplings tested:** FOM-FOM, FOM-ROM, ROM-ROM, implicit-explicit, implicit-implicit, explicit-explicit.
- ROMs are **reproductive** and based on the **POD/Galerkin** method.
 - 50 POD modes capture ~100% snapshot energy



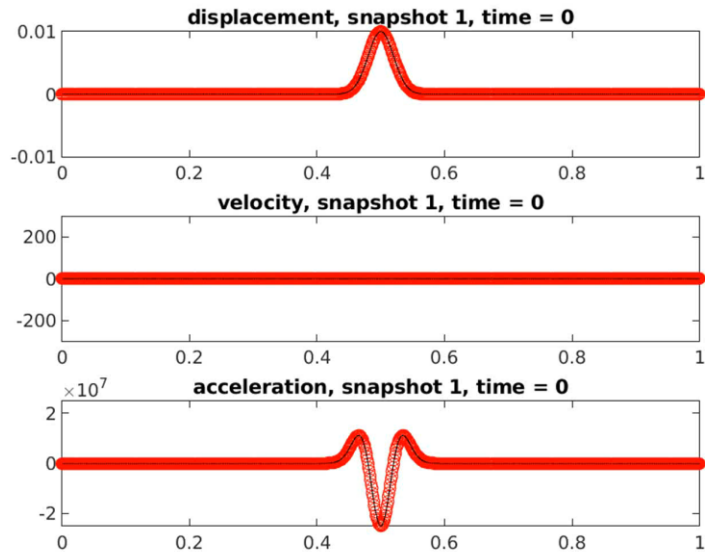
Above: 3D rendering of clamped beam with Gaussian initial condition.
Right: Initial condition (blue) and final solution (red). Wave profile is negative of initial profile at time $T = 1.0e-3$.



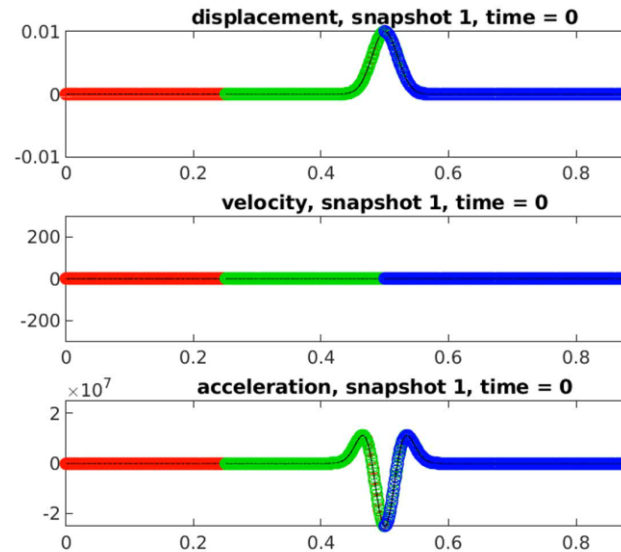
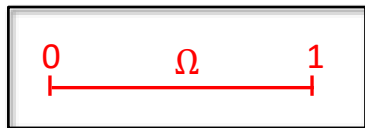
Linear Elastic Wave Propagation Problem: FOM-ROM and ROM-ROM Couplings



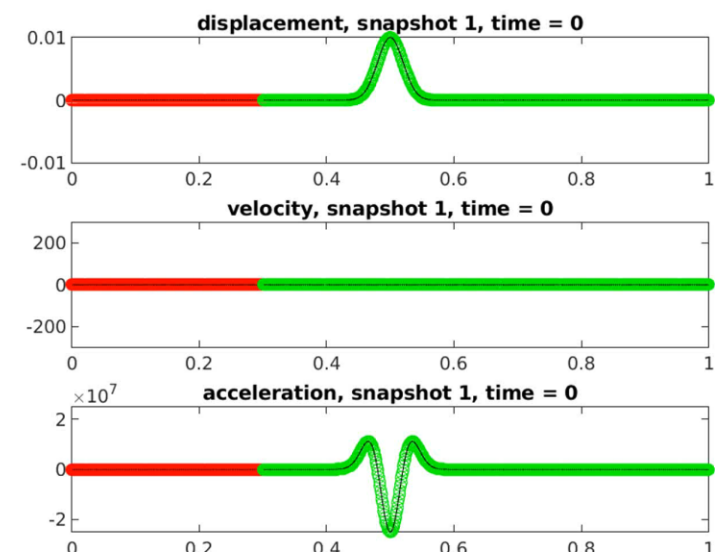
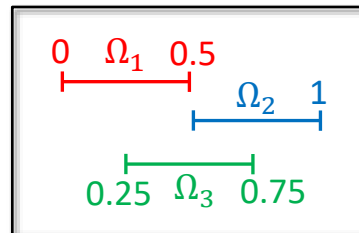
Coupling delivers accurate solution if each subdomain model is reasonably accurate, can couple different discretizations with different Δx , Δt and basis sizes.



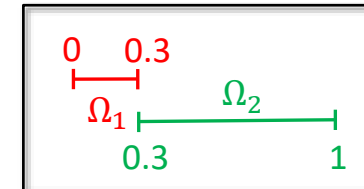
Single Domain FOM



3 overlapping subdomain
ROM¹-FOM²-ROM³



2 non-overlapping subdomain
FOM⁴-ROM⁵ ($\theta = 1$)



¹Implicit 40 mode POD ROM, $\Delta t=1e-6$, $\Delta x=1.25e-3$

²Implicit FOM, $\Delta t=1e-6$, $\Delta x=8.33e-4$

³Explicit 50 mode POD ROM, $\Delta t=1e-7$, $\Delta x=1e-3$

⁵Implicit FOM, $\Delta t=2.25e-7$, $\Delta x=1e-6$

⁴Explicit 50 mode POD ROM, $\Delta t=2.25e-7$, $\Delta x=1e-6$

Linear Elastic Wave Propagation Problem: FOM-ROM and ROM-ROM Couplings



Coupled models are reasonably accurate w.r.t. FOM-FOM coupled analogs and convergence with respect to basis refinement for FOM-ROM and ROM-ROM coupling is observed.

	disp MSE ⁶	velo MSE	acce MSE
Overlapping ROM ¹ -FOM ² -ROM ³	1.05e-4	1.40e-3	2.32e-2
Non-overlapping FOM ⁴ -ROM ⁵	2.78e-5	2.20e-4	3.30e-3

¹Implicit 40 mode POD ROM, $\Delta t = 1e-6$, $\Delta x = 1.25e-3$

²Implicit FOM, $\Delta t = 1e-6$, $\Delta x = 8.33e-4$

³Explicit 50 mode POD ROM, $\Delta t = 1e-7$, $\Delta x = 1e-3$

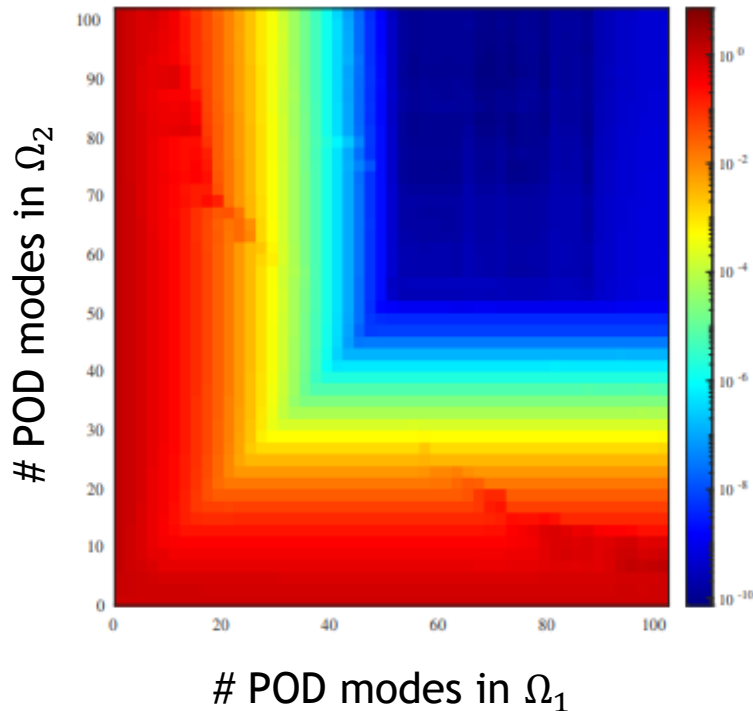
⁴Implicit FOM, $\Delta t = 2.25e-7$, $\Delta x = 1e-6$

⁵Explicit 50 mode POD ROM, $\Delta t = 2.25e-7$, $\Delta x = 1e-6$

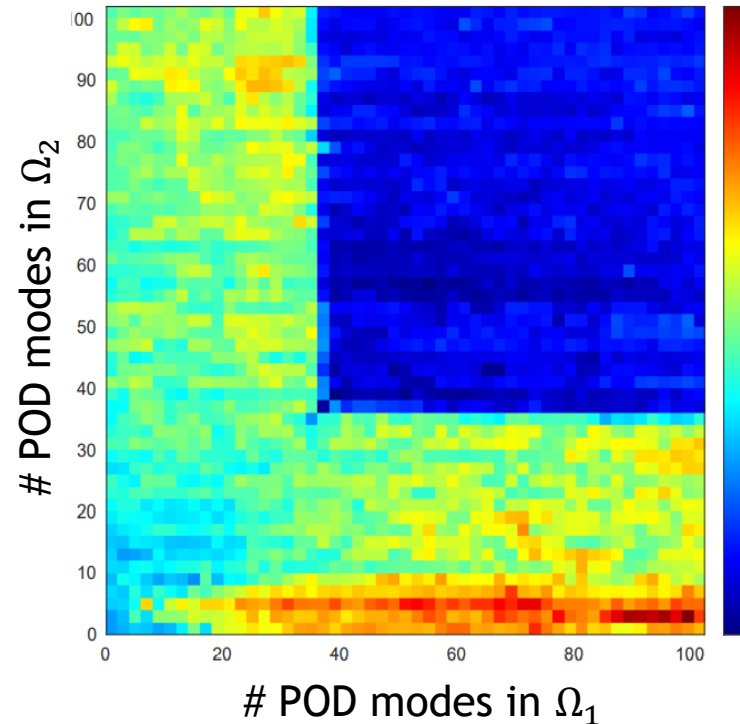
$$^6\text{MSE} = \text{mean squared error} = \sqrt{\sum_{n=1}^{N_t} \|\tilde{\mathbf{u}}^n(\boldsymbol{\mu}) - \mathbf{u}^n(\boldsymbol{\mu})\|_2^2} / \sqrt{\sum_{n=1}^{N_t} \|\mathbf{u}^n(\boldsymbol{\mu})\|_2^2}.$$

ROM-ROM coupling gives errors $< O(1e-6)$ & speedups over FOM-FOM coupling for basis sizes > 40 .

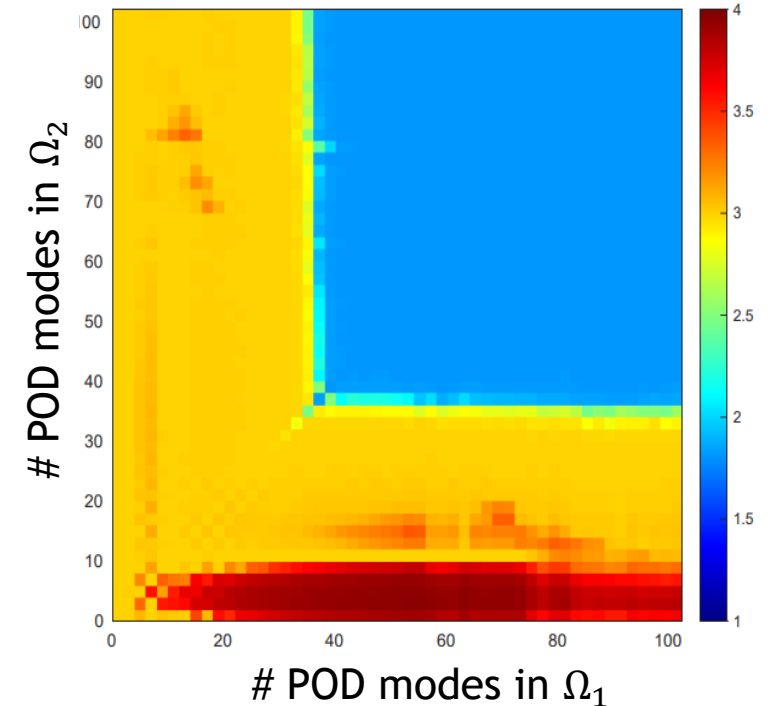
MSE in displacement for 2 subdomain ROM-ROM coupling



CPU times for 2 subdomain ROM-ROM coupling normalized by FOM-FOM CPU time



Average # Schwarz iterations for 2 subdomain ROM-ROM coupling



- **Smaller ROMs are not the fastest:** less accurate & require more Schwarz iterations to converge.
- All couplings converge in ≤ 4 Schwarz iterations on average (FOM-FOM coupling requires average of 2.4 Schwarz iterations).

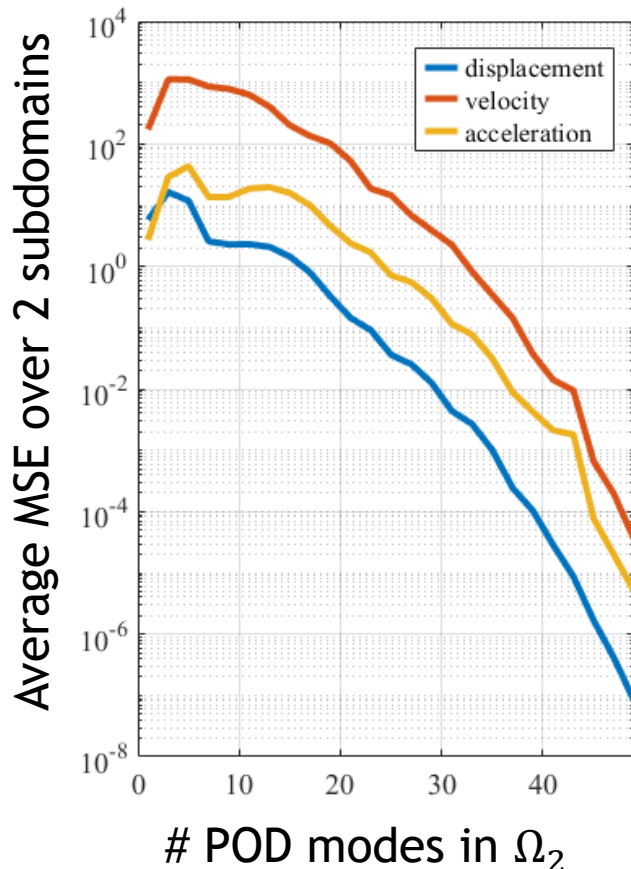
Overlapping implicit-implicit coupling
with $\Omega_1 = [0, 0.75]$, $\Omega_2 = [0.25, 1]$

Linear Elastic Wave Propagation Problem: FOM-ROM Couplings

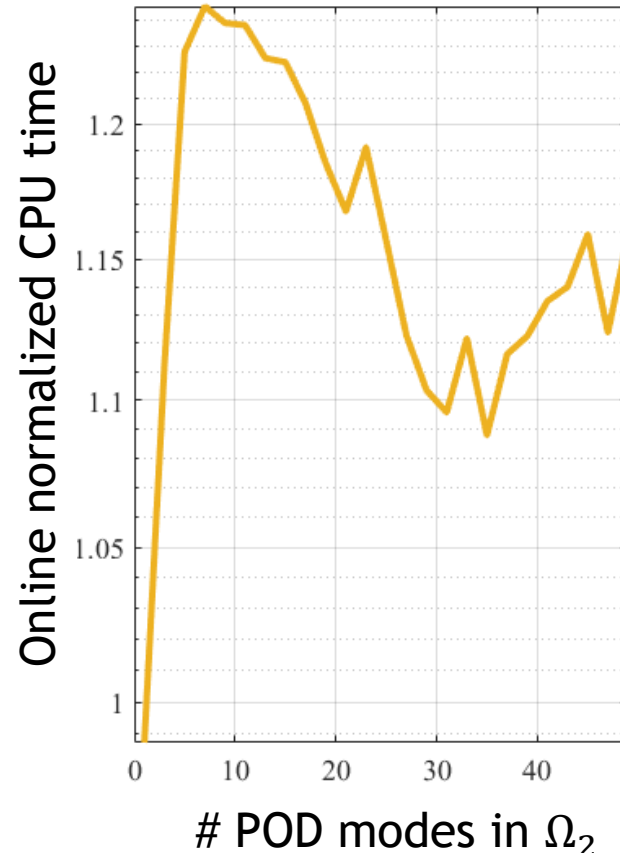


FOM-ROM coupling shows convergence with basis refinement. FOM-ROM couplings are 10-15% slower than comparable FOM-FOM coupling due to increased # Schwarz iterations.

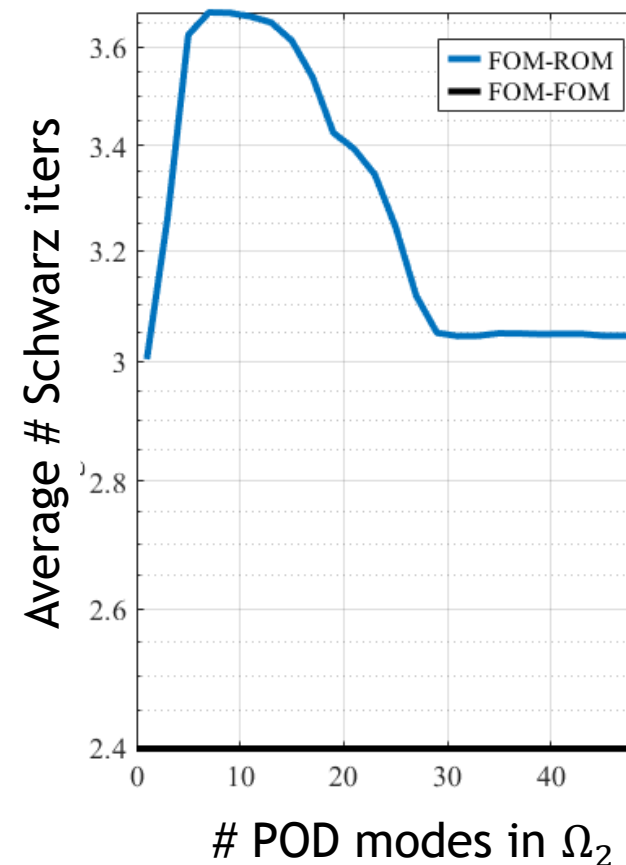
MSE for 2 subdomain FOM-ROM coupling



CPU times for 2 subdomain FOM-ROM coupling normalized by FOM-FOM CPU time



Average # Schwarz iterations for 2 subdomain couplings



WIP:
understanding & improving FOM-ROM coupling performance.

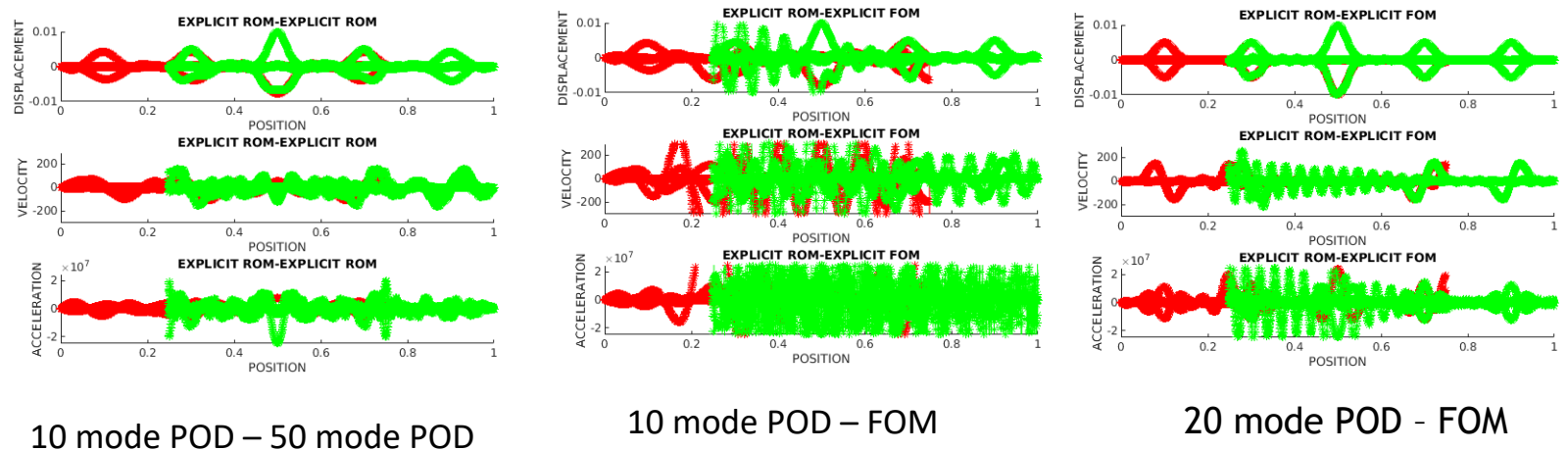
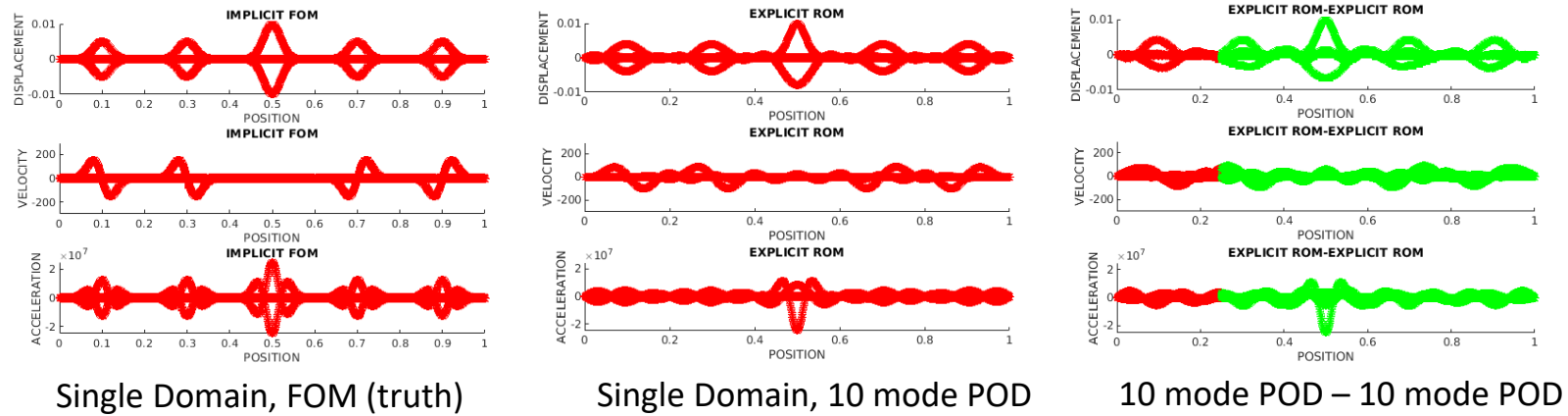
Overlapping implicit-implicit coupling with $\Omega_1 = [0, 0.75]$, $\Omega_2 = [0.25, 1]$

Linear Elastic Wave Propagation Problem: FOM-ROM and ROM-ROM Couplings



Inaccurate model + accurate model \neq accurate model.

Accuracy can be improved by “gluing” several smaller, spatially-local models



Figures above: $\Omega_1 = [0, 0.75]$, $\Omega_2 = [0.25, 1]$

Observation suggests need for “smart” domain decomposition.

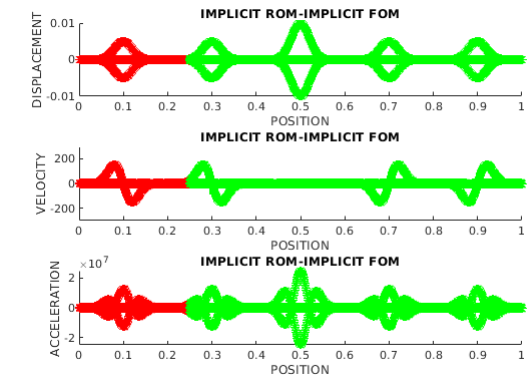
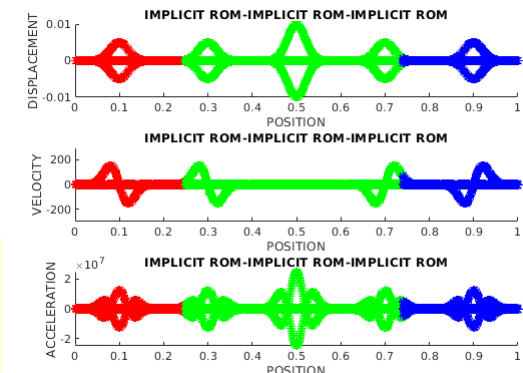


Figure above: $\Omega_1 = [0, 0.3]$, $\Omega_2 = [0.25, 1]$, 20 mode POD - FOM

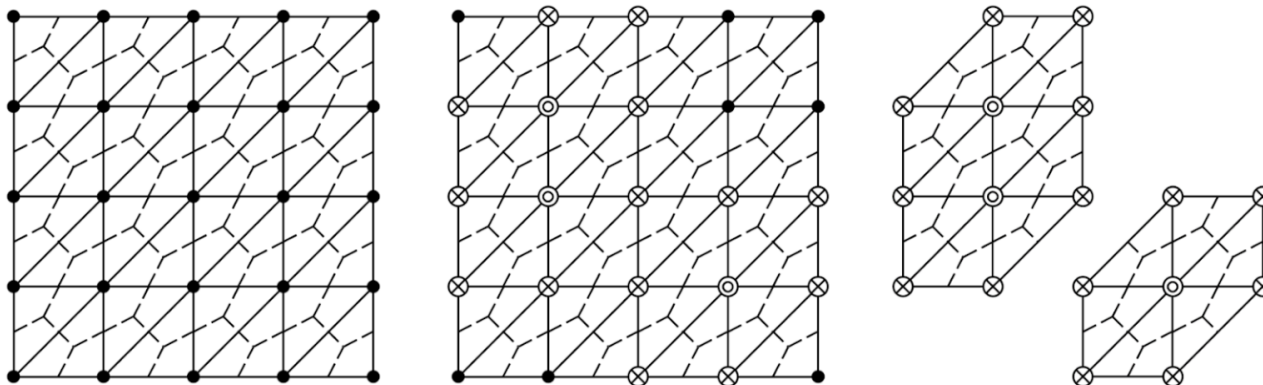
Figure below: $\Omega_1 = [0, 0.26]$, $\Omega_2 = [0.25, 0.75]$, $\Omega_3 = [0.74, 1]$, 15 mode POD - 30 mode POD - 15 mode POD



- **Project-then-approximate** paradigm (as opposed to approximate-then-project)

$$\begin{aligned} r_k(q_k, t) &= W^T r(\tilde{u}, t) \\ &= \sum_{e \in \mathcal{E}} W^T L_e^T r_e(L_{e+} \tilde{u}, t) \end{aligned}$$

- $L_e \in \{0,1\}^{d_e \times N}$ where d_e is the **number of degrees of freedom** associated with each mesh element (this is in the context of meshes used in first-order hyperbolic problems where there are N_e mesh elements)
- $L_{e+} \in \{0,1\}^{d_e \times N}$ selects degrees of freedom necessary for **flux reconstruction**
- Equality can be **relaxed**



Augmented reduced mesh: \odot represents a selected node attached to a selected element; and \otimes represents an added node to enable the full representation of the computational stencil at the selected node/element

ECSW: Generating the Reduced Mesh and Weights



- Using a subset of the same snapshots $u_i, i \in 1, \dots, n_h$ used to generate the **state basis** V , we can train the reduced mesh
- Snapshots are first **projected** onto their associated basis and then **reconstructed**

$$c_{se} = W^T L_e^T r_e \left(L_e + \left(u_{ref} + V V^T (u_s - u_{ref}) \right), t \right) \in \mathbb{R}^n$$

$$d_s = r_k(\tilde{u}, t) \in \mathbb{R}^n, \quad s = 1, \dots, n_h$$

- We can then form the **system**

$$\mathbf{C} = \begin{pmatrix} c_{11} & \dots & c_{1N_e} \\ \vdots & \ddots & \vdots \\ c_{n_h 1} & \dots & c_{n_h N_e} \end{pmatrix}, \quad \mathbf{d} = \begin{pmatrix} d_1 \\ \vdots \\ d_{n_h} \end{pmatrix}$$

- Where $\mathbf{C}\xi = \mathbf{d}, \xi \in \mathbb{R}^{N_e}, \xi = \mathbf{1}$ must be the solution
- Further relax the equality to yield **non-negative least-squares problem**:

$$\xi = \arg \min_{x \in \mathbb{R}^n} \|\mathbf{C}x - \mathbf{d}\|_2 \text{ subject to } x \geq \mathbf{0}$$

- Solve the above optimization problem using a **non-negative least squares solver** with an **early termination condition** to **promote sparsity** of the vector ξ

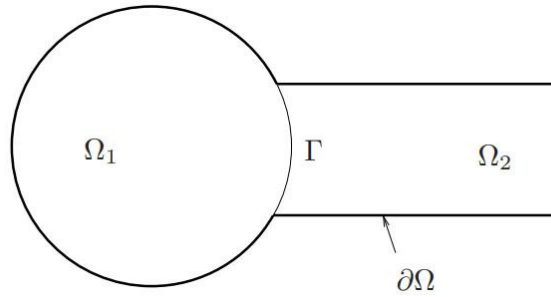
Numerical Example: 1D Dynamic Wave Propagation Problem



- Alternating **Dirichlet-Neumann** Schwarz BCs with **no relaxation** ($\theta = 1$) on Schwarz boundary Γ

$$\begin{cases} \text{Div } \mathbf{P}_1^{(n+1)} + \rho \mathbf{B}(t_i) = \mathbf{0}, & \text{in } \Omega_1 \\ \boldsymbol{\varphi}_1^{(n+1)} = \boldsymbol{\chi}, & \text{on } \partial\Omega_1 \setminus \Gamma \\ \boldsymbol{\varphi}_1^{(n+1)} = \boldsymbol{\lambda}_{n+1} & \text{on } \Gamma \end{cases}$$

$$\begin{cases} \text{Div } \mathbf{P}_2^{(n+1)} + \rho \mathbf{B}(t_i) = \mathbf{0}, & \text{in } \Omega_2 \\ \boldsymbol{\varphi}_2^{(n+1)} = \boldsymbol{\chi}, & \text{on } \partial\Omega_2 \setminus \Gamma \\ \mathbf{P}_2^{(n+1)} \mathbf{n} = \mathbf{P}_1^{(n+1)} \mathbf{n}, & \text{on } \Gamma \end{cases}$$



$$\boldsymbol{\lambda}_{n+1} = \theta \boldsymbol{\varphi}_2^{(n)} + (1 - \theta) \boldsymbol{\lambda}_n, \text{ on } \Gamma, \text{ for } n \geq 1$$

θ	Min # Schwarz Iters	Max # Schwarz Iters	Total # Schwarz Iters
1.10	3	9	59,258
1.00	1	4	24,630
0.99	1	5	35,384
0.95	3	6	45,302
0.90	3	8	56,114

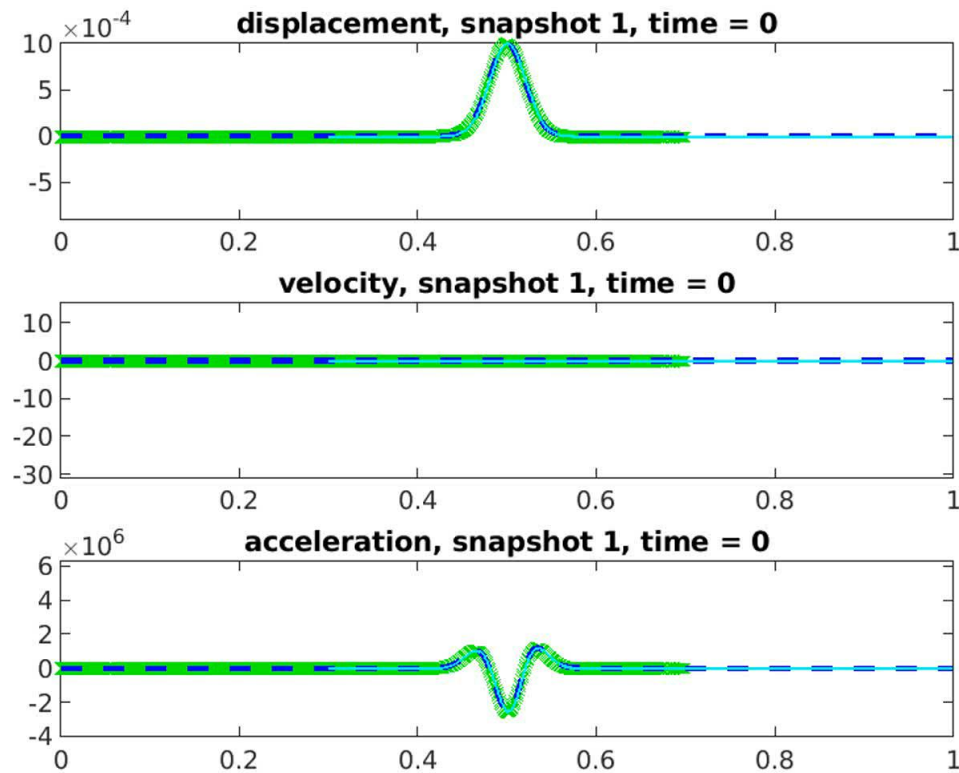
- A **parameter sweep study** revealed $\theta = 0$ gave best performance (min # Schwarz iterations)
- All couplings were **implicit-implicit** with $\Delta t_1 = \Delta t_2 = \Delta T = 10^{-7}$ and $\Delta x_1 = \Delta x_2 = 10^{-3}$
 - Time-step and spatial resolution chosen to be small enough to resolve the propagating wave
- All reproductive cases run on the **same RHEL8 machine** and all predictive cases run on the **same RHEL7 machine**, in MATLAB
- Model **accuracy** evaluated w.r.t. analogous FOM-FOM coupling using **mean square error (MSE)**:

$$\varepsilon_{MSE}(\tilde{\mathbf{u}}_i) := \frac{\sqrt{\sum_{n=1}^S \|\tilde{\mathbf{u}}_i^n - \mathbf{u}_i^n\|_2^2}}{\sqrt{\sum_{n=1}^S \|\mathbf{u}_i^n\|_2^2}}$$

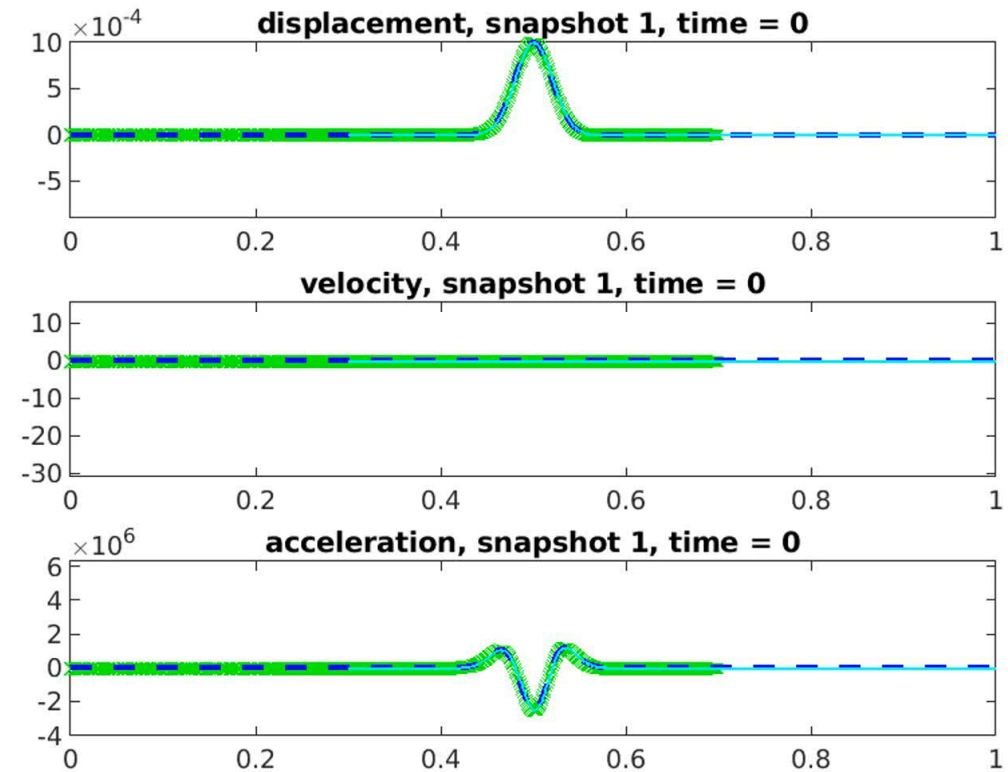
Overlapping Coupling, Nonlinear Henky MM, 2 Subdomains



- $\Omega = [0, 0.7] \cup [0.3, 1]$, implicit-implicit FOM-FOM coupling, $dt = 1e-7$, $dx = 1e-3$.

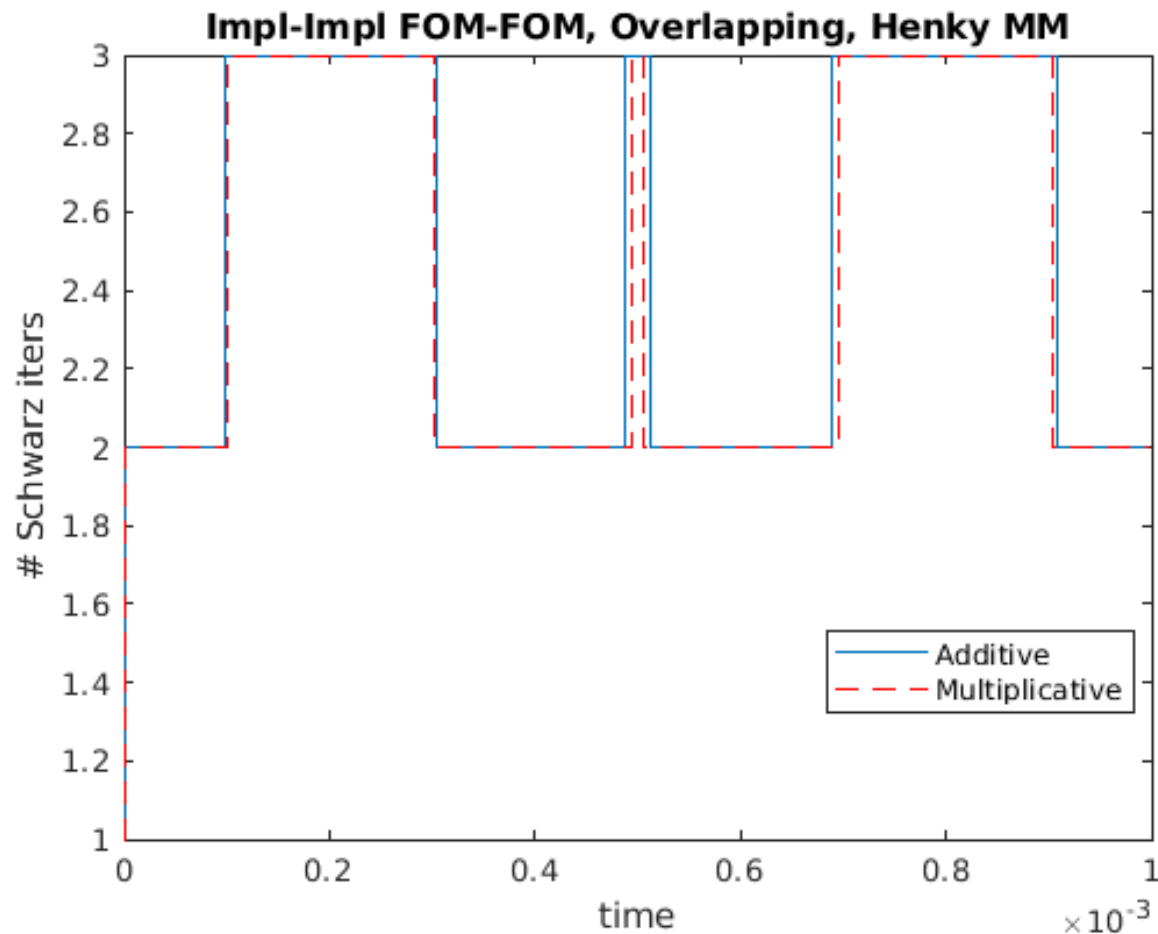


Multiplicative Schwarz



Additive Schwarz

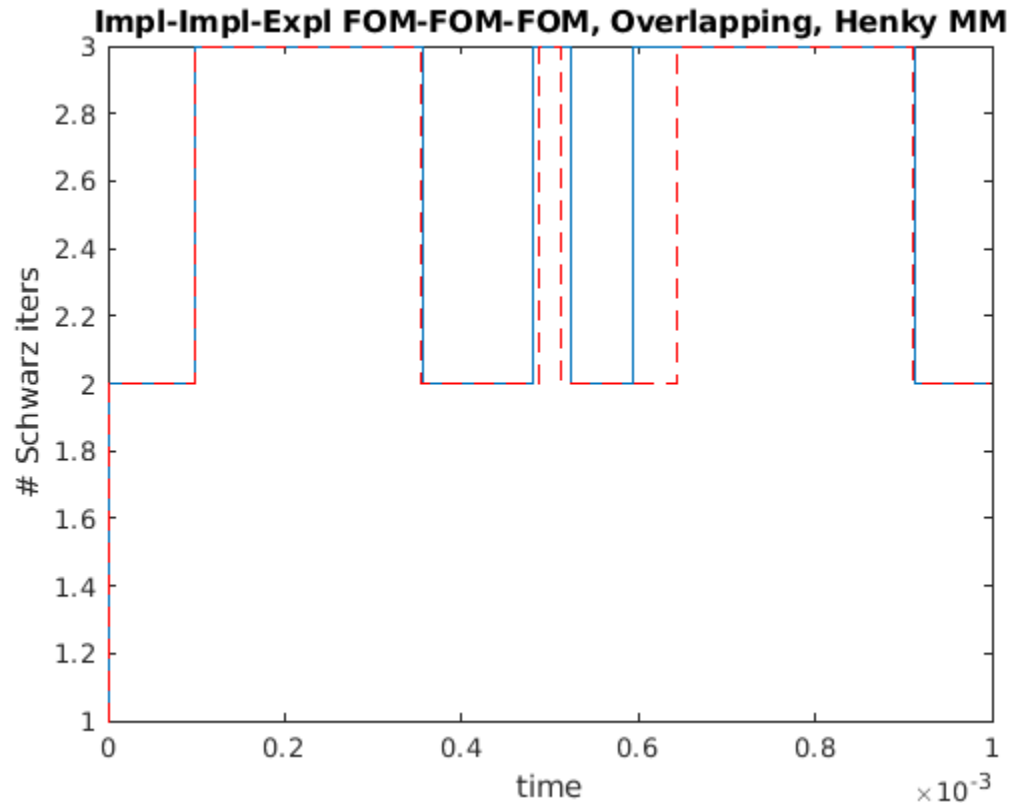
Overlapping Coupling, Nonlinear Henky MM, 2 Subdomains



- $\Omega = [0, 0.7] \cup [0.3, 1]$, implicit-implicit FOM-FOM coupling, $dt = 1e-7$, $dx=1e-3$.
- Additive Schwarz requires slightly more Schwarz iterations but is actually faster.
- Solutions agree effectively to machine precision in mean square (MS) sense.

	Additive	Multiplicative
Total # Schwarz iters	24495	24211
CPU time	2.03e3s	2.16e3
MS difference in disp	6.34e-13/6.12e-13	
MS difference in velo	1.35e-11/1.86e-11	
MS difference in acce	5.92e-10/1.07e-9	

Overlapping Coupling, Nonlinear Henky MM, 3 Subdomains



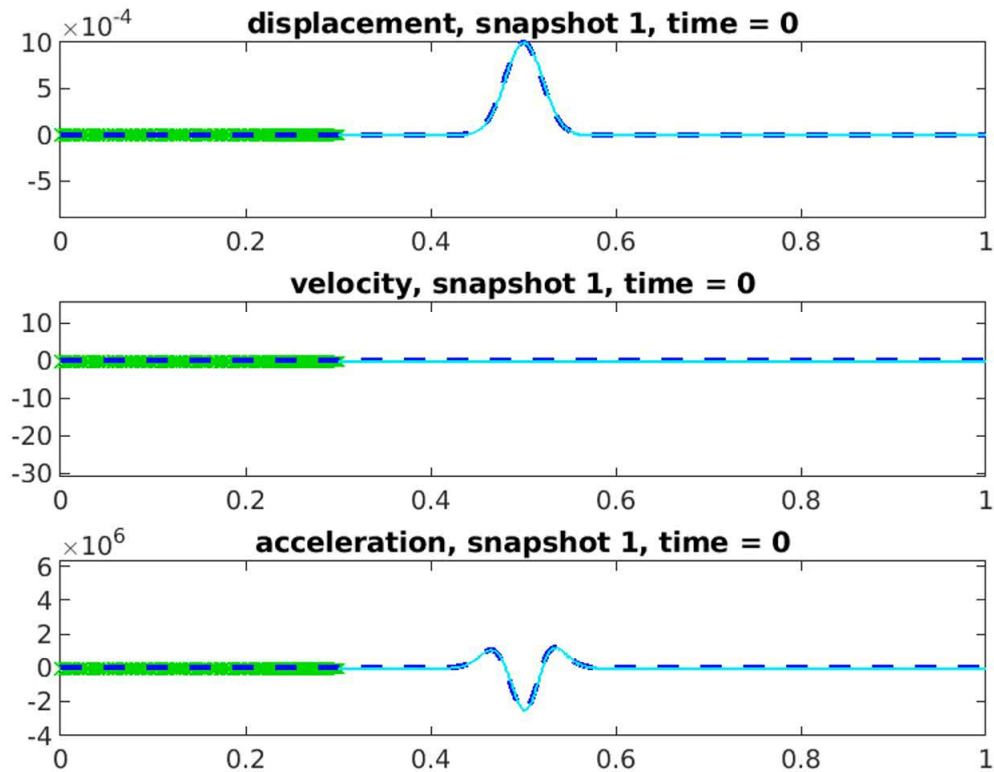
- $\Omega = [0, 0.3] \cup [0.25, 0.75] \cup [0.7, 1]$, implicit-implicit-explicit FOM-FOM-FOM coupling, $dt = 1e-7$, $dx = 0.001$.
- Solutions agree effectively to machine precision in mean square (MS) sense.
- Additive Schwarz has slightly more Schwarz iterations but is slightly faster than multiplicative.

	Additive	Multiplicative
Total # Schwarz iters	26231	25459
CPU time	1.89e3s	2.05e3s
MS difference in disp	5.3052e-13/9.3724e-13/6.1911e-13	
MS difference in velo	7.2166e-12/2.2937e-11/2.4975e-11	
MS difference in acce	2.8962e-10/1.1042e-09/1.6994e-09	

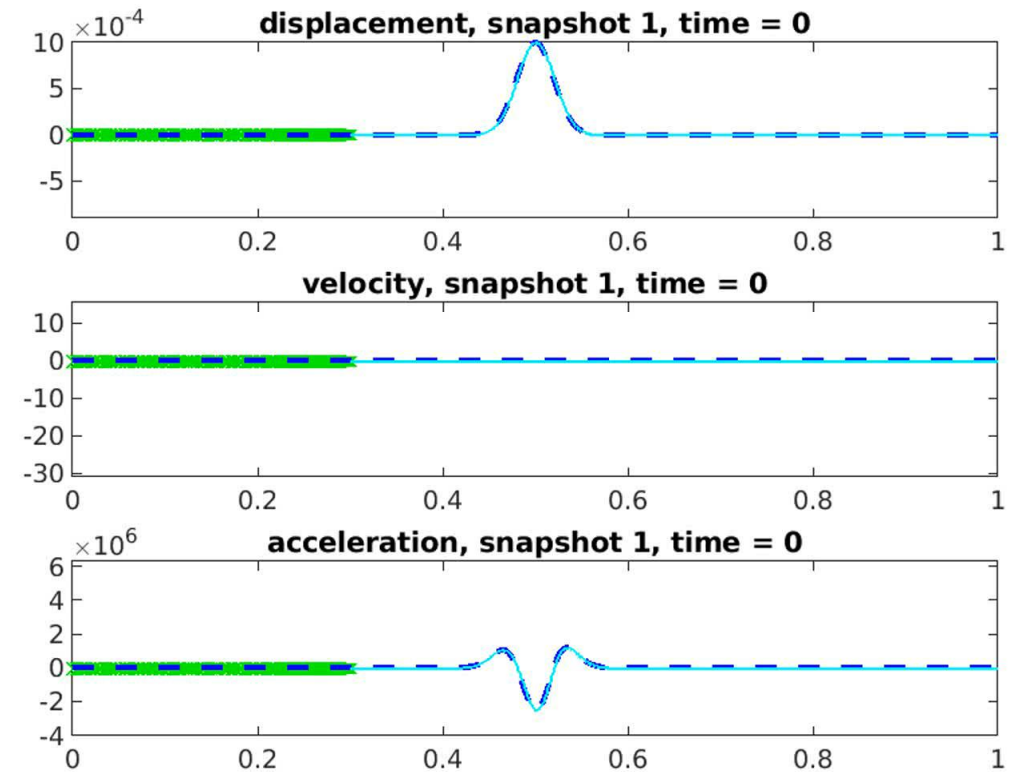
Non-overlapping Coupling, Nonlinear Henky MM, 2 Subdomains



- $\Omega = [0, 0.3] \cup [0.3, 1]$, implicit-implicit FOM-FOM coupling, $dt = 1e-7$, $dx = 1e-3$.

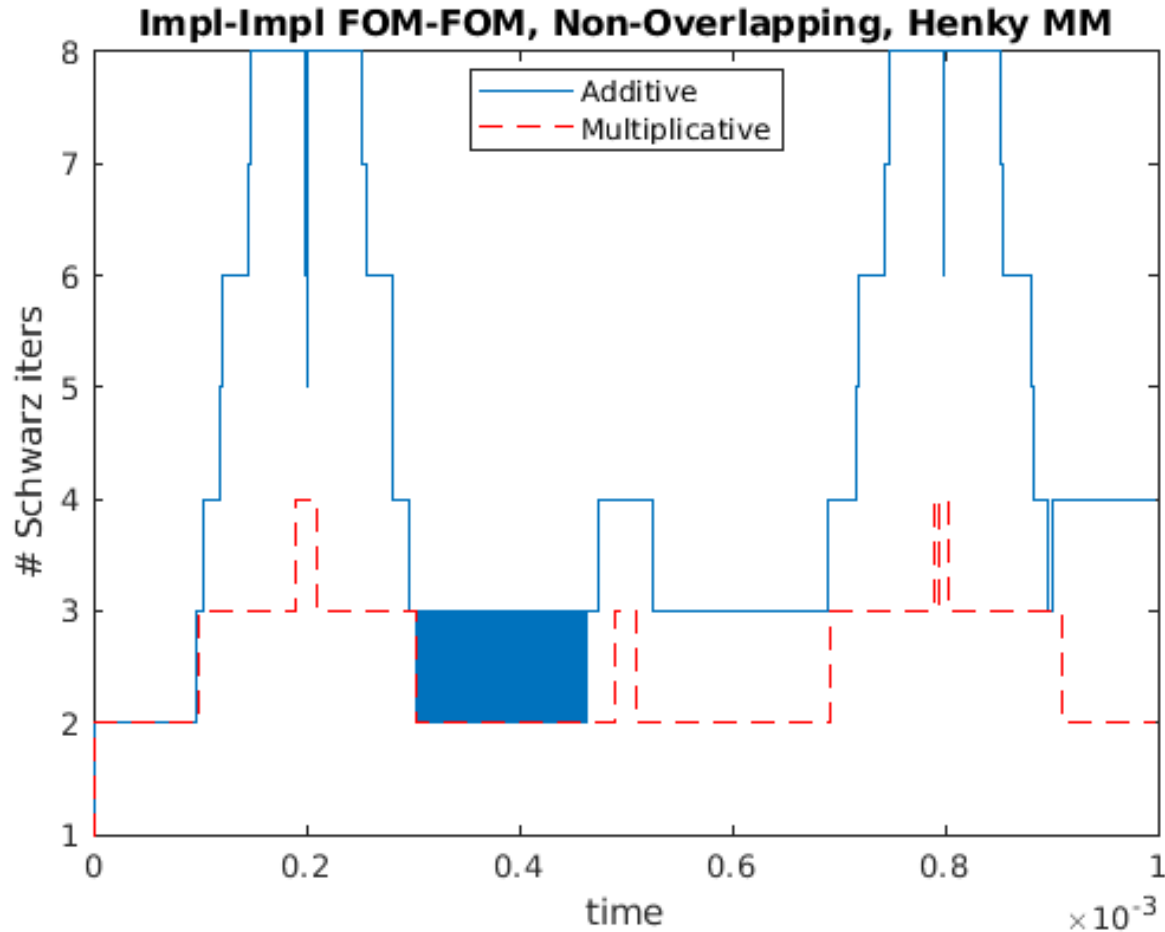


Multiplicative Schwarz



Additive Schwarz

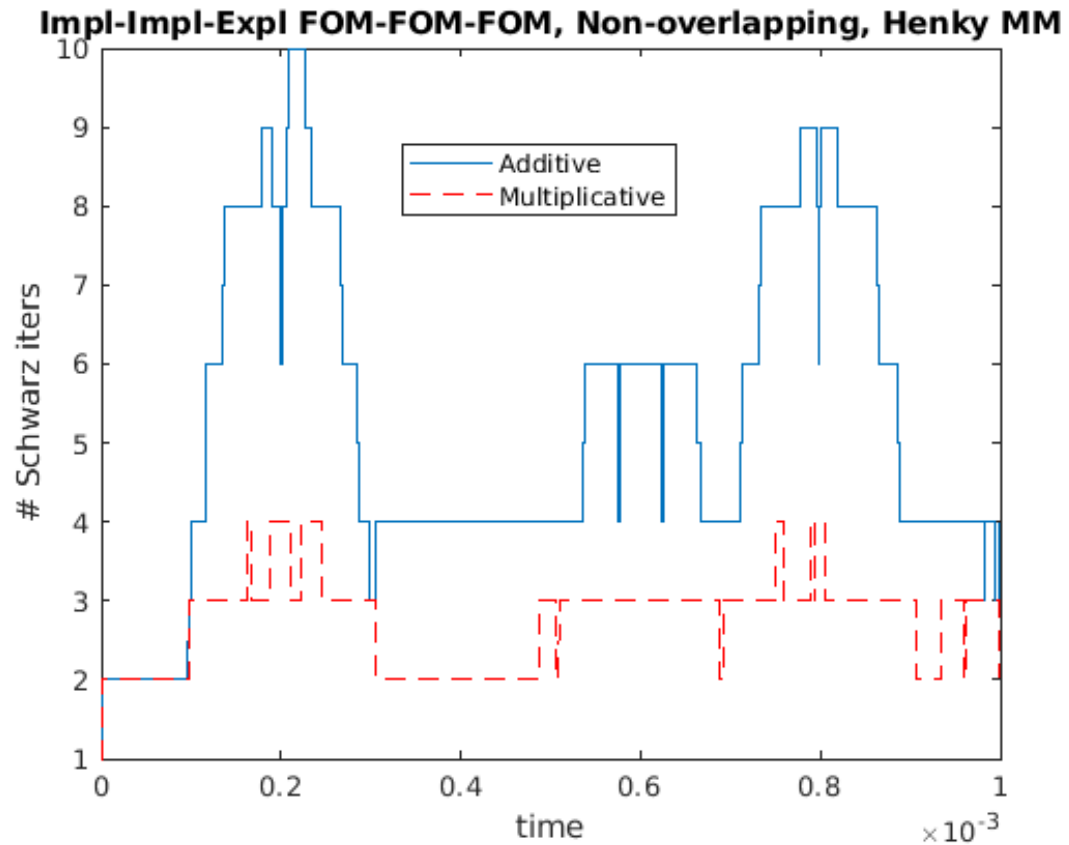
Non-overlapping Coupling, Nonlinear Henky MM, 2 Subdomains



- $\Omega = [0, 0.3] \cup [0.3, 1]$, implicit-implicit FOM-FOM coupling, $dt = 1e-7$, $dx = 1e-3$.
- Additive Schwarz requires 1.81x Schwarz iterations (and 1.9x CPU time) to converge. CPU time could be reduced through added parallelism of additive Schwarz.
 - Note blue square for additive Schwarz...
- Additive and multiplicative solutions differ in mean square (MS) sense by $O(1e-5)$.

	Additive	Multiplicative
Total # Schwarz iters	44895	24744
CPU time	1.87e3s	982.5s
MS difference in disp	4.26e-5/2.74e-5	
MS difference in velo	1.02e-5/5.91e-6	
MS difference in acce	5.84e-5/1.21e-5	

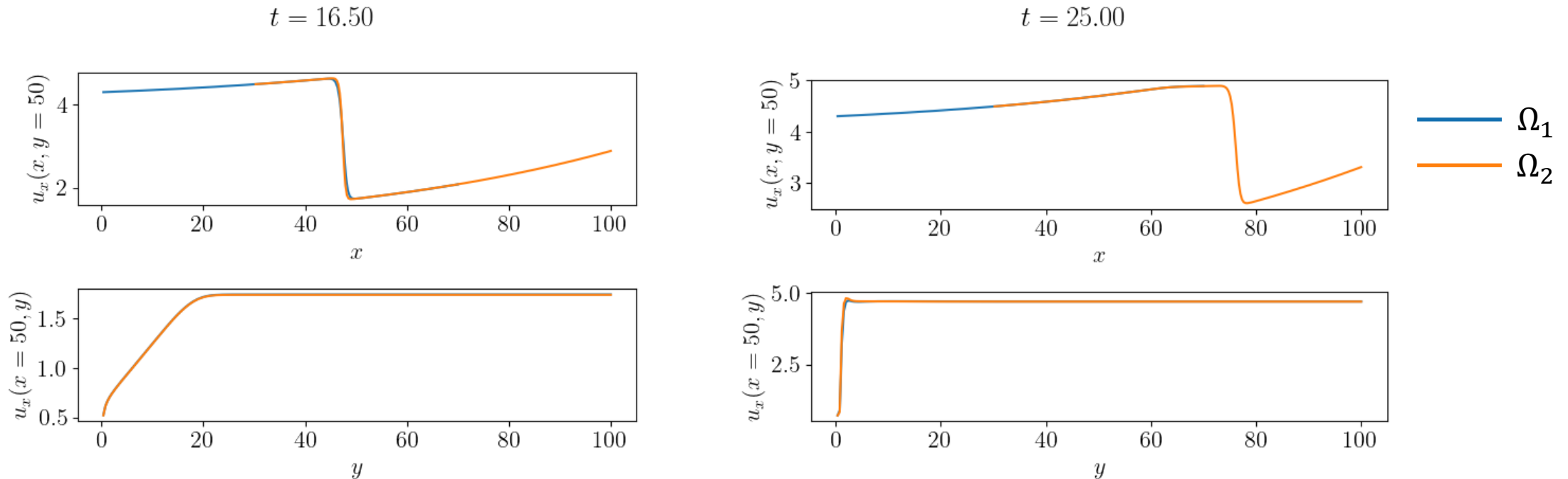
Non-overlapping Coupling, Nonlinear Henky MM, 3 Subdomains



- $\Omega = [0, 0.3] \cup [0.3, 0.7] \cup [0.7, 1]$, implicit-implicit-explicit FOM-FOM-FOM coupling, $dt = 1e-7$, $dx = 0.001$.
- Additive Schwarz has about 1.94x number Schwarz iterations and is about 2.06x slower - similar to 2 subdomain variant of this problem. No “blue square”.
 - Results suggest you could win with additive Schwarz if you parallelize and use enough domains.
- Additive/multiplicative solutions differ by $O(1e-5)$, like for 2 subdomain variant of this problem.

	Additive	Multiplicative
Total # Schwarz iters	53413	27509
CPU time	5.91e3s	2.87e3s
MS difference in disp	2.8036e-05/3.1142e-05/ 8.8395e-06	
MS difference in velo	1.4077e-05/1.2104e-05/6.5771e-06	
MS difference in acce	8.7885e-05/3.2707e-05/1.3778e-05	

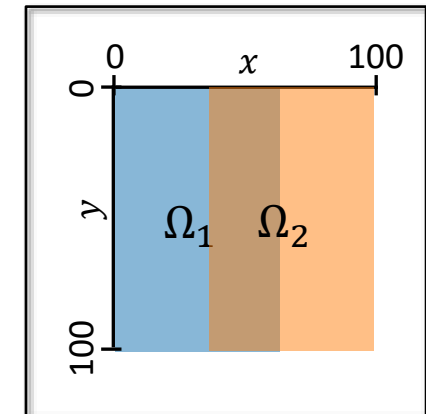
FOM-FOM Coupling: Differing Resolution



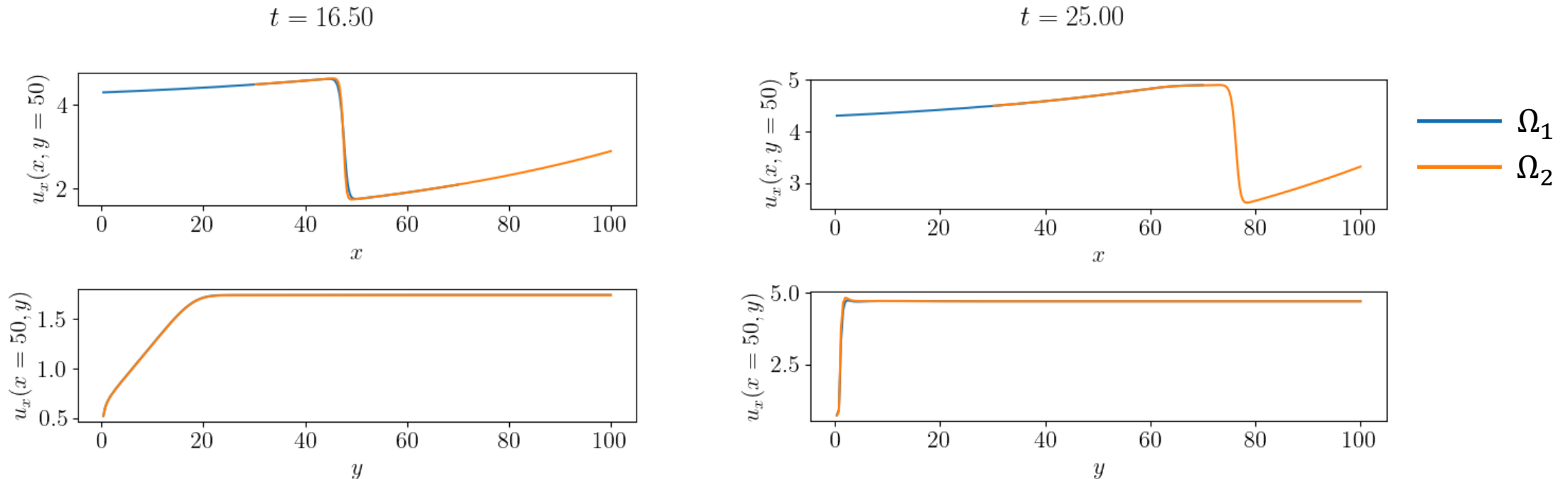
Figures above: Two-subdomain explicit-explicit overlapping coupling in x -axis $[0, 70] \cup [30, 100]$ where $\mu = [4.3, 0.021]$, $\Delta t = 0.005$, $\Delta x_1 = 0.4$, $\Delta x_2 = 0.3$

- Figures show the mid-plane slice of the solution for u_x at various times
- The right subdomain is a finer mesh, and the difference in how the shock is resolved can be seen
- $\Omega_1 \rightarrow \Omega_2$ ordering gives 2 Schwarz iterations per global time step
- $\Omega_2 \rightarrow \Omega_1$ ordering gives 3 Schwarz iterations per global time step

Order can be important!

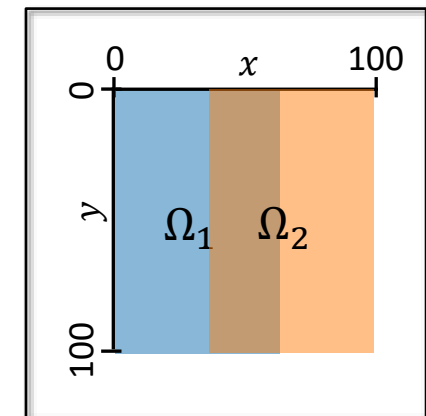


FOM-FOM Coupling: Differing time integrators and Δt

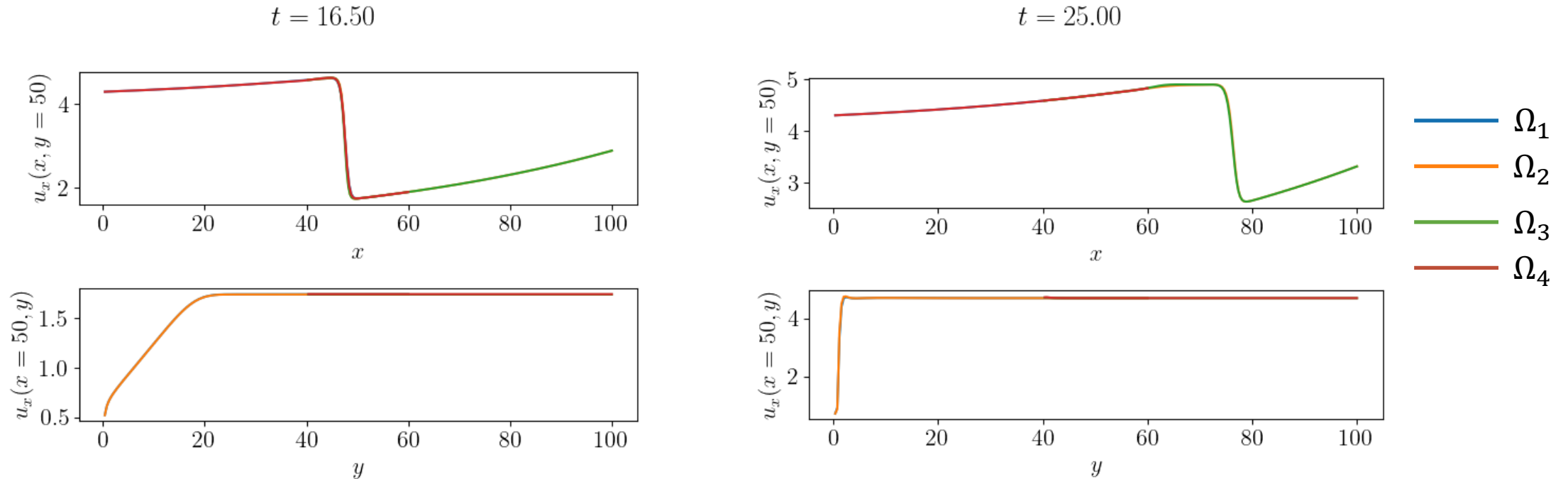


*Figures above: Two-subdomain implicit-explicit overlapping coupling in x-axis $[0, 70]$
 $U [30, 100]$, $\mu = [4.3, 0.021]$, $\Delta t_1 = 0.05$, $\Delta t_2 = 0.005$, $\Delta x_1 = 0.4$, $\Delta x_2 = 0.3$*

- Introducing a different time stepper in Ω_1 has not introduced artifacts and produces visually identical solution
- Choosing $\Omega_1 \rightarrow \Omega_2$ still only requires 2 Schwarz iterations per global time step

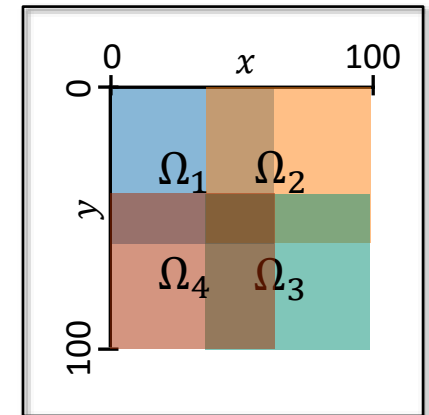


FOM-FOM Coupling: >2 Subdomains



Figures above: Four-subdomain implicit-explicit-implicit-explicit overlapping coupling in x-axis $[0, 60] \cup [40, 100]$ and y-axis $[0, 60] \cup [40, 100]$, $\mu = [4.3, 0.021]$, $\Delta t_1 = \Delta t_3 = 0.05$, $\Delta t_2 = \Delta t_4 = 0.005$, $\Delta x_1 = \Delta x_4 = 0.4$, $\Delta x_2 = \Delta x_3 = 0.3$

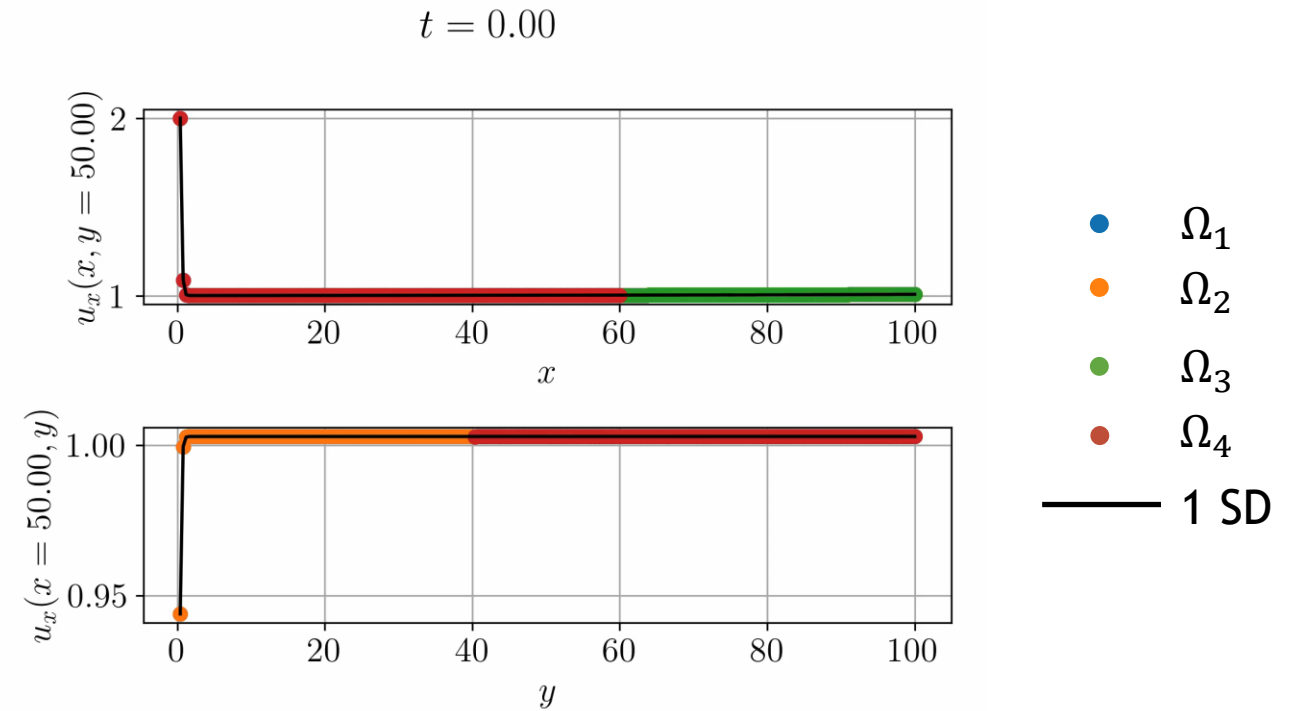
- Despite a heterogeneous mixture of different subdomains coupled in multiple dimensions with different solvers, resolutions, etc. the solution is still consistent
- Choosing $\Omega_1 \rightarrow \Omega_2 \rightarrow \Omega_3 \rightarrow \Omega_4$ requires 3 Schwarz iterations per global time step



FOM-FOM Coupling: >2 Subdomains

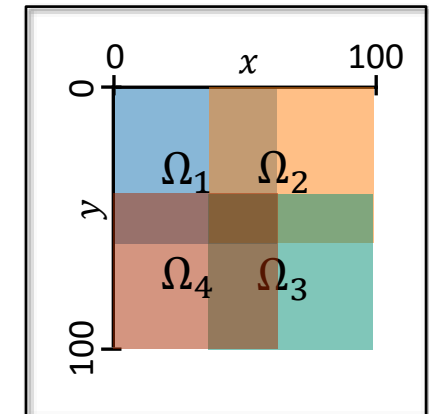


Subdomain	Wall Clock Time (s)	Total (s)
Monolithic	124	124
Ω_1	75	300
Ω_2	62	
Ω_3	62	
Ω_4	77	



Figures above: Four-subdomain implicit-implicit-implicit-implicit overlapping coupling in x -axis $[0, 60] \cup [40, 100]$ and y -axis $[0, 60] \cup [40, 100]$, $\mu = [4.3, 0.021]$, $\Delta t = 0.05$, $\Delta x_1 = \Delta x_4 = 0.4$, $\Delta x_2 = \Delta x_3 = 0.3$

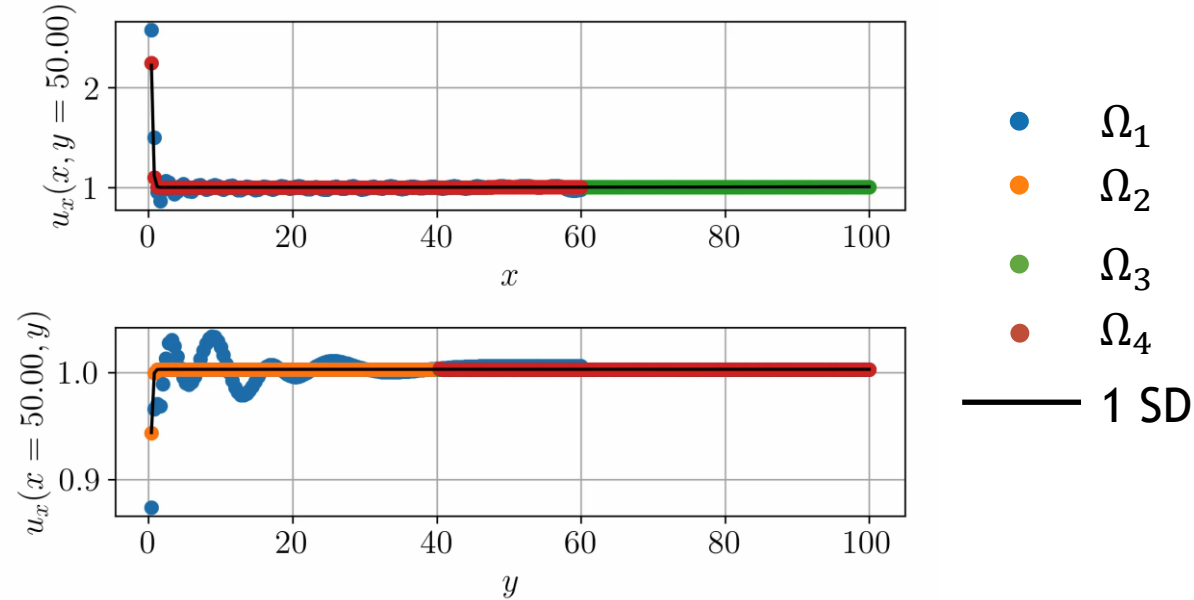
- Despite a heterogeneous mixture of different subdomains coupled in multiple dimensions with different solvers, resolutions, etc. the solution is still consistent
- Choosing $\Omega_1 \rightarrow \Omega_2 \rightarrow \Omega_3 \rightarrow \Omega_4$ requires 3 Schwarz iterations per global time step



HROM-FOM-FOM-FOM Coupling

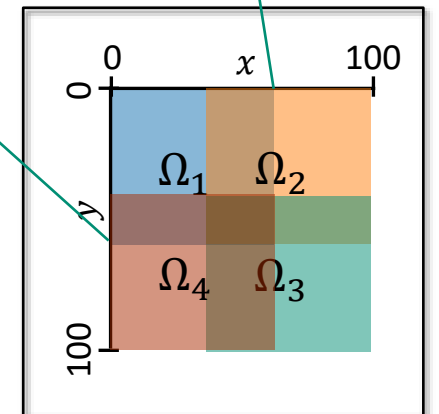


$t = 0.00$



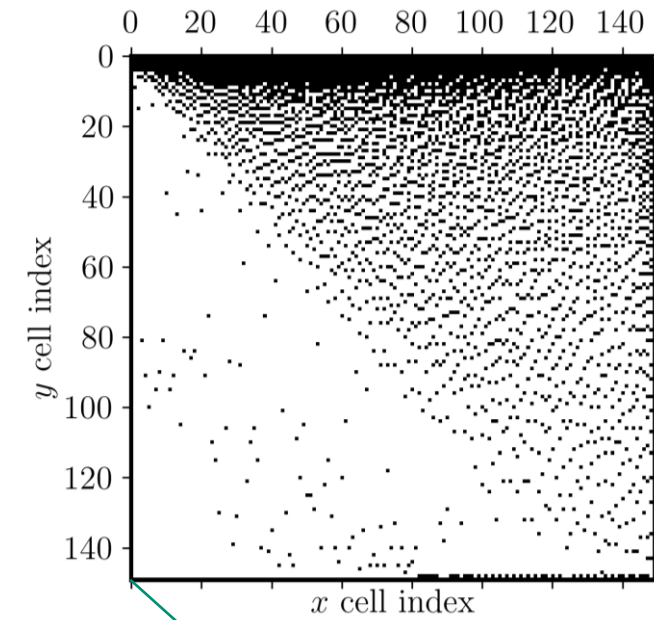
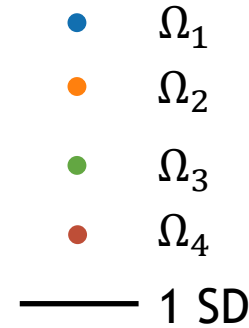
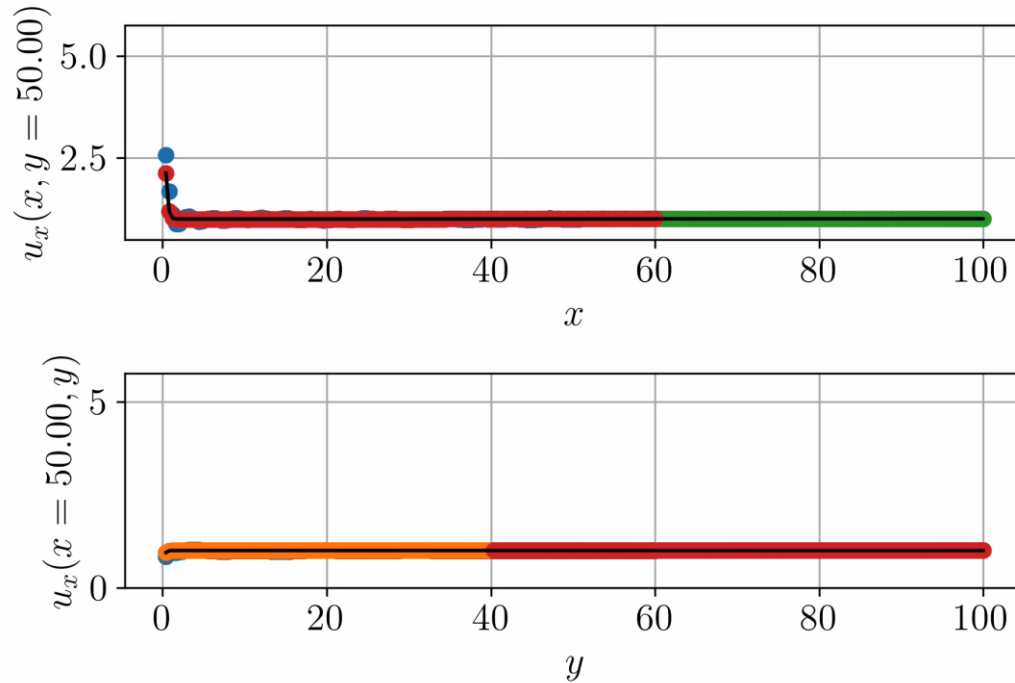
$n_e = 4,346$ (19% of N_e)

Domain	M	MSE (%)	HROM-FOM-FOM-FOM Wall Clock Time (s)	FOM-FOM-FOM-FOM Wall Clock Time (s)	Speedup
Ω_1	76	1.5	30	68	2.3
Total	—	—	276	300	1.1

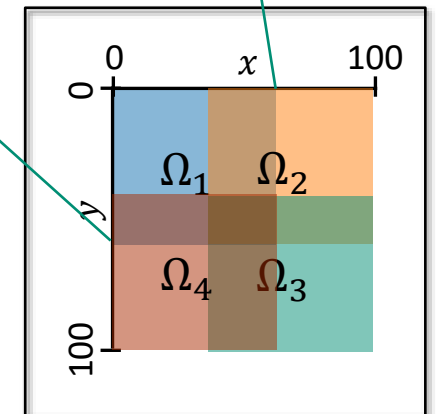


- We have **computational gain** even when choosing the “worst” subdomain for HROM
- No speedup over single-domain FOM (wall clock time = 124 s)
 - **Mitigation:** additive Schwarz, which admits more parallelism

HROM-FOM-FOM-FOM Coupling



$n_e = 4,346$ (19% of N_e)



- HROM is in Ω_1 and retains **95% of snapshot energy** \Rightarrow 57 modes
 - HROM assignment is “**worst-case-scenario**”
- **Reduced mesh** trained only using a single parameter instance of $\mu = [4.25, 0.0225]$
- Method converges in **3 Schwarz iterations** per controller time-step.
- Some **spurious oscillations** in first/last time steps due to **under-resolved solution**

Spurious oscillations *do not* impact Schwarz coupling.



Opinion: *hybrid FOM-ROM models are the future!*

- We have developed an **iterative** coupling formulation based on the **Schwarz alternating method** and an **overlapping** or **non-overlapping DD**
- Numerical results show **promise** in using the proposed methods to create **heterogeneous coupled models** comprised of arbitrary combinations of **ROMs** and/or **FOMs**
 - Coupled models can be **computationally efficient** w.r.t analogous FOM-FOM couplings
 - Coupling introduces **no numerical artifacts** into the solution
- FOM-ROM and ROM-ROM have potential to **improve** the **predictive viability** of projection-based ROMs, by enabling the **spatial localization of ROMs** (via DD) and the **online integration of high-fidelity information** into these models (via FOM coupling)



Alternating Schwarz-based Coupling Method

- Can do FOM-FOM, FOM-ROM, ROM-ROM coupling
- **Overlapping or non-overlapping DD**
- **Iterative** formulation (less intrusive but likely requires more CPU time)
- Can couple **different mesh resolutions and element types**
- Can use **different time-integrators** with **different time-steps** in different subdomains
- **No interface bases** required
- **Sequential subdomain solves** in multiplicative Schwarz variant
 - **Parallel subdomain solves** possible with **additive Schwarz** variant (not shown)
- **Extensible** in **straightforward** way to **PINN/DMD** data-driven model

Lagrange Multiplier-Based Partitioned Coupling Method

- Can do FOM-FOM, FOM-ROM, ROM-ROM coupling
- **Non-overlapping DD**
- **Monolithic** formulation requiring hybrid formulation (more intrusive but more efficient)
- Can couple **different mesh resolutions and element types**
- Can use **different explicit** time-integrators with **different time-steps** in different subdomains
- Provably convergent variant requires **interface bases**
- **Parallel subdomain solves** if explicit or IMEX time-integrator is employed
- **Extensions to PINN/DMD** data-driven models are **not obvious**



- Extension/prototyping on more multi-D (2D/3D compressible flow¹, 2D/3D solid mechanics²) and multi-physics problems (FSI, Air-Sea coupling)
- Implementation/testing of **additive Schwarz variant**, which admits more parallelism
- **Analysis** of method's convergence for ROM-FOM and ROM-ROM couplings
- **Learning** of “**optimal**” **transmission conditions** to ensure **structure preservation**
- Extension of coupling methods to coupling of **Physics Informed Neural Networks (PINNs)** (WIP)
- Exploration of **connections** between **iterative Schwarz** and **optimization-based coupling** [Iollo *et al.*, 2022]
- Development of **smart domain decomposition approaches** based on error indicators, to determine optimal placement of ROM and FOM in a computational domain (including **on-the-fly ROM-FOM switching**)
- Extension of couplings to POD modes built from snapshots on **independently-simulated subdomains**
- **Journal article** currently in preparation.

¹ [https://github.com/ Pressio/pressio-demoapps](https://github.com/Pressio/pressio-demoapps)

² <https://github.com/lxmota/norma>